“Adaptation to climate change through management and restoration of European estuarine ecosystems”.

A2.1: Assessment of the co-benefits of Climate Change provided by estuarine ecosystems and application to three European estuarine regions

Deliverable ID	**DA2.1**
Action	**A2**
Issue	**1.1**
Due Date of Deliverable	**30/07/2020**
Submission Date	**31/12/2021**
Dissemination level[1]	**PU**
Lead partner	**FIHAC**
Contributors	**MARE-IP-Leiria**
Grant Agreement No.	**LIFE18 CCA/ES/001160**

A2.1: Assessment of the co-benefits of Climate Change provided by estuarine ecosystems and application to three European estuarine regions

With the contribution of the LIFE Programme of the European Union

[1]PU = Public; CO = Confidential. only for members of the consortium (including the Commission Services); CL = Classified. as referred to in Commission Decision 2001/844/EC

A2.1: Assessment of the co-benefits of Climate Change provided by estuarine ecosystems and application to three European estuarine regions

Prepared by	Reviewed by	Approved by
Inés Mazarrasa. María Recio. Miriam Jiménez. Saúl Torres. Joao Neto	Joao Neto. José A. Juanes	José A. Juanes

Issue	Date	Description	Authors
1.0	31/12/2021	Methodology and results of the coastal protection and carbon sequestration services provided by European estuarine habitats	Inés Mazarrasa. María Recio. Miriam Jiménez. Saúl Torres. Joao Neto

TABLE OF CONTENTS

LIST OF TABLES

No se encuentran elementos de tabla de ilustraciones.

LIST OF FIGURES

1 INTRODUCTION

Coastal areas are particularly vulnerable to the impacts of climate change through sea level rise and extreme weather events (e.g. storms, floods). Given the high concentration of economic activity and the exposure to hazards, coastal areas are regions particularly under a high disaster risk (Kron, 2013; Reguero et al., 2015). The expected scenarios of Climate Change and coastal urbanization increase the need of the world's coastal communities to adapt and manage the risks derived from Climate Change on a sustainable way (Hallegatte et al., 2013; Hinkel et al., 2013; Reguero et al., 2015). In Europe, where approximately one fifth of the EU population lives within 10 km of the coast and where many densely populated coastal areas are already below sea level adaptation strategies are necessary and already in place in many areas.

Thus far traditional coastal defences have been dominated by built engineering measures or ´grey´ infrastructure (Mccreless and Beck, 2016). However since Katrina (2005) or Sandy (2012) hurricanes or the Indonesia tsunami (2004) coastal managers worldwide have started to consider alternative solutions based on the natural protection provided by coastal ecosystems, which are known as Nature Based Solutions (NbS, Cohen-Shacham et al., 2016). In particular. estuaries and estuarine ecosystems play a significant role for adaptation to CC in coastal areas. Estuaries serves as buffers of flooding and extreme sea levels and some estuarine ecosystems, such as saltmarshes, seagrass meadows, mangroves and reefs forming organisms (e.g. oysters) protect coastal areas from erosion by dampening wave energy (Ondiviela et al., 2014; Temmerman et al., 2013). For example, saltmarshes prevented over $625 million in flood losses during Hurricane Sandy in the United States (Narayan et al., 2017). These ecosystems are also able to build land through the enhancement of sediment accretion and soil elevation (Duarte et al., 2013; Potouroglou et al., 2017). particularly useful for keeping pace with sea level rise (Temmerman and Kirwan, 2015). In addition, estuarine vegetated ecosystem (i.e. saltmarshes and mangroves) are significant carbon sinks, contributing to CC mitigation through CO2 sequestration, forming, along with mangroves the so-called group of Blue Carbon ecosystems (Nellemann et al., 2009). Estuaries also support multiple other ecosystem services relevant for coastal communities, such as fisheries support, biodiversity, water quality improvement and recreational and cultural benefits (Barbier et al., 2011).

Thus, the sustainable management and conservation of estuarine ecosystems can serve as an efficient ecosystem-based approach to reduce risk, adapt to climate change and mitigate its effects and achieve a sustainable and resilient development in coastal areas (Cheong et al., 2013; Spalding et al., 2014; Sutton-Grier et al., 2015; Temmerman et al., 2013). However. estuaries and coastal ecosystems worldwide have been threatened by different anthropogenic pressures such as eutrophication, land reclamation and the spread of invasive species. In particular in Europe, two thirds of European coastal wetlands that existed at the start of the 20th century are lost (Airoldi and Beck, 2007). The loss of estuarine ecosystems leads to the loss of all the ecosystem services provided and to an increase in the exposure to climate change hazards. On the contrary, the protection and restoration of estuarine ecosystems provides an opportunity for coastal climate change adaptation and mitigation while enhancing biodiversity and all other ecosystem services provided. Therefore, it is very important to quantify the different adaptation and mitigation services that estuarine vegetation communities can provide. When carrying out the quantification of these ecosystem services, it should be considered what are the different methodological approaches that can be found in the scientific literature.

The LIFE ADAPTA BLUES project aims to demonstrate that the sustainable management, conservation and restoration of estuarine degraded and reclaimed areas is an efficient strategy to enhance adaptation to climate change in coastal areas of the European Atlantic coast. For this purpose, the project aimed to develop tools that support stakeholders in the implementation of conservation and restoration projects in estuaries as CC adaptation strategies. The development of such tools requires a deep knowledge on the benefits against climate change that estuarine ecosystems provide, considering the broad variability of vegetated communities and environmental conditions that can affect their capacity for coastal protection and carbon sequestration. Thus, the project LIFE ADAPTA BLUES includes a preparatory action (action A2) that specifically aims to assess the climate co-benefits that estuarine habitats provide in Europe in 5 estuaries of study distributed in three European Atlantic regions: Coimbra (in Portugal), Cantabria (in Spain) and Zeeland (The Netherlands). **The protocols applied in this action shall be applicable to other European estuaries. In addition, the knowledge generated in this action is critical for the development of other actions in the project such as action A4 and C1.**
This report presents the method used and the results obtained in the preparatory action A2 of the project LIFE ADAPTABLUES.

1.1 Goals

The goal of the action A2 of the project LIFE ADAPTA BLUES is to assess the climate co-benefits (adaptation and mitigation) that estuarine habitats provide in Europe based on five estuaries of study, using a protocol applicable to any other European estuary. To meet with this general purpose, the action A2 established three main goals.

1.1.1. Protocol to develop a detailed cartography of estuarine habitats (considering the EU habitats directive) within the estuaries of study.

1.1.2. Protocol to To assess the capacity for coastal protection against erosion and flooding of the most representative habitats in the estuaries of study.

1.1.3. Protocol to To assess the carbon sink capacity of the most representative habitats in the estuaries of study.

It should be noted that these protocols are intended to be applied by technical teams in order to carry out a robust quantification of the ecosystem services provided by estuarine plant communities.

2 METHODS

2.1 Habitats cartography

Mapping is a key role for Habitats monitoring (Bunce et al., 2013). The spatial distribution of the plant communities will shape the availability of goods and services, including climate services (coastal protection and carbon storage). Therefore, the recognition of this distribution should be the first step to take into account in the assessment of climate services.

Within the framework of this project, the cartography of intertidal habitats of the estuaries of study should be conducted through fieldwork campaigns in 2019. Habitats should be classified according to the EU habitats directive (92/43/EEC) based on the floristic composition of the plant community, although EUNIS classification will also be acceptable. It is important to note that areas occupied by alien species should also be mapped, as well as artificial barriers to natural tidal or riverine flow.

The recommended representation scale is, at least, 1:10000.

In this action the habitats cartography distribution was applied in 5 estuaries located in 3 Atlantic European Region: Oyambre estuary, Santander Bay, Santoña marshes, Mondego estuary and Western Scheldt estuary.

2.2 Coastal protection against erosion and flooding

Sustainable management of estuarine environments requires a reliable quantification of the different ecosystem services provided by the estuary. This section defends the need to define a protocol that allows to quantify the coastal protection offered by estuarine vegetation. This protocol will establish the basis for a study whose objective is to analyze the risk of erosion and flooding on the socioeconomic system around the estuary and the risks of flooding due to sea level rise, considering the role played by estuarine ecosystems.

Coastal protection services will be evaluated considering a vegetated and an unvegetated estuary. Each of the different steps in the development of the protocol will be described below.

In this action the protocol was applied in 4 estuaries located in 2 Atlantic European Region: Oyambre estuary, Santander Bay, Santoña marshes and Mondego estuary. This protocol has not been applied in the Western Scheldt estuary because since 2017 the Dutch flood

protection legislation establishes the safety standard for dike segments that are defined as the maximum allowed probability of flooding.

2.2.1 Definition of spatial and time scales

The impacts of flooding and erosion will be analyzed considering the role of estuarine ecosystems. Floods are usually caused by short-lived extreme events. These events exceed a certain infrequent water level, after which the water level returns to its average situation. On the other hand, the erosion-sedimentation equilibrium that occurs in estuarine environments is conditioned by a variety of spatio-temporal scales: short-scale processes (erosion processes caused by extreme events), medium-scale processes (seasonal variability of sediment transport) and long-scale processes (evolution of the system towards a dynamic equilibrium position). All these scales interact and must be considered when predicting the behavior of these systems.

For this reason, both impacts (flooding and erosion) should be analyzed from different time scales.

- The study of flood analysis should be approached from a short-term point of view, by means of the extreme regime analysis.
- The study of erosion-sedimentation analysis should be approached considering different time scales, through the characterization of the average and extreme regime.

It should be noted that the increase of mean sea level due to climate change is an important element to consider in the assessment of flooding and erosion impacts in estuarine environments, since it can cause the permanent loss of low-lying areas. This loss will cause significant alterations to the hydrodynamic and morphological characteristics of estuaries, and therefore in their sediment balance. Therefore, not only the role of estuarine ecosystems will be evaluated, but also the changes that estuaries may experience under different climate change scenarios.

The behavior of an estuary is the result of the nonlinear interaction between hydrodynamics, sediment transport, ecosystem functioning and bed level change. However, the difficulty to simulate nonlinear processes and the intervention of a wide variety of spatio-temporal scales must be evaluated in order to select the most appropriate approaches to solve our system. For this reason, before tackling any task, it is necessary to know the information available, the scale of the processes to be solved and the existing computational limitations. Table 1 shows the list of criteria to be considered before approaching the study.

		Equilibrium models	Pseudo-empirical models	Processes models
Spatial scale	High resolution (m -dam)	🔴	🔴	🟢
	Medium resolution (hm)	🔴	🟢	🟢
	Low resolution (km)	🟢	🟢	🟢
Temporal scale	Short term (hours- days)	🔴	🔴	🟢
	Medio term (weeks - months)	🔴	🟢	🟢
	Long term (years -decades)	🟢	🟢	🟢
Processes to study	Hydrodynamic	🔴	🔴	🟢
	Sediment transport or balance mass	🟢	🟢	🟢
	Sea Level Rise	🟢	🟢	🟢
	Vegetation	🔴	🟢	🟢
Computational cost	Low	🟢	🔴	🔴
	Medium	🔴	🟢	🟢
	High	🔴	🔴	🟢
Information requirements	Low	🟢	🔴	🔴
	Medium	🔴	🟢	🔴
	High	🔴	🔴	🟢

Table 1. Criteria to be considered in the study of different spatial and time scales.

This study analyzes the impact of floods, which are extreme events that occur and develop their impact in short time scales. A model based on physical processes was selected to perform the flood analysis according to the criteria presented in Table 1. This approach allows us to reproduce the hydrodynamic behavior at short time scales, and at a suitable spatial resolution. In the evaluation of the erosion-sedimentation impact, a process-based model was also selected, despite the high computational cost and the large amount of information required to analyze the erosion-sedimentation patterns at a high spatial resolution. This decision has been taken to obtain the spatial distribution of erosion and sedimentation in each estuary.

2.2.2 State of knowledge

The Intergovernmental Panel on Climate Change (IPCC) Fifth Assessment Report shows that the combined effect of changes in hazard, associated with extreme events and long-term changes, as well as an increased exposure of assets and activities, and vulnerability of human settlements and coastal ecosystems, will be the main causes of growth in risk levels (Wong et al., 2014). Risk management and adaptation represent a major investment challenge that the present society is forced to face. One of the main challenges we face when analyzing climate change risks is the choice of the most appropriate strategy to model the impact of interest. Although there is much research focused on the analysis of flood risk due to sea level (Rosenzweig et al., 2011; Hallegatte et al., 2013), few authors take into account the effect of waves (Dawson et al., 2009), even though they have been responsible for significant coastal damage. In addition to marine dynamics, precipitation and river flow can contribute to coastal inundation (Muis et al., 2015), and should be considered in estuarine environments. Additionally, estuaries can alter the erosion/accretion patterns of adjacent beaches (Ranasinghe et al., 2013). While the use of high-resolution historical databases (Camus et al., 2013; Pérez et al., 2017) is essential for assessing interannual variability, as well as for analyzing changes in extreme regimes or modeling past events (Muis et al., 2016), numerous studies have been conducted based on design storms (Ranasinghe et al., 2012) or directly employing sea level extremes provided by the Dynamic Interactive Vulnerability Assessment model tool (DIVA) (Hinkel et al., 2014). Regarding how climate change is usually incorporated, while adding SLR (sea level rise) to the current distribution of extremes is common practice (Muis et al., 2015). Few works include wave and meteorological tidal projections or consider in the analysis the combined action with fluvial dynamics.

Another relevant aspect in risk assessment is the selection of the most appropriate impact model. While more sophisticated process models may seem the best option to carry out a detailed study, depending on the type of statistical analysis required and the geographical scale, among other criteria, the approach followed may consider the use of simpler and more efficient methods and equilibrium formulations, where appropriate. Because the problem is not a mere question of computational cost, but sometimes of the incomplete knowledge that we have of the processes and of the number of model calibration parameters that limit the suitability of certain numerical strategies. In recent years, many methodologies have been developed to analyze coastal erosion with different levels of complexity. These vary from indicator-based approaches, such as the simple BTM (bathtub method) (Reguero et al., 2015; Muis et al., 2016) that coarsely resolves the propagation of inundation over land by slicing the Digital Terrain Model (DTM) at a given elevation; to much more sophisticated analyses that incorporate 2D or 3D modeling, computationally more demanding, and that are applicable at a local scale only.

A detailed representation of the coastal protection behavior against flooding and erosion is needed. Therefore, a sophisticated analysis of the behavior of vegetation has been carried out in this action by means of a 2D model in the different estuaries analyzed.

Once the most appropriate approach has been selected, the different methodological steps to be followed for the evaluation of flood and morphodynamic evolution based on process-based modeling are described below.

2.2.3 Flood assessment protocol.

Figure 1 shows a schematic representation of the methodology used to carry out the analysis of the flooding areas in the analyzed estuaries.

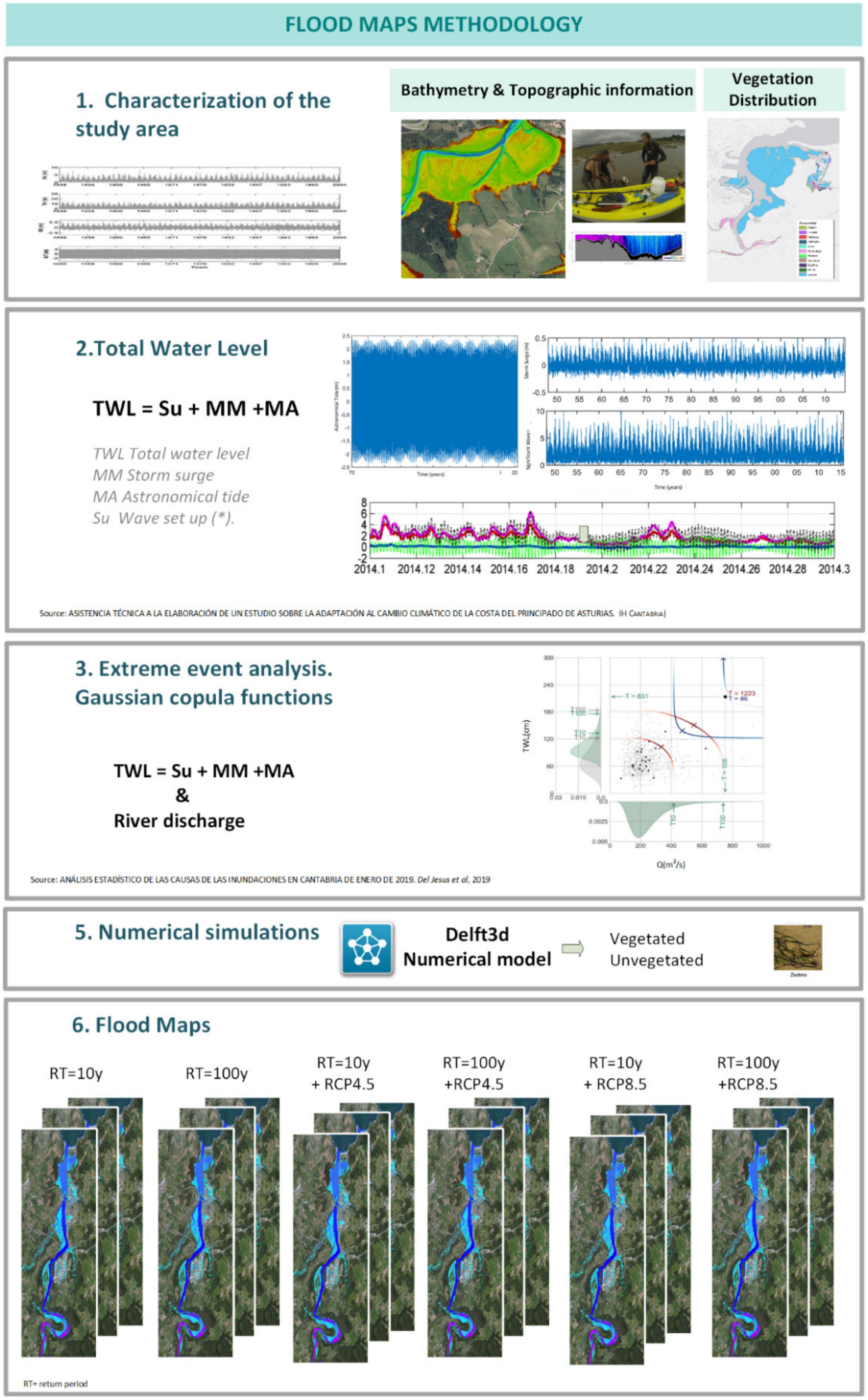

Figure 1. Methodological scheme for the calculation of flooding area.

For the analysis of flood maps (considering the role of estuarine vegetation), the following methodological steps must be carried out:

1. **Gathering of information and analysis of main dynamics.** The gathering of information is an essential step in order to obtain flood maps that provide robust and reliable information. Therefore, in order to be able to approach this type of study, at least the following information is required.

   Bathymetric information. A compilation of bathymetric information of the study area will be collected. If different bathymetric maps are available, the one with the highest spatial resolution will be used. The vertical reference levels (which are crucial to obtain robust results) at which bathymetric measurements are made must be known.
   Digital Terrain Model. A compilation of topographic information of the study area will be collected, using the information available from the source with the highest spatial resolution. When assembling the bathymetric information with the topographic information, all the information must be homogenized to the same reference level, making the necessary corrections.
   Information of Estuarine Vegetation. A proper assessment of the role played by coastal vegetation in coastal protection involves representing the behavior of the vegetation in the development of the flow. A physical description of the different plant species to be considered is necessary. This includes the spatial distribution of the different species, their physical characteristics (height and diameter) and the drag coefficients of each species typology (obtained from bibliographic information).

   Analysis of dynamics. It is necessary to identify the dynamics that cause flooding in the study areas. Once identified, a statistical analysis of each one of the dynamics must be carried out in order to know the role played by each one of them and to be able to characterize their average behavior. This analysis will dilucidated whether the most important dynamics are marine or continental.

The analysis of the dynamics will be accompanied by a study of climate change projections in order to capture the long-term behavior.

2. **Computation of the Flooding indicator: Total Water Level (TWL).** Although the total water level is not a marine dynamic *per se*, it is an indicator of coastal inundation that combines the three most important marine dynamics (astronomical tide, storm surge

and waves). Its quantification is important for the assessment of the role of coastal dynamics in the total inundation of estuarine environments.

3. **Extreme event analysis of dynamics.** As mentioned above, inundation events are linked to extreme events. For this reason, an extreme event analysis of the dynamics that produce flooding in the study area should be carried out.

   Univariate analysis. If the flood events have only a coastal origin (aggregated in the TWL), it will be considered a univariate flood. Those events are induced mainly by one mechanism that can be easily analyzed by means of an extreme value analysis using the Generalized Extreme Value (GEV) distribution.

   Multivariate analysis. If the flood events are the result of the combination of coastal (TWL) and continental dynamics (river discharge), a multivariate analysis using Gaussian copulas should be performed.

4. From this analysis the different extreme scenarios to be simulated with the numerical model are obtained.**Numerical model.** Process-based models for flooding analysis rely on the description of the underlying physical processes that derive from the dynamics of the estuaries. At the estuarine scale, finite differences, grid-based models such as Delft3D is applied,. These models are based on considerable simplifications that allow for fast computations but limit the range of problems they can solve. Generally, hydromorphodynamic models involve a combination of different interconnected models that are called from a control module. This control module successively calls hydrodynamic, sediment transport and bed level update modules, linked through a feedback loop (Lesser et al., 2004). The hydrodynamics are solved using the unsteady shallow water equations for currents and the spectral wave action balance equation for waves (Booij et al., 1999). Biogeomorphic models add a fourth -biology-module to this scheme. Various types of biology modules exist: rule-based cellular automata, physics-based habitat models and individuals-based models (Hidralab+, 2016). In this study, the Delft3D model will be used to combine the behavior of the hydrodynamic and the wave module, incorporating the spatial interaction of vegetation species.

5. **Flood maps.** The results obtained from the numerical model will serve to perform the analysis of flood maps considering different climatic scenarios. The comparison of the maps considering a vegetated or unvegetated estuary will allows to quantify the protective role provided by these vegetated ecosystems.

It should be remarked that the analysis of flood in the Western Scheldt should not be evaluated with this kind of protocol, since the coastal protection context is framed within another typology. Around the Western Scheldt estuary, and throughout the Netherlands, a large proportion of the territory are below sea level or the high-water levels of rivers and lakes. Due to this situation, without the protection of dikes, dunes and hydraulic structures, about the 60% of the country is prone to regular flooding at present.

Therefore, it is also highly susceptible to both sea level rise and river flooding. Flooding of protected areas around the Western Scheldt estuary may occur as a result of the failure or overtopping of dikes. The study of the damage probabilities of this type of structures is out of scope of this study, however, the role of plant communities on the structures will be analyzed from a bibliographic point of view. An analysis of damage probabilities of all these kinds of infrastructures is out of the scope of this work, however, the role of vegetation communities in the foreshore of the dikes will be analyzed studying the results found in scientific literature.

2.2.4 Morphological evolution assessment protocol.

The morphology of an estuary is the result of the non-linear interactions among hydrodynamics, sediment transport, seabed configuration and biological processes occurring in these water bodies (Figure 2). In recent years, several scientific research works have been carried out to predict the long-term morphological evolution (scale of years - decades) of coastal zones and estuaries. However, the difficulty in simulating non-linear processes and the intervention of a wide variety of spatio-temporal scales means that this predictive capacity is still limited. Several approaches have been used in order to be able to predict the behavior of the estuaries to be analyzed.

Figure 3 shows a schematic representation of the methodology used to carry out the analysis of the morphodynamic evolution in the analyzed estuaries.

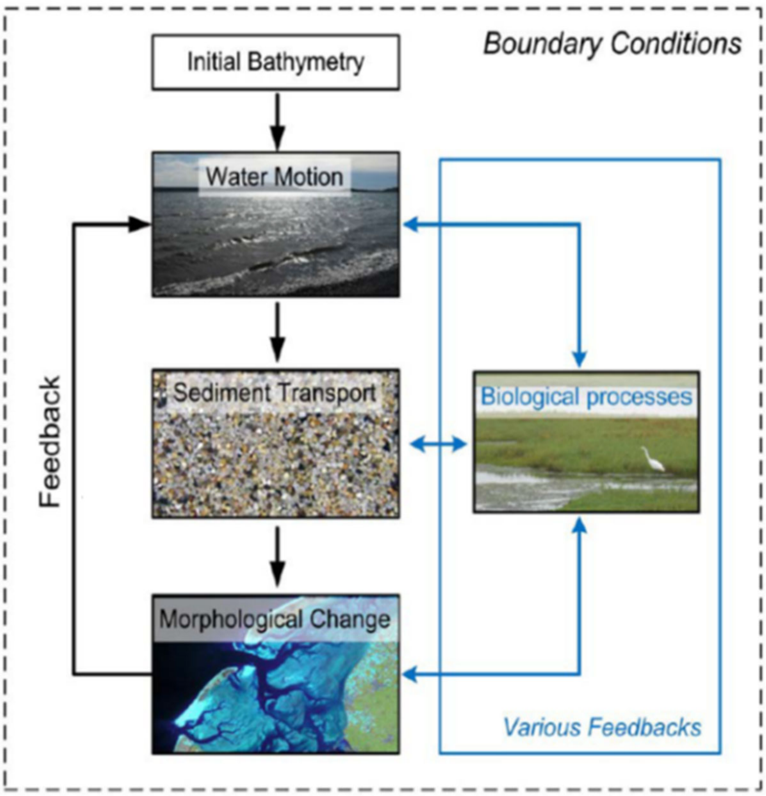

Figure 2. Working structure of a typical morphodynamic model where connections between different components give rise to the "morphodynamic loop". Adapted from Coco et al. 2013.

For the analysis of morphodynamic evolution (considering the role of estuarine vegetation), the following methodological steps must be carried out:

1. **Gathering of information and analysis of main dynamics.** The gathering of information is an essential step in order to obtain flood maps that provide robust and reliable information. Therefore, in order to be able to approach this type of study, at least the following information is required.

   Bathymetric information. A compilation of bathymetric information of the study area will be collected. If different bathymetric maps are available, the one with the highest spatial resolution will be used. The vertical reference levels (which are crucial to obtain robust results) at which bathymetric measurements are made must be known.

   Digital Terrain Model. A compilation of topographic information of the study area will be collected, using the information available from the source with the highest spatial resolution. When assembling the bathymetric information with the topographic information, all the information must be homogenized to the same reference level, making the necessary corrections.

Information of Sediment distribution. A compilation of the sedimentological information of the study area will be carried out. This information should consist of grain size classification and its spatial distribution in the study area. This information can be complemented with stratigraphic information, providing the thickness of sediment available on the seabed.

Information of Estuarine Vegetation. A proper assessment of the role played by coastal vegetation in coastal protection involves representing the behavior of the vegetation in the development of the flow. A physical description of the different plant species to be considered is necessary. This includes the spatial distribution of the different species, their physical characteristics (height and diameter) and the drag coefficients of each species typology (obtained from bibliographic information).

2. **Statistical analysis of marine and continental dynamics.** An analysis of the average and extreme regimes of the coastal and continental dynamics should performed. The statistical analysis of the dynamics will be complemented by a study of climate change projections in order to analyze different climate change scenarios.

3. **Model and Input reduction techniques.** To analyze the long-term morphological evolution of an estuary using process-based models, it is necessary to perform continuous simulations over a long period of time (years-decades). However, in the first place, these models use the hydrodynamic and sediment transport governing equations, and thus, the results obtained from multi-year simulations are highly uncertain. Secondly, these simulations are computationally expensive; often unaffordable to obtain the results. To solve this problem, Vriend et al. (1993) described two different techniques:

   Model reduction techniques. They are based on using the different time scales in which hydrodynamic (much faster) and morphological processes occur to accelerate numerical simulations by means of a factor, such as the so-called MorFac.

   Input reduction techniques. They are based on methods that allow to reduce the length of the dynamics time series that enter the model as inputs and at the same time to obtain, with these reduced series, the same results. Techniques such as morphological tide and input clustering can been considered.

The decision to apply one approach or the other will depend on the computational cost and the experience of the technicians. The model reduction techniques require less technical experience during its application.

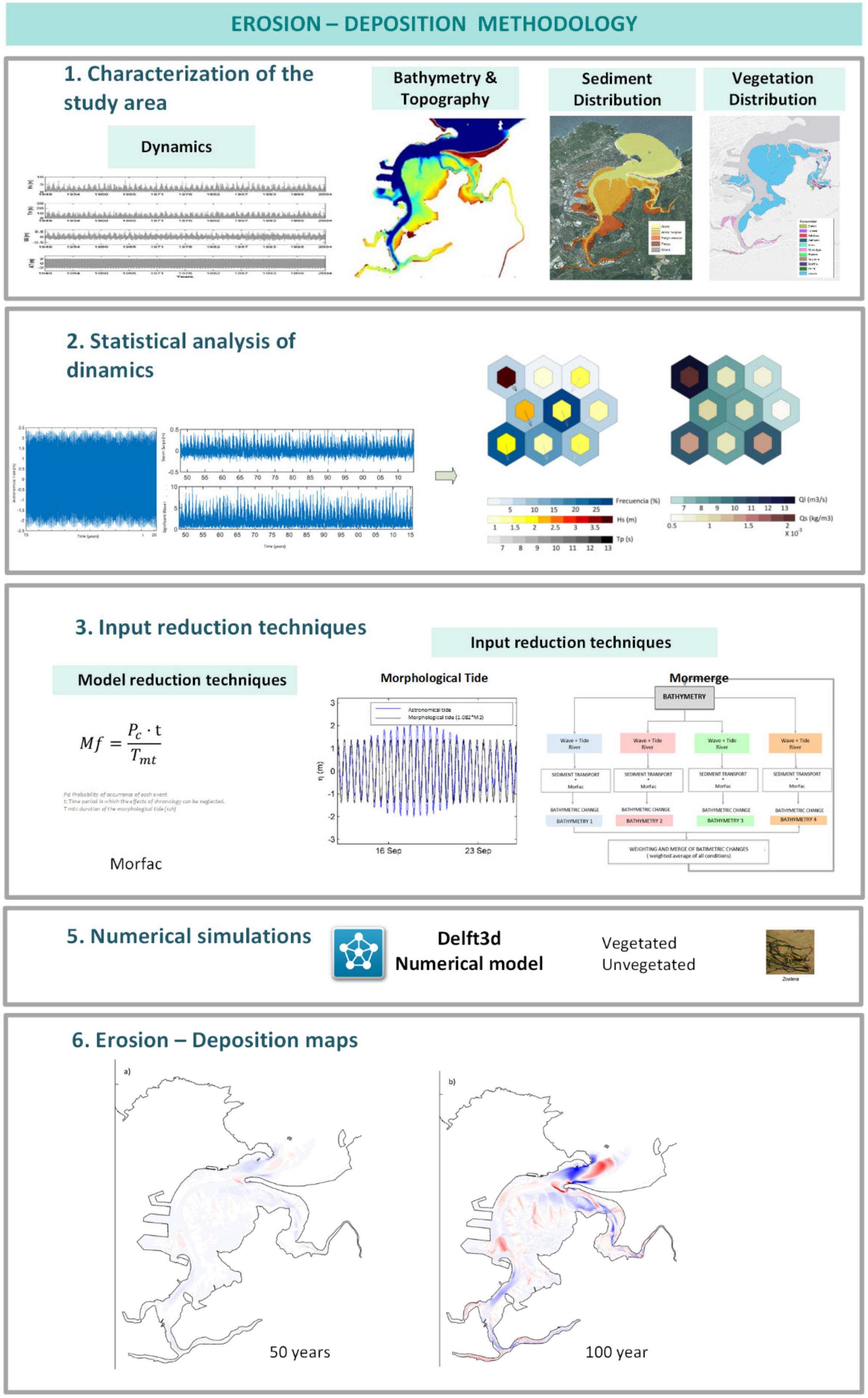

Figure 3. Methodological scheme for the morphodynamic evolution assessment.

4. **Numerical model.** Process-based models for flooding analysis rely on the description of the underlying physical processes that derive from the dynamics of the estuaries. At the estuarine scale, finite differences, grid-based models such as Delft3D is applied. These models are based on considerable simplifications that allow for fast computations but limit the range of problems they can solve Generally, hydromorphodynamic models involve a computational control shell that successively calls hydrodynamic, sediment transport and bed level update modules, linked through a feedback loop (Lesser et al., 2004).

   The hydrodynamics are solved using the unsteady shallow water equations for currents and the spectral wave action balance equations for waves (Booij et al., 1999). Sediment transport rates are calculated using one of the many available sediments transport equations Engelund and Hansen, 1967 or Van Rijn, 2007a, b. Biogeomorphic models add a fourth – biology-module to this scheme.

   Various types of biology modules exist: rule-based cellular automata, physics-based habitat models and individuals-based model. In this study, the Delft3D model will be used to combine the behavior of the hydrodynamic, sediment transport and the wave module, incorporating the spatial interaction of vegetation species. A physical description of the different plant species to be considered is necessary. This includes the spatial distribution of the different species and their physical characteristics (height and diameter). These morphological characteristics have been obtained during the field campaigns done by FIHAC in the framework of other projects and during the habitats' cartography (all this information has been completed from several identification guides and bibliographic information) and the drag coefficients of each species typology (obtained from bibliographic information)

5. **Erosion - sedimentation maps.** The results obtained from the numerical model will allow the analysis of erosion-sedimentation patterns considering different climatic scenarios and considering a vegetated and an unvegetated estuary. These results will allow establishing the basis for the quantification of the protective role provided by these ecosystems.

Additionally, the protocols developed in this action will be applied in 3 new study sites in the action C.4 ("C.4.To explore jointly with the insurance sector the feasibility of development of an innovative coastal flood insurance based on the capacity of estuarine ecosystems to reduce total cost of flood risk"). The results obtained from the application of the protocol at these new study sites will increase the information on estuaries to establish the feasibility of flood resilience insurance mechanisms for European estuarine ecosystem-based restoration projects in collaboration with the insurance industry.

2.2.5 Quantification of the coastal protection protocol.

The proposed risk analysis is framed within a more general risk methodology adopted by the IPCC (IPCC, 2014). In this more general framework, risk (R) has been defined as a combination of the probability of an event and its negative consequences, which in turn is a result of the combination of hazard (P), defined through coastal and continental dynamics, exposure (E), associated with the physical environment, and vulnerability (V), linked to the socioeconomic characteristics of the area, and is expressed through the following equation:

$$Risk = \text{Hazard} * \text{Exposure} * \text{Vulnerability}$$

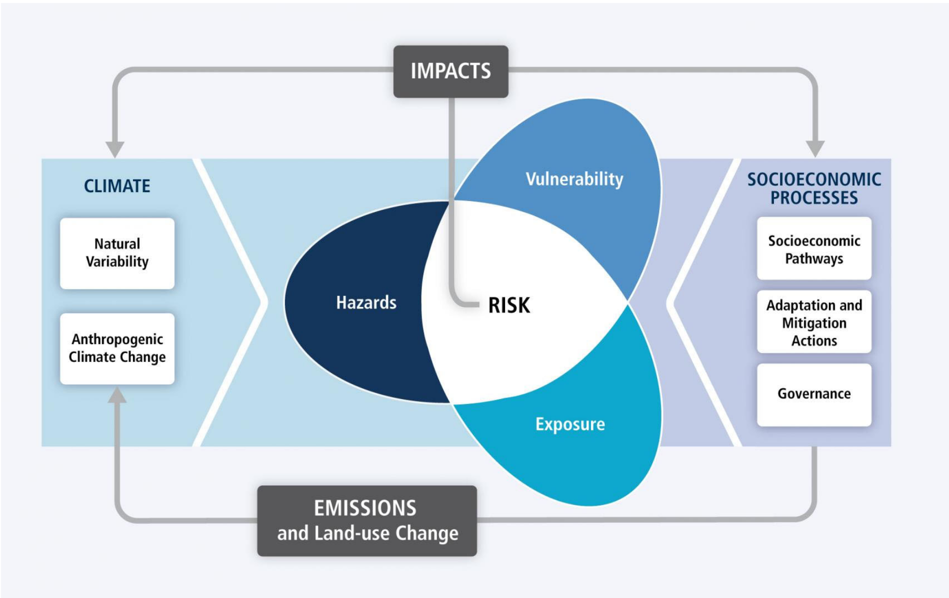

Figure 4. General framework of risk assessment defined by the IPCC (IPCC, 2014)

In this analysis, the general IPCC framework has been applied to the assessment of climate change risks on the estuaries of Mondego (Portugal), Oyambre (Spain), the Bay of Santander (Spain) and the Santoña Marhes (Spain), considering the impacts of coastal flooding on the socio-economic system.

The result of the Hazard analysis has been combined with exposure data and vulnerability functions. Exposure has been characterised through geospatial databases of present population and buildings. Regarding the characterisation of vulnerability, damage functions have been defined for different sectors of the socio-economic system.

The consequences integrate the previous components of risk, and have been expressed with various indicators to obtain the level of risk in terms of:

- Affected population
- Affected buildings

The quantification of coastal protection provided by vegetation shall be measured in terms of consequences in the population and in the built capital (physical assets) on the margins of the estuaries.

To characterize the exposure:

1. **Definition of the analysis unit.** The evaluation of the consequences will be carried out at a defined spatial scale. In this project, a hexagonal grid with polygons of about 15,000 m^2 was created in each estuary.
2. **Gathering exposure information.** A critical point in exposure characterization processes is to find and gather all available information. We recommend to use the best, most updated and more detailed information available.
   - For population, this normally includes working with census, usually at city or district level.
   - For other assets, (built capital, economic activity) it is rare to have the information at the same level, so regional disaggregation can be used.
3. **Homogenisation and downscaling.** When analysing different hotspots, it is usual to have different sources of data, with different variables and spatial resolution. It is therefore necessary to carry out a process of homogenisation of variables and scale adjustments so that similar information is available at all study points to enable the results obtained to be compared. This work will be carried out at this stage, using the polygons developed in step 1 as spatial aggregation elements.

To characterize the vulnerability:

Vulnerability is characterized by introducing individual functions that act as attributes of the exposed elements. These functions, called vulnerability curves or damage curves, quantify the level of damage suffered by the exposed asset for a given level of hazard, and are also capable of assessing the losses caused by the disruption of economic flow.

2.2.6 Databases and information.

This section will show the information and databases used to implement the protocols shown in Figure 1 and Figure 3.

DEM and bathymetric information

Digital Terrain Model (DTM) information. In this study a digital terrain model with a grid resolution of 5m have been used in Oyambre, Santoña and Santander estuaries. - DTM05 (1st cover, year 208-2015). This information can be requested through the download center. https://centrodedescargas.cnig.es/CentroDescargas/index.jsp. In Mondego estuary a digital terrain model with a grid resolution of 20m -MDT20 has been used. This information can be requested through the download center. https://sniamb.apambiente.pt/content/geo-visualizador?language=pt-pt. In the Mondego estuary the topographic information where the traditional marshes are located has a low resolution and it should be noted that in these areas the water level is anthropogenically regulated.

Bathymetric information. Bathymetric data has been gathered. Data from several nautical charts and field campaigns have been used to obtain the bathymetry with the highest spatial resolution. In order to homogenize and unify all the information, coordinates systems and the vertical reference level of bathymetric measurements must be known. In those areas where bathymetric information was not available, this information was supplemented by bathymetry provided by European Marine Observation and Data Network (EMODnet) https://emodnet.ec.europa.eu/geoviewer/. This information presents a grid resolution of 1/16 * 1/16 arc minutes (115 * 115 meters) covering all European seas from the Mediterranean Sea, the Black Sea, the North-East Atlantic Ocean, up to the Arctic Ocean and Barents Sea.

Figure 5 shows the bathymetric and topographic information used in the study sites.

Sediment information

The analysis of sediment transport and the morphological evolution of estuaries requires granulometric information from field campaigns or, alternatively, a mapping of the granulometric characteristics of the study area must be available. Generally, this information is expressed in Attemberg scale: cohesive sediment (clays) and non-cohesive sediment (silt, fine sand, medium sand, coarse sand, fine gravel and coarse gravel).

In this study, for the estuaries of Oyambre, Santander Bay and Santoña Marshes, granulometric information is available from several field campaigns carried out by IHCantabria between 2005 and 2018 in the framework of the project “Red de Calidad del Litoral de Cantabria”. In the Mondego estuary, a detailed sedimentological mapping was available (Figure 6).

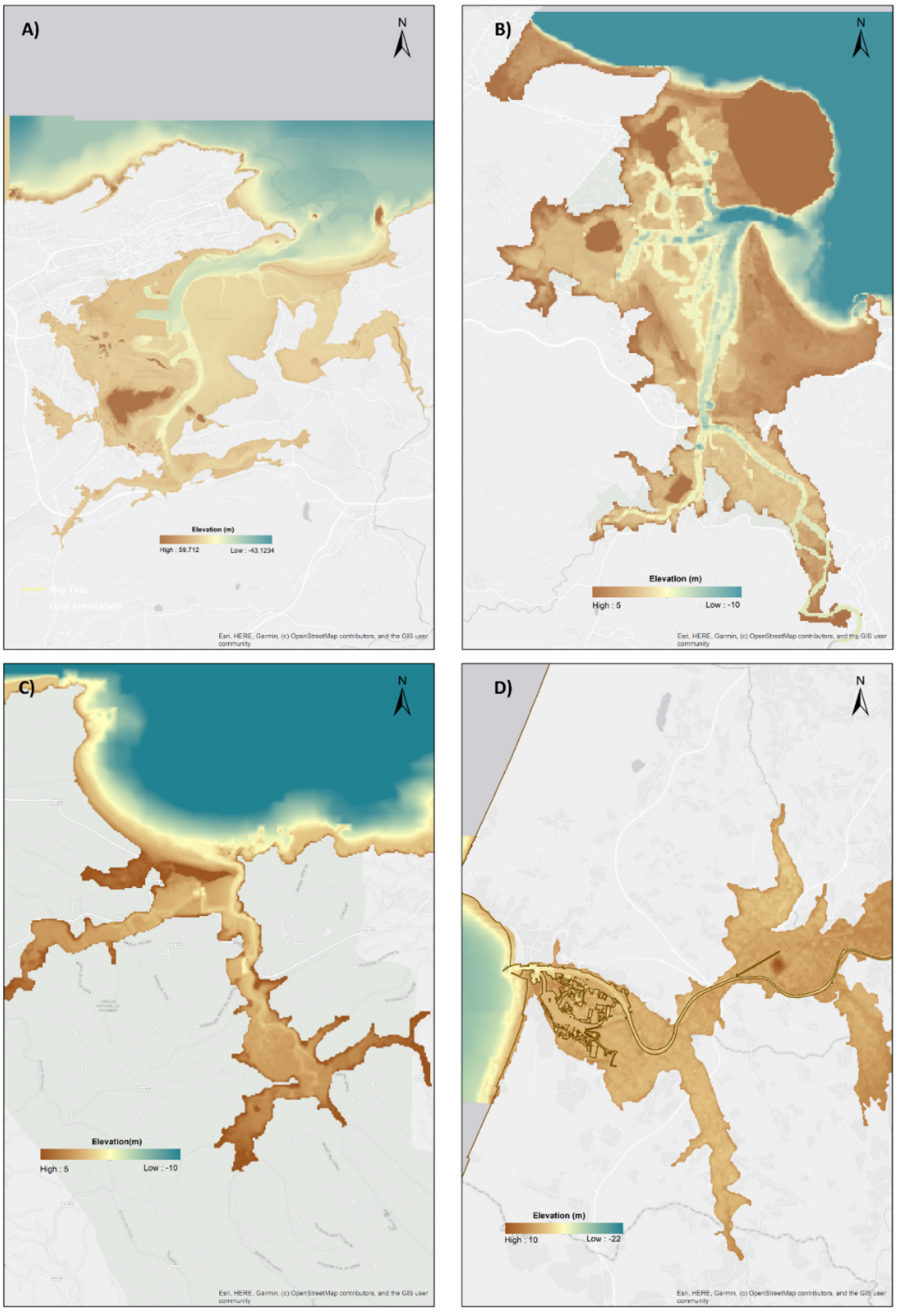

Figure 5. Bathymetric and topographic information used in the study areas: A) Santander Bay B) Santoña Marshes C) Oyambre estuary and D) Mondego estuary.

Figure 6. Location of sediment sampling: A) Santander Bay B) Santoña Marshes C) Oyambre estuary and D) Mondego estuary.

Vegetation information

The spatial distribution of vegetation communities is obtained from results of section 2.1. This information is key to the quantification of the protective role offered by vegetation communities.

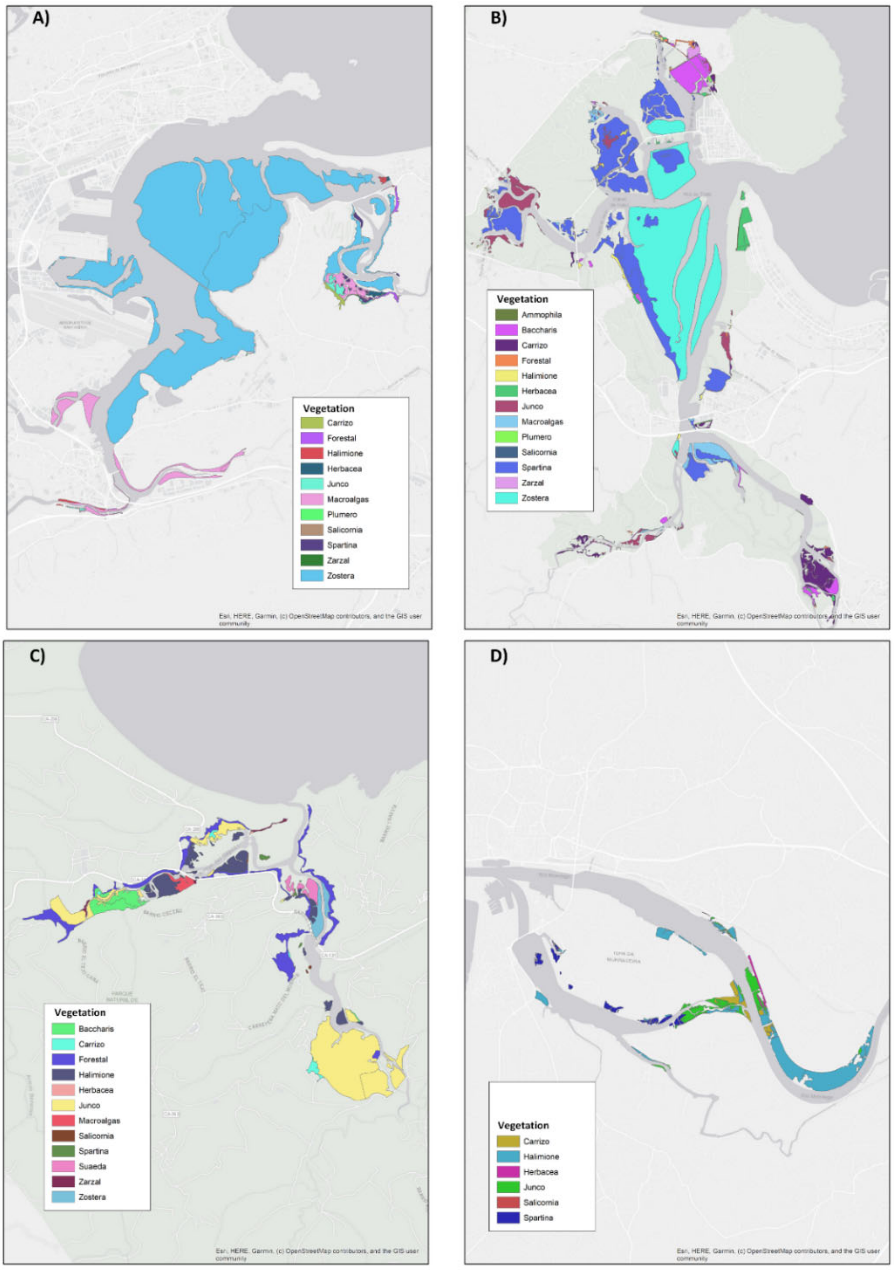

Figure 7. Spatial distribution of vegetation communities A) Santander Bay, B) Santoña Marshes, C) Oyambre estuary and D) Mondego estuary.

This includes the spatial distribution of the different species and their physical characteristics (height and diameter). These morphological characteristics have been obtained during the field campaigns done by FIHAC in the framework of other projects and during the habitats' cartography (all this information has been completed from several identification guides and bibliographic information) and the drag coefficients of each species typology (obtained from scientific literature)

Each estuary presents a variety of species. Figure 7 shows the classification by communities. As shown in Figure 8, the vegetation morphology is varied and it must be considered in order to model their behavior (see Section 2.2.6.4).

Figure 8. Photographs of different plant species found in the estuaries to be analyzed.

Coastal and continental dynamics dataset.

The information used to analyse the marine and continental dynamics should be long time series, which allow a correct statistical characterization of the average and extreme regimes. The length of the time series data should cover a period of 20 - 30 years. In this study, different databases have been used to perform a robust analysis of all the variables.

Waves. The wave information is provided by two databases: Global Ocean Wave (GOW) database for the Mondego estuary and the DOW (Downscaling Ocean Waves) database for Oyambre, Santander and Santoña estuaries.

GOW is a historical reconstruction of ocean waves, developed by IHCantabria. GOW has been generated from the spectral model WaveWatch III (WWIII, Tolman, 2014) to obtain homogeneous, continuous and long records of wave climate. Wavewatch III is a third-generation wave model developed at NOAA-NCEP. It solves the spectral action density balance equation for wave number direction spectra. The model can generally be applied to large spatial scales and outside the surf zone. Parameterizations of physical processes include wave growth and decay due to the actions of wind, nonlinear resonant interactions, dissipation (whitecapping) and bottom friction. Apart from the setup of the model, bathymetry, ice cover and wind forcings, databases are crucial for a good historical hindcast of ocean waves.

DOW is a historical reconstruction of coastal waves. In order to obtain wave data in shallow waters and due to the scarcity of coastal observation measurements, ocean wave reanalysis databases ought to be downscaled to increase the spatial resolution and simulate the wave transformation process. Due to the computational cost of hindcasting 60 years of hourly coastal waves, DOW is a hybrid downscaling combining a numerical wave model (dynamical downscaling) with mathematical tools (statistical downscaling).

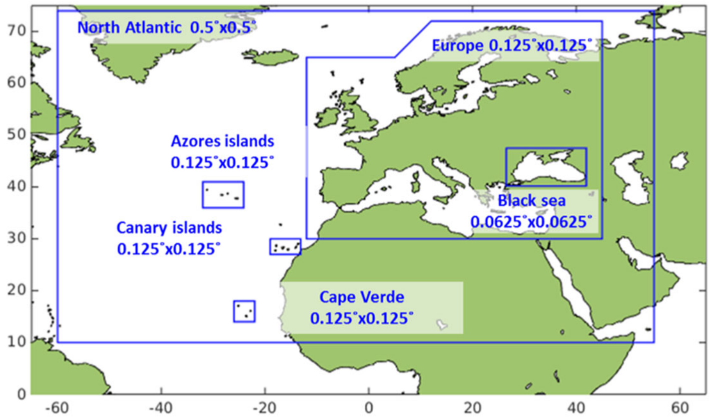

Figure 9. Spatial domains of regional GOW dataset.

Astronomical tide. The database Global Ocean Tidel (GOT) has been used to obtain timeseries of storm surge in all estuaries analyzed. This database is generated using the harmonic constants derived from the TPXO global tides model, developed by Oregon State University. TPXO is a series of fully-global models of ocean tides, which best-fits, in a least-squares sense. The database includes eight primary (M2, S2, N2, K2, K1, O1, P1, Q1), two long period (Mf,Mm), and 3 non-linear (M4, MS4, MN4) harmonic constituents (plus 2N2 and S1 for TPXO9). The database provides the harmonic constituents data over a global grid, the spatial resolution depends of the database version, the TPXO8-atlas provide the data at 1/30-degree resolution in zones near to the coast and 1/6-degree resolution for the rest of the Ocean. This information is used to reconstruct hourly time series of tide in any location worlwide using OSU Tidal Prediction Software.

Storm Surge. The database Global Ocean Surges (GOS) has been used to obtain timeseries of storm surge in all estuaries analyzed. The storm surge is the sea level variations generated by the wind speed and low air pressures. GOS encompasses 3 regions: Europe, Arabian Sea and Latin-America (including Caribbean, Atlantic and Pacific areas). The historical reconstruction of storm surge in the south European region (Cid et al. 2014) has a spatial resolution of 1/8º (~30km), while the American region has 1/4º.

The databases used are managed by the IHCantabria through https://ihdataprot-a.ihcantabria.com/.

Table 2 shows a summary of the characteristics of the different databases used in this study.

Estuary	Variable (*)	Database Name (**)	Mesh Name	Long (decimal degrees)	Lat (decimal degrees)	Time
Santander	AT	GOT	-	-3.75	43.5	01/01/1970 - 01/12/2020
	SS	GOS	South Europe / SW NCEP	-3.75	43.503	01/01/1984 - 30/06/2014
	Waves	DOW	G01	3.73	43.504	01/02/1984 -31/08/2015
Santoña	AT	GOT	-	-3.25	43.5	01/01/1970 - 01/12/2020
	SS	GOS	South Europe / SW NCEP	-3.39	43.452	01/01/1984 -30/06/2104
	Waves	DOW	G01	-3.375	43.458	01/02/1984 - 31/08/2015
Oyambre	AT	GOT	-	-4.25	43.5	01/01/1970 - 01/12/2020
	SS	GOS	South Europe / SW NCEP	-4.3125	43.4582	01/01/1984 - 30/06/2014
	Waves	DOW	G02	-4.32	43.416	01/02/1984 -31/08/2015
Mondego	AT	GOT	-	-8.75	41	01/01/1970 - 01/12/2020
	SS	GOS	South Europe / SW NCEP	-9	40.101	01/01/1984 - 30/ 06/ 2014
	Waves	GOW	Europe	-8.75	41.125	01/02/1984 - 31/08/2015

(*) AT = Astronomical Tide
SS = Storm Surge

(**) GOT= Hourly time series of astronomical tide.
GOS = Coastal meteo-induced sea level (storm surges).
GOW: Oceanic Waves at global/regional scale.
DOW: Coastal Waves at high spatial resolution.

Table 2. Location and characteristics of points analyzed from the databases.

River discharge. The riverine sources should be considered in the assessment of flooding events in estuarine environments. For this reason, it is necessary to collect information from the gauging stations of the hydrological network (Table 3). In this study, in 3 of the estuaries analyzed, river dynamics will be taken into account.

Estuary	River	Name Station	CoordX	CoordY	Period
Santander	Cubas River	La Cavada	464639	4797560	01/01/1970 - 31/12/2018
Santoña	Asón River	Coterillo	441915	4806326	01/01/1970 - 31/12/2018
Mondego	Mondego River	Ponte Coimbra	173868	360830	01/11/2005 - 31/12/2021

Table 3. Location and characteristics of gauging stations used in this study.

Climate change scenarios

Sea Level Rise

The assessment of flooding and erosion in future scenarios requires considering the role of climate change in sea level changes. The report of Working Group II of the Intergovernmental Panel on Climate Change (IPCC, 2014) provides a mean value and confidence bands of sea level rise over the 21st century for each of the greenhouse gas concentration scenarios. These scenarios consider the spatial variability of sea level rise and take into account mainly: the contribution of ocean thermal expansion, the movement of water within the oceans in response to coupled ocean-atmosphere variability patterns, including ENSO and the NAO, variations in the mass of the Greenland and Antarctic ice sheets as well as glaciers and ice caps (GIA), and the depletion of groundwater resources. Table 4 shows projections of global sea level rise for the periods 2046-2065 and 2081-2100 based on the 20-year period 1986-2005.

RCP scenarios	Sea level rise, $\Delta\eta$	
	2046-2065	**2081-2100**
RCP 4.5	0.26 [0.19 – 0.33]	0.47 [0.32 – 0.63]
RCP 8.5	0.30 [0.22 – 0.38]	0.63 [0.45 – 0.82]

Table 4. Projected changes in global mean sea level rise for the mid- to late 21st century, relative to the 1986-2005 baseline period, for each RCP scenario (IPCC, 2014).

River discharge

Projections of climate change in the fluvial environment must also be considered. However, this type of projections is usually inferred from changes in the hydrometeorological variables: precipitation and temperature. Thus, a detailed quantification of river discharge changes requires the use of a hydrological and a hydraulic model, to analyse basins. This analysis is out of the scope of the present work and, therefore, we have assumed the hypothesis that the change in precipitation directly transfers to river discharge, that is, that if rainfall suffers a reduction of 30%, river discharge will suffer the same reduction. In this study, these projections have been obtained from 2 different sources:

- Web platform "Adaptación al Cambio climático en España" (AdapteCCa) (https://www.adaptecca.es). AdapteCCa is a joint initiative of the Spanish Climate

Change Office and the Biodiversity Foundation, which allows us to obtain regionalized projections of climate change for Spain (Figure 10), based on the global projections of the Fifth Assessment Report (AR5) of the IPCC. These projections have been transferred to the fluvial discharge of the Miera River and the Asón River.

- Web platform "Portal do Clima" (http://portaldoclima.pt/en/). Portal do Clima has been developed in the framework of the Instituto Português do Mar e da Atmosfera within the ADAPT Program Alteracões Climáticas in Portugal, which allows obtaining regionalized projections of climate change for Portugal, based on the global projections of the Fifth Assessment Report (AR5) of the IPCC Spain (Figure 10). These projections have been transferred to the fluvial discharge of the Mondego River.

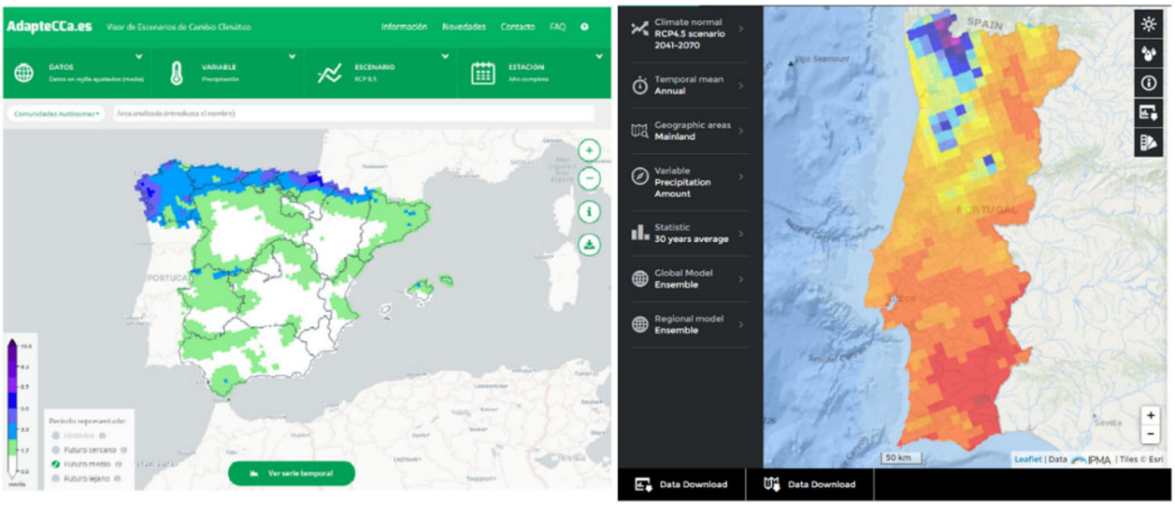

Figure 10. Spatial domain covered by the projections of AdapteCCa (España) and Portal do Clima (Portugal).

River Basin	Climate Change Projections. Precipitation changes (%)	
	RCP 4.5	RCP 8.5
Miera River	-7.45	-12.55
Asón River	-4.14	-12.68
Mondego River	35.1	22.54

Table 5. Projections of climate change in precipitation by the end of the 21st century, relative to the 1971-2000 reference period, for each RCP scenario (IPCC, 2014).

2.2.7 Statistical analysis of variables for the assessment of flooding and morphodynamic evolution

Coastal flooding depends mainly on waves, astronomical tide (AT), storm surge (SS) and mean sea level rise (Figure 11). These variables can be combined in different ways depending on the main climatic dynamics in the study area. They used to be combined into different indices. These indices can be defined as the lineal sum of the SS, AT and the sea level rise due to the transfer of momentum flux from the wave to the water column when waves are breaking (Su). This latter term is calculated using the formulation of Stockdon et al. (2006). Additionally, if sea level rise is to be considered, the TWL would require the incorporation of the SLR term

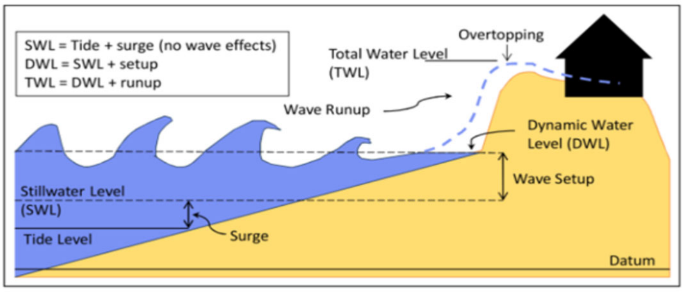

Figure 11. Definition of SWL= Still Water Level, DWL =Dynamic Water Level and TWL = Total Water Level

$$TWL = SS + \mathrm{AT} + \mathrm{Su} + \mathrm{SLR}$$

$$Su = \alpha\sqrt{H_s L_0}$$

where α = 0.04 if it is a seafront or a beach and α = 0.08 if it is a rocky seafront or cliffs. H_s is the significant wave height and L_0 is the deep-water wavelength.

It should be noted that estuaries are generally protected from wave action. The mouth and adjacent areas can be affected by wave set-up in flooding events and by the sediment transport capacity of these coastal dynamics. For this reason, a prior analysis of the need to include this variable in the TWL analysis should be carried out according to the area to be analyzed.

To perform a TWL analysis, time series of astronomical tide, meteorological tide, swell and river discharge in the different estuaries must be analyzed. Figure 12, Figure 13, Figure 14, Figure 15 show the information used.

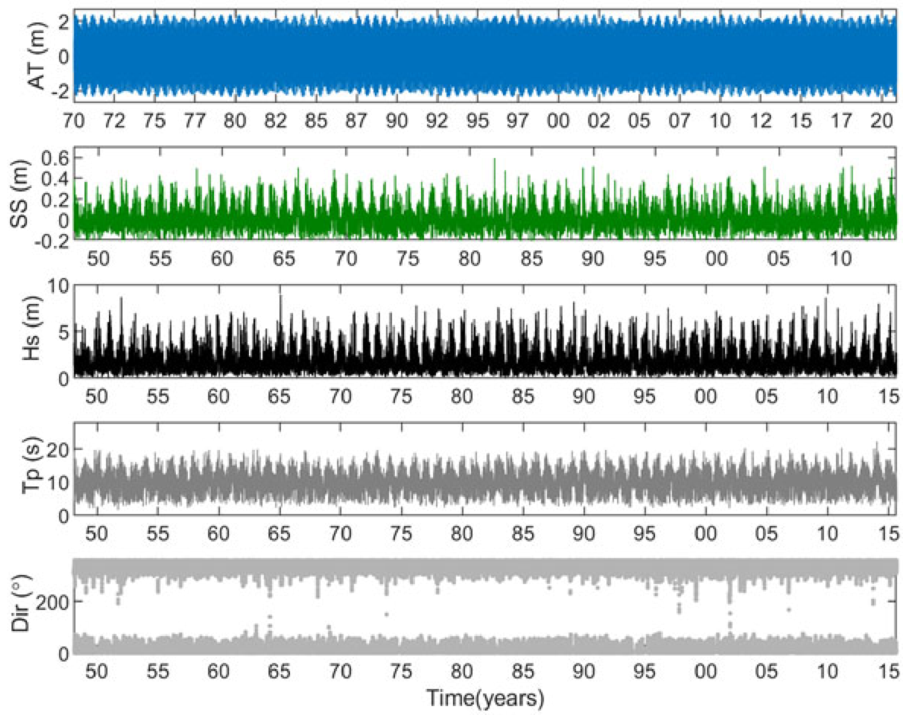

Figure 12. Time series data of dynamics in Oyambre estuary: AT= astronomical Tide, SS= Storm surge, Hs= significant wave height, Tp= Peak wave Period and Dir= mean wave direction

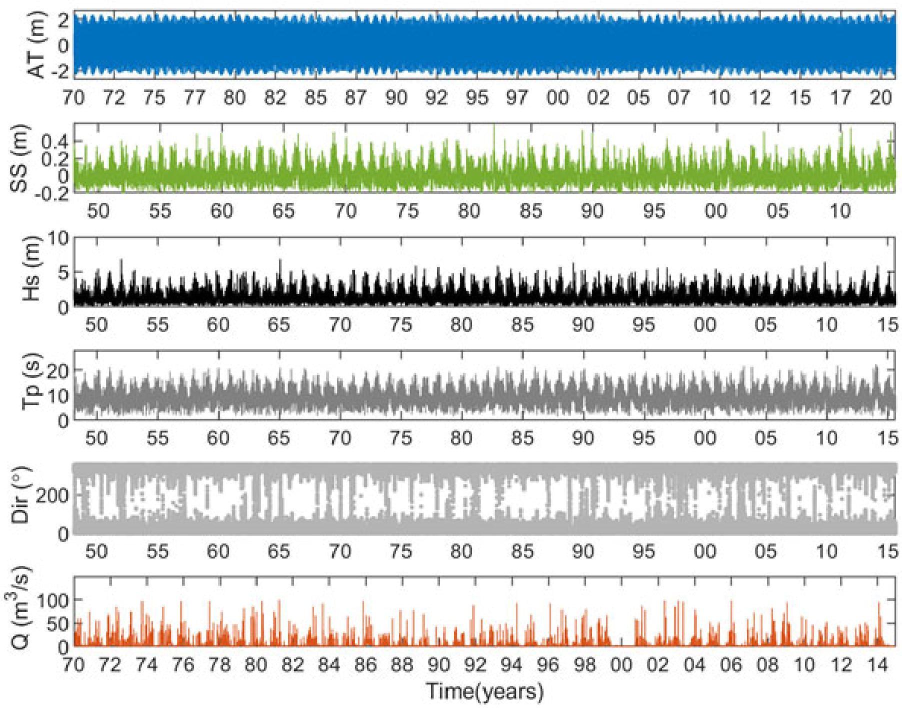

Figure 13. Time series data of dynamics in Santander Bay: AT= astronomical Tide, SS= Storm surge, Hs= significant wave height, Tp= Peak wave Period and Dir= mean wave direction

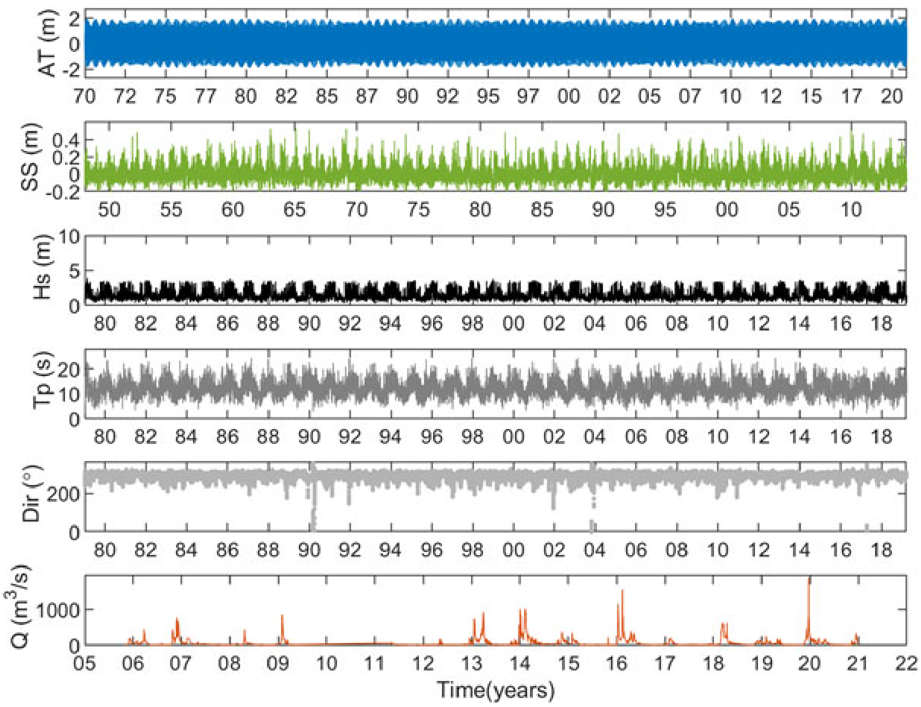

Figure 14. Time series data of dynamics in Mondego estuary: AT= astronomical Tide, SS= Storm surge, Hs= significant wave height, Tp= Peak wave Period and Dir=mean wave direction

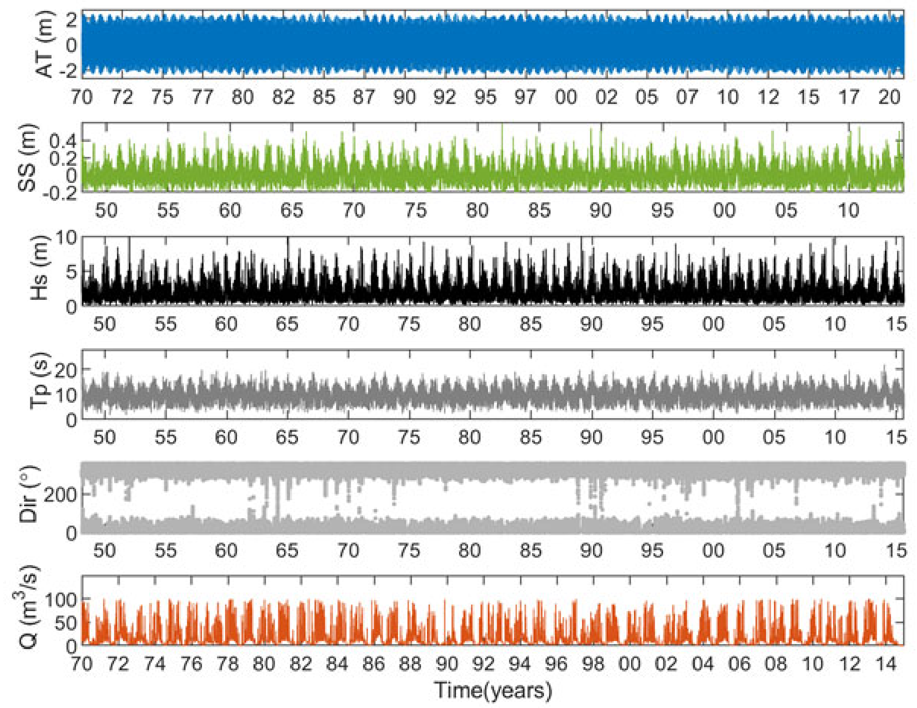

Figure 15. Time series data of dynamics in Santoña marshes: AT= astronomical Tide, SS= Storm surge, Hs= significant wave height, Tp= Peak wave Period and Dir= mean wave direction

Time series of coastal and continental dynamics have been analyzed using several statistics techniques depending on whether coastal flooding or morphodynamics evolution is analyzed.

Flood assessment

Extreme event analysis is required to assess the flood hazard. It will be performed using two different approaches depending on whether the fluvial dynamics is included as a key dynamic in flood events.

- If the flood analysis has a univariate component (only coastal dynamics are considered) an extreme analysis will be performed in the TWL variable.
- If the flood analysis has a multivariate component (coastal and river dynamics are considered), an extreme analysis using Gaussian copulas will be performed.

Univariate analysis

TWL has been fitted by a GEV (Generalized Extreme Value) and it has been represented on Gumbel probability paper. This distribution function combines the three distributions for fitting extreme values (Gumbel, Fréchet and Weibull) according to the three-tailed theorem (Fisher and Tippett, 1928) and is usually expressed as:

$$F(x;\mu,\psi,\xi) = exp\left(-\left(1+\xi\left(\frac{x-\mu}{\psi}\right)\right)^{-\frac{1}{\xi}}\right)$$

Where: μ: location parameter, ψ: scale parameter, ξ: shape parameter.

When:

ξ=0 Gumbel distribution.

ξ>0 Fréchet distribution.

ξ<0 Weibull distribution.

Multivariate analysis

The multivariate analysis is carried out using Gaussian copulas. Different inducing variables are tested to determine the return period of the events from the return period of the combination of those variables. Gaussian copulas provide a robust tool to characterize return periods. These kinds of analysis have been widely used evaluating river flooding scenarios (del Jesus et al., 2020)

As we are interested in the analysis of return periods, the marginal distributions of the variables are taken to be Generalized Extreme Value (GEV) distributions. All fits are done in Gaussian space and then transformed back to GEV space. The scenarios to be propagated with the numeric model will be the combination of both variables (Figure 16).

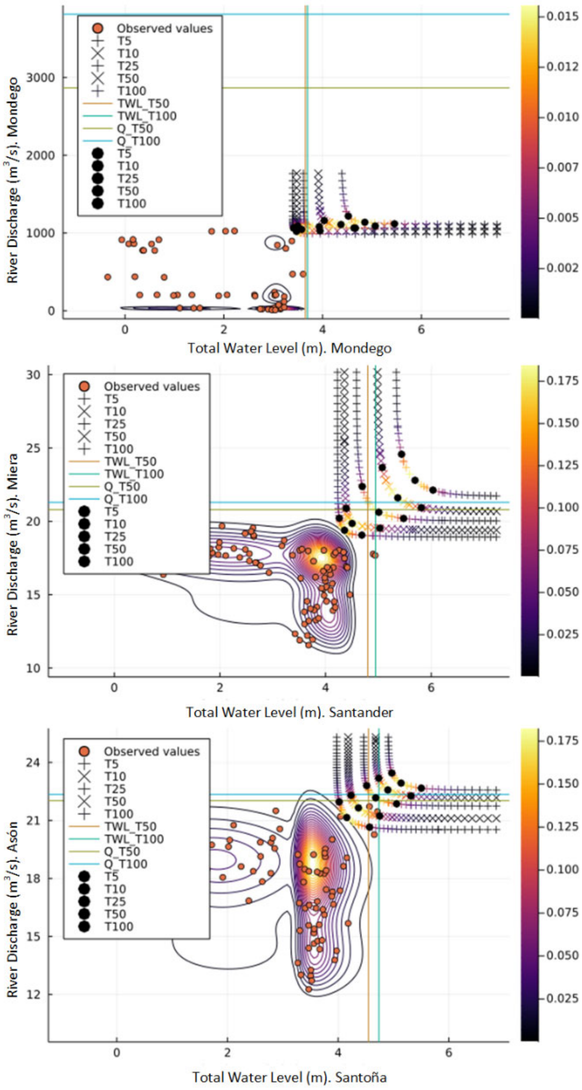

Figure 16. Primary return periods of TWL and River discharge in Mondego, Santander Bay and Santoña marshes.

Morphodynamic evolution

In the analysis of long-term evolution, process-based modeling has been used. As we have mentioned previously, this type of modeling requires a high computational effort to analyze all the scales proposed in this study. For this reason, input reduction approaches must be applied to simplify the boundary conditions in the model. These input reduction techniques are based on methods that allow to reduce the length of the dynamic series that enter the model and obtain a reliable solution in our study site.

Morphological Tide

According Lesser (2009), many authors have used tidal input reduction (tidal schematization) to extend their morphological models into the medium term. The concept of morphological tide seeks to reduce the natural input conditions of tides in a model. The most commonly used technique is based on Latteux (1995), that is, a morphological tide can be chosen where the pattern of sediment transport, or morphological change, over the area of interest most closely matches the pattern of transport, or morphological change over an entire neap-spring tidal cycle.

Lesser (2009) describes a standard method based on Latteaux's idea and previous studies developed by Delft Hydraulics. This method can be described as follows: first, the harmonic analysis of the water level time series is performed and the relationship between the amplitudes of the tidal components O1, K1, M2 and M4 is checked.

- If the relationship $2 \cdot O1 \cdot K1 < M2 \cdot M4$ is satisfied, it means that the nonlinear interaction between the tidal components O1, K1 and M2 is not important. In this case the morphological tide is chosen as that tide of amplitude (A_{MM}) and period (T_{MM}) defined as follows:

  $A_{MM} = f_1 \cdot M2$

  $T_{MM} = 12$ hours

  where: f_1 is an amplifying factor y M2 es la amplitud de la componente de marea M2.

- If $2 \cdot O1 \cdot K1 > M2 \cdot M4$, then the amplitude ($A_{MM}$) and period ($T_{MM}$) of the morphological tide are defined as: $A_{MM} = f2 \cdot M2 + C1$; $C1 = 2 \cdot O1 \cdot K1$

  $T_{MM} = 24$ hours

  where: f2 is a calibration factor for residual sediment transport due to non-tidal effects, C1 is the amplitude of an artificial tidal component, and M2 residual sediment transport due to non-tidal effects, C1 is the amplitude of an artificial tidal component and M2, O1 and K1 are the amplitudes of the M2, O1 and K1 tidal components, respectively. In this study, the first approach described above will be used since the linear interaction of the O1, K1 and M2 components is not relevant in the study areas.

This means that in the study area the diurnal components O1 and K1 are not significant. Consequently, according to the described methodology a morphological tide of amplitude equal to f1-M2 has been chosen, where f1 is a factor equal to 1.08 (Lesser, 2009) and M2 is the amplitude of such tidal component (~1.34 m), and period of (TMM) of 12 hours (see Figure 17).

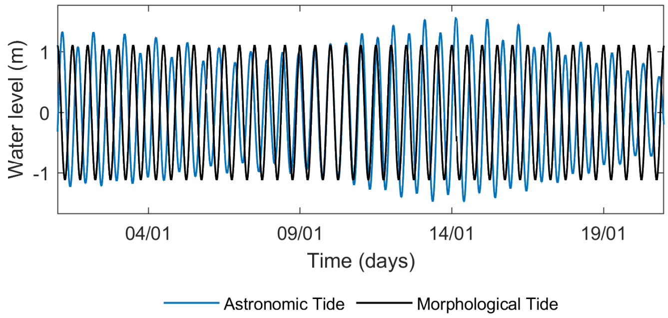

Figure 17. Time series Astronomical Tide and Morphological Tide.

<u>Clustering of dynamics</u>

The configuration of estuaries depends on mean conditions of several dynamics (waves, storm surge and river discharge), while extreme events are those that characterize the morphological variability around this mean configuration. Therefore, in order to select the most representative wave (Hs, Tp, θ) and river (Ql, Qs) conditions in the study area, the use of the statistical classification technique K-means is proposed.

This technique consists of selecting a limited number of representative conditions (forcings) that allow reproduce the long-term morphological evolution. Currently, the advantages and disadvantages of this technique have been evaluated by different authors, e.g. Lesser (2009), Walstra et al. (2013) and Luijendijk (2019).

The K-means classification technique divides the starting dataset, in this case the wave and river variables, into a certain number of subsets (NC). Each subset is represented by a centroid or prototype (Ci) and is constituted by the data for which that data for which that prototype is the closest. The classification process consists of the following steps: first, the desired number of groups is established, then the prototypes are initialized and finally, the algorithm proceeds iteratively by moving these centroids until the total intra-group variance is minimized (Hastie et al., 2001), i.e., at the end of the process, for each subset of data it must be satisfied that the sum of distances between the prototype and the data is minimum.

The procedure used is to perform the classification at a point located at deep water so as to take into account all the existing wave climate variability (DOW and GOW data) analyzed at each of the study sites (see section 2.2.5.4). The extracted time series are clustered in 9 clusters (N_c), the climatic variability is well represented.

Figure 18 shows the classification result obtained with 9 clusters. Each of the clusters is characterized by four variables: frequency of occurrence (panel A), significant wave height (H_s), peak period (T_p) and mean direction (θ) (panel B). The frequency of occurrence of each group was represented by the intensity of the blue color of each outer hexagon. The warm color scale of the inner hexagon represents the magnitude of H_s. The range of grays and the direction of the arrows indicate the value of T_p and the direction of the swell (θ), respectively. The marine dynamics must be associated with fluvial conditions, which is why we consider in each cluster the mean river flow during the period of time in which the cluster is presented.

Figure 19 shows how the real wave series (H_s, T_p) (in black) is represented with the categorical series (in color) constructed from the clusters resulting from the classification.

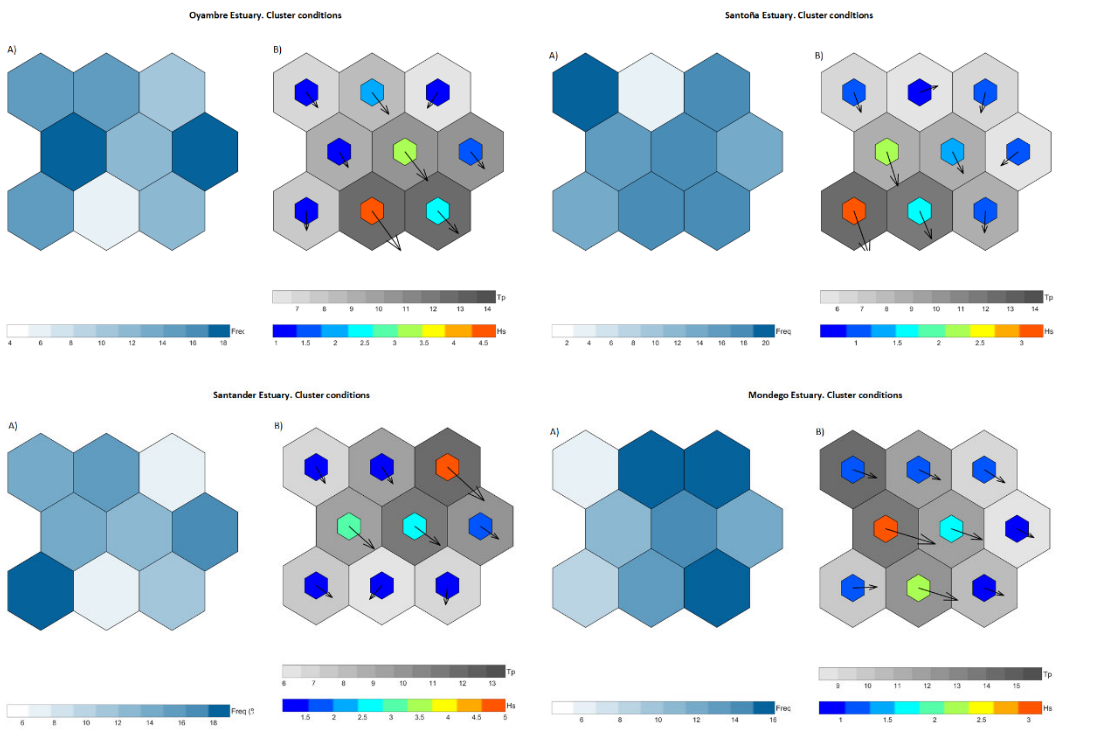

Figure 18. K-mean wave clustering at the GOW (for the Mondego estuary) and DOW (for the Santander Bay, Santoña marshes and Oyambre estuary): 3x3 centroid frequency map (Panel A) and map of Hs, Tp and mean propagation direction (Panel B).

Figure 19. Reconstruction of the real wave time series using C_i values from the clusters.

Oyambre Estuary

ID Cluster	Frequency	Hs(m)	Tp(s)	Dir(º)
C1	20.808	0.870	6.647	342.174
C2	9.169	2.206	9.022	343.974
C3	4.708	3.260	14.334	342.828
C4	0.651	0.573	5.321	248.600
C5	15.801	1.141	9.711	336.018
C6	12.350	1.699	13.011	338.925
C7	16.311	0.860	6.247	11.133
C8	6.444	0.872	5.348	47.992
C9	13.757	0.956	9.650	1.817

Table 6. Values of Hs, Tp and Θ values of the 9 centroids obtained from the k-means techniques.

Santander Bay

ID Cluster	Frequency	Hs(m)	Tp(s)	Dir(º)	River discharge (m^3/s)
C1	10.977	1.179	6.993	333.424	8.033
C2	11.748	3.013	9.831	314.783	7.451
C3	19.039	1.27	7.811	309.705	21.28
C4	13.082	1.33	9.853	328.995	11.167
C5	9.782	2.699	12.966	309.511	5.898
C6	5.414	1.102	5.956	38.278	18.414
C7	5.042	5.001	13.441	315.494	9.523
C8	16.089	1.526	10.69	307.801	8.875
C9	8.828	1.329	7.174	4.824	8.591

Table 7. Values of Hs, Tp, Θ, and River Discharge values of the 9 centroids obtained from the k-means techniques.

Mondego Estuary

ID Cluster	Frequency	Hs(m)	Tp(s)	Dir(º)	River discharge (m^3/s)
C1	4.453	1.218	15.861	291.048	28.349
C2	8.3	3.141	15.109	288.712	50.433
C3	6.146	1.11	9.697	267.269	206.235
C4	15.241	1.143	12.407	297.36	37.323
C5	13.06	1.755	12.289	291.263	110.433
C6	10.883	2.357	13.594	289.137	66.03
C7	16.082	1.194	9.179	305.193	61.605
C8	10.356	0.774	8.377	300.192	28.363
C9	15.478	0.898	10.814	292.939	42.548

Table 8. Values of Hs, Tp, Θ, and River Discharge values of the 9 centroids obtained from the k-means techniques.

Santoña Marshes					
ID Cluster	Frequency	Hs(m)	Tp(s)	Dir(º)	River discharge (m^3/s)
C1	20.808	0.870	6.647	342.174	1.771
C2	9.169	2.206	9.022	343.974	1.923
C3	4.708	3.260	14.334	342.828	7.912
C4	0.651	0.573	5.321	248.600	1.280
C5	15.801	1.141	9.711	336.018	2.046
C6	12.350	1.699	13.011	338.925	2.129
C7	16.311	0.860	6.247	11.133	1.405
C8	6.444	0.872	5.348	47.992	9.164
C9	13.757	0.956	9.650	1.817	0.848

Table 9. Values of Hs, Tp, Ɵ, and River Discharge values of the 9 centroids obtained from the k-means techniques.

2.2.8 Numerical modelling with Delf3d model.

Hydrodynamic model

In this study will be used the Delft3D-Flow model, with the aim to reproduce the hydrodynamic condition in the study site. This code is based on finite differences and solves the unsteady shallow water equations in two (depth-averaged) or three dimensions (hydrostatic assumption), derived from the three-dimensional Navier-Stokes equations for incompressible free surface flow (Roelvink, J. A. and van Bannin, 1994; Delft3D-Flow User Manual, 2011). It's based on a system of three equations that are solved using a finite difference grid. The governing equations system are composed by the horizontal equations of motion and the continuity equation for conservative constituent. They are expressed as follows:

<u>Continuity equation</u>

$$\frac{\partial\zeta}{\partial t}+\frac{1}{\sqrt{G_{\xi\xi}}\sqrt{G_{\eta\eta}}}\frac{\partial\left[(d+\zeta)u\sqrt{G_{\eta\eta}}\right]}{\partial\xi}+\frac{1}{\sqrt{G_{\xi\xi}}\sqrt{G_{\eta\eta}}}\frac{\partial\left[(d+\zeta)v\sqrt{G_{\xi\xi}}\right]}{\partial\eta}+\frac{\partial\omega}{\partial\sigma}=H\left(q_{in}-q_{out}\right)+P+E$$

in which u is the flow velocity in the ξ-direction [m/s], v is the flow velocity in the η-direction [m/s], w is the velocity in the σ-direction in the σ-co-ordinate system [m/s], qin is the local source per unit volume [1/s], qout is the local sink per unit volume [1/s], $\sqrt{G_{\eta\eta}}$ and $\sqrt{G_{\xi\xi}}$ are the coefficients used to transform curvilinear to rectangular co-ordinates [m], P is the precipitation [m/s] and E is the evaporation [m/s].

Momentum equations in horizontal direction

The momentum equations in ξ- and η-direction are given respectively by:

$$\frac{\partial u}{\partial t}+\frac{u}{\sqrt{G_{\xi\xi}}}\frac{\partial u}{\partial \xi}+\frac{v}{\sqrt{G_{\eta\eta}}}\frac{\partial u}{\partial \eta}+\frac{\omega}{d+\zeta}\frac{\partial u}{\partial \sigma}-\frac{v^2}{\sqrt{G_{\xi\xi}}\sqrt{G_{\eta\eta}}}\frac{\partial\sqrt{G_{\eta\eta}}}{\partial \xi}+\frac{uv}{\sqrt{G_{\xi\xi}}\sqrt{G_{\eta\eta}}}\frac{\partial\sqrt{G_{\xi\xi}}}{\partial \eta}-fv=$$
$$-\frac{1}{\rho_0\sqrt{G_{\xi\xi}}}P_\xi+\frac{1}{\sqrt{G_{\xi\xi}}}\frac{\partial\tau_{\xi\xi}}{\partial\xi}+\frac{1}{\sqrt{G_{\eta\eta}}}\frac{\partial\tau_{\xi\eta}}{\partial\eta}+\frac{1}{(d+\zeta)^2}\frac{\partial}{\partial\sigma}\left(\nu_V\frac{\partial u}{\partial\sigma}\right)+M_\xi$$

$$\frac{\partial v}{\partial t}+\frac{u}{\sqrt{G_{\xi\xi}}}\frac{\partial v}{\partial \xi}+\frac{v}{\sqrt{G_{\eta\eta}}}\frac{\partial v}{\partial \eta}+\frac{\omega}{d+\zeta}\frac{\partial v}{\partial \sigma}-\frac{uv}{\sqrt{G_{\xi\xi}}\sqrt{G_{\eta\eta}}}\frac{\partial\sqrt{G_{\eta\eta}}}{\partial \xi}+\frac{u^2}{\sqrt{G_{\xi\xi}}\sqrt{G_{\eta\eta}}}\frac{\partial\sqrt{G_{\xi\xi}}}{\partial \eta}+fu=$$
$$-\frac{1}{\rho_0\sqrt{G_{\eta\eta}}}P_\eta+\frac{1}{\sqrt{G_{\xi\xi}}}\frac{\partial\tau_{\eta\xi}}{\partial\xi}+\frac{1}{\sqrt{G_{\eta\eta}}}\frac{\partial\tau_{\eta\eta}}{\partial\eta}+\frac{1}{(d+\zeta)^2}\frac{\partial}{\partial\sigma}\left(\nu_V\frac{\partial v}{\partial\sigma}\right)+M_\eta$$

where P_ξ is the gradient hydrostatic pressure in ξ-direction [kg/m^{2}s^2], P_η is the gradient hydrostatic pressure in η-direction [kg/m^{2}s^2], $\tau_{\xi\xi}$, $\tau_{\eta\eta}$ and $\tau_{\xi\eta}$ are the contributions secondary flow to shear stress tensor [kg/ms^2], M_ξ source or sink of momentum in ξ-direction [m/s^2], Mη source or sink of momentum in η-direction [m/s^2], f Coriolis parameter (inertial frequency) [1/s] and ν_V vertical eddy viscosity [m^2/s]. The numerical models will be represented by a discretization of the domain using regular grids with resolutions of 15 x 15m in Oyambre estuary, 40 x 40 in the Santander Bay and Santoña marshes estuaries and 50 x 50 m in the Mondego estuary (Figure 20 and Figure 21).

Figure 20. Representation of numerical grids: A) Oyambre estuary grid and B) Santoña marshes grid.

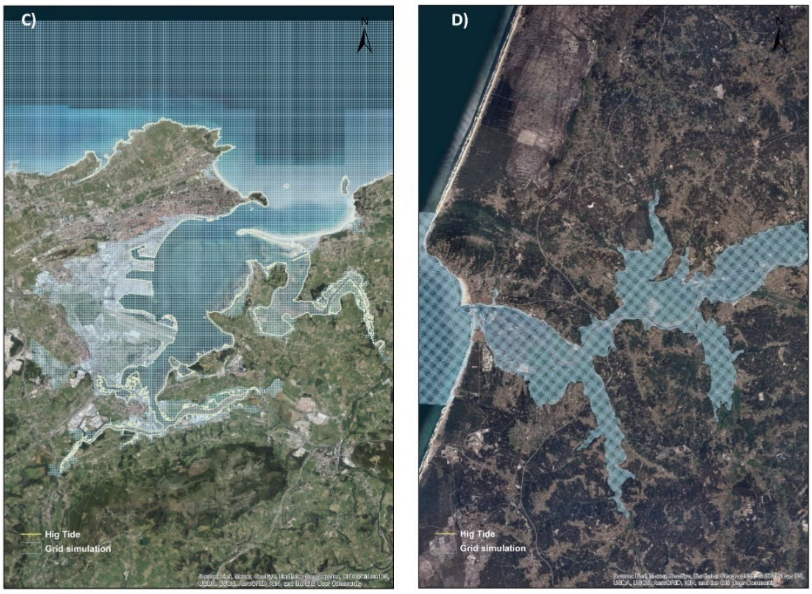

Figure 21. Representation of numerical grids: C) Santander Bay grid and D) Mondego estuary grid.

Wave model

The wave module includes the implementation of the SWAN wave propagation model (Holthuijsen et al., 1993, Booij et al., 1999, Ris et al., 1999), allowing the online coupling with FLOW module. In this way it is possible to simulate processes such as wave-current interaction.

The SWAN model accounts for the following physics:

- Wave refraction over a bottom of variable depth and/or a spatially varying ambient current.
- Depth and current-induced shoaling.
- Wave generation by wind.
- Dissipation by whitecapping.
- Dissipation by depth-induced breaking.
- Dissipation due to bottom friction (three different formulations).
- Nonlinear wave-wave interactions (both quadruplets and triads).
- Wave blocking by flow.
- Transmission through, blockage by or reflection against obstacles.
- Diffraction.

In SWAN the evolution of the wave spectrum is described by the spectral action balance equation (Hasselman et al., 1973)

$$\frac{d}{dt}N+\frac{d}{dx}c_xN+\frac{d}{dy}c_yN+\frac{d}{d\sigma}c_\sigma N+\frac{d}{d\theta}c_\theta N=\frac{S}{\sigma}$$

where:

N is the action density, cx y cy: propagation velocities in the space x-y, cσ y cθ: propagation velocities in the spectral space σ-θ and S: source term in terms of energy density representing the effect of generation, dissipation and non-linear wave interaction.

Morphodynamic model.

Delft3D-FLOW also calculates sediment transport (bed load transport and suspension transport) and the morphological changes associated with it, allowing to consider different fractions of sediment.

The three - dimensional transport of suspended solids is calculated by solving the three - dimensional advection - diffusion equation for solids in suspension:

$$\frac{\partial c^{(\ell)}}{\partial t}+\frac{\partial uc^{(\ell)}}{\partial x}+\frac{\partial vc^{(\ell)}}{\partial y}+\frac{\partial\left(w-w_s^{(\ell)}\right)c^{(\ell)}}{\partial z}-\frac{\partial}{\partial x}\left(\varepsilon_{s,x}^{(\ell)}\frac{\partial c^{(\ell)}}{\partial x}\right)-\frac{\partial}{\partial y}\left(\varepsilon_{s,y}^{(\ell)}\frac{\partial c^{(\ell)}}{\partial y}\right)-\frac{\partial}{\partial z}\left(\varepsilon_{s,z}^{(\ell)}\frac{\partial c^{(\ell)}}{\partial z}\right)=0$$

where $c^{(\ell)}$ mass concentration of sediment fraction (ℓ) (kg/m3), u,v,w flow velocity components (m/s), $\varepsilon_{s,x}^{(\ell)},\varepsilon_{s,y}^{(\ell)},\varepsilon_{s,z}^{(\ell)}$ Eddy diffusivities of sediment fraction (ℓ) (m2/s) y $w_s^{(\ell)}$ sediment settling velocity of sediment fraction (ℓ) (m/s).

According to the characteristics of the sediment, the Delft3D model uses different equations, being the differential characteristic the cohesive or non-cohesive nature of the sediment.

Non-cohesive sediment

The settling velocity of a non-cohesive ("sand") sediment fraction is computed following the method of van Rijn (1993). The formulation used depends on the diameter of the sediment in the suspension:

$$w_{s,0}^{(\ell)} = \begin{cases} \dfrac{\left(s^{(\ell)}-1\right) g D_s^{(\ell)2}}{18\nu}, & 65\,\mu m < D_s \le 100\,\mu m \\ \dfrac{10\nu}{D_s}\left(\sqrt{1+\dfrac{0.01\left(s^{(\ell)}-1\right) g D_s^{(\ell)3}}{\nu^2}}-1\right), & 100\,\mu m < D_s \le 1000\,\mu m \\ 1.1\sqrt{\left(s^{(\ell)}-1\right) g D_s^{(\ell)}}, & 1000\,\mu m < D_s \end{cases}$$

where $s^{(\ell)}$ is the relative density of sediment fraction(l), $D_s^{(\ell)}$ is the representative diameter of sediment fraction (ℓ) and ν is the kinematic viscosity coefficient of water (m2/s).

Delft3d model allows the selection of different sediment transport equations for non-cohesive sediment (see Table 10). Some sediment transport equations calculate total transport and other distinguish between bed load transport and suspension transport. In addition, not all of them can be applied with waves.

Formula	Bed load	Waves
Van Rijn (1993)	Bed load + suspension	Yes
Engelund-Hansen (1967)	total	No
Meyer-Peter-Muller (1948)	total	No
General formula	total	No
Bijker (1971)	Bed load + suspension	Yes
Van Rijn (1984)	Bed load + suspension	No
Soulsby/Van Rijn	Bed load + suspension	Si
Soulsby	Bed load + suspension	Si
Ashida-Michiue (1974)	Bed load + suspension	No

Table 10. Non-cohesive sediment transport formulations available in Delft3d model.

Cohesive sediment

In salt water, cohesive sediments tend to form sediment flocs, with the degree of flocculation dependent on the salinity concentration in the medium. These flocs, much larger than individual sediment particles, have a higher sedimentation rate. The sedimentation rate of cohesive sediment flocs is calculated with the following expression:

$$w_{s,0}^{(l)} = \begin{cases} \frac{w_{s,\max}^{(l)}}{2}\left(1 - cos\left(\frac{\pi S}{S_{max}}\right)\right) + \frac{w_{s,f}^{(l)}}{2}\left(1 + cos\left(\frac{\pi S}{S_{max}}\right)\right) & , \ si\ S \leq S_{max} \\ w_{s,max}^{(l)} & , \ si\ S < S_{max} \end{cases}$$

where $w_{s,0}^{(l)}$ is the settling velocity (unattenuated) of the sediment fraction. (l), ($w_{s,max}^{(l)}$), is the settling velocity of the sediment fraction (l) for the maximum salinity concentration ($w_{s,f}^{(l)}$), is the freshwater settling velocity of the sediment fraction (l) and Smax is the maximum salinity specified for $w_{s,max}^{(l)}$). In the evaluation of cohesive sediment dispersion, the diffusion coefficient is equal to that used by the model to solve for hydrodynamics and does not take into account the increase in turbulence due to waves.

The calculation of erosion and deposition of cohesive sediment, i.e., the flux of cohesive sediment fractions between the water column and the bed, is carried out with the Partheniades-Krone formulations (Partheniades, 1965).

These formulations allow the evaluation of the transport patterns of the system on a spatial and temporal scale.

Model reduction techniques

For the modeling of the long-term morphodynamic evolution in computationally feasible times, techniques known as model reduction are used. These techniques are based on the idea that that the model can be reformulated to describe only those processes that belong to the scale of interest. Among these techniques, two of them stand out, which have been used in the framework of this study.

1. **Morfac** is the first model reduction method that allows running flow, sediment transport and bottom updating all at the same small-time steps. Lesser et al. (2004), based on the different time scales characterizing hydrodynamic (faster) and morphodynamic (slower) processes, proposed to multiply the sediment fluxes at each hydrodynamic step by a constant factor "MorFac (M_f)" (morphological acceleration factor). This factor allows to perform morphodynamic simulations equivalent to a “real” duration equal to the product of the duration of the hydrodynamic simulation by the morphological factor. This technique makes it possible to optimize the computational cost of the numerical simulations. The value of this factor is set within certain limits, depending on the type of dynamics of the study area.

The duration of the morphological simulation (T_{morpho}) is the product of M_f and the duration of hydrodynamic simulation (T_{hydro}):

$$M_f = \frac{T_{morpho}}{T_{hydro}}$$

In Delft3D, this multiplication is applied to the net sediment transports (bed load and/or suspended load) which are calculated every half time step (in water level points and half a time step later in the velocity points). The depth change based on the net sediment transports can be calculated, if desired, every half a time step too (Wilmink, 2015). In order to avoid the violation of the continuity of sediment mass in the model, expressions are included that limit the erosion if the quantity of sediment at the bed approaches zero (Lesser et al., 2004). It is therefore important to check the thickness of the sediment layer in the model regularly.

2. Mormerge approach

Another method that has the stability and rate of accuracy of Morfac, but can perform the computations parallel, is Mormerge (Roelvink, 2006). In this approach it is assumed that the hydrodynamic conditions vary much more than the morphology. If the time interval in which all hydrodynamic conditions occur (ebb, flood, spring tide, neap tide, storms etc.) is small compared to the morphological time-scale, these processes can be run in parallel, using the same bathymetry and same acceleration factor for all conditions. This bathymetry is subsequently updated using a weighted average of the sediment transport rates for all hydrodynamic conditions based on the occurrence of the wave classes (Wilmink, 2015). The flow scheme of the method can be seen in Figure 22. The various parallel processes for flow, wave and sediment transport can be defined based on different conditions that are present in a study area. These processes (input conditions) in this study are derived by applying input reduction techniques.

By computing the processes parallel, it is possible to include an instantaneously counteraction of conditions as is in reality. An example is that other tidal phases can be assigned to different wave conditions. This will lead to ebb and flood sediment transports counteracting each other at all times (as most times in reality) and can allow for the use of much higher morphological acceleration factors because of the reduced short-term amplitude changes (Roelvink, 2006). The tidal phase shift applied in this study is equally divided over the number of conditions included. A particular phase shift is randomly assigned to a wave class. For Mormerge, the bathymetric changes are weighted every flow time step.

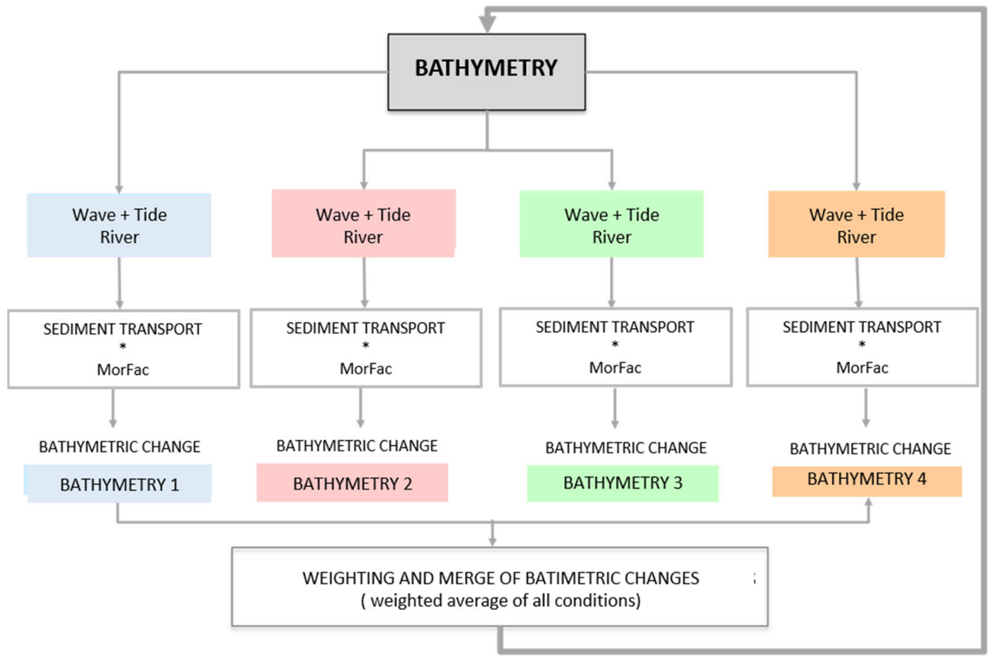

Figure 22.Flow scheme of the Mormerge approach with an acceleration factor included for all conditions

Vegetation

To simulate the influence of vegetation on hydrodynamics in Delft3D-FLOW can be modeled with a vegetation module. This module is based on a model developed by Uittenbogaard (2003), in which vegetation is represented by a number of rigid cylindrical rods. These rods influence the momentum and turbulence equations by adding extra source terms for drag and turbulence. The vegetation is characterized by a number of parameters: **the number of stems per unit area (stem density), the stem diameter and the stem height and the drag coefficient (**Figure 23**).** The main input parameter for this formulation is the plant geometry. The implementation of vegetation resistance can also be applied for 2DH computations.

The influence of the vegetation on drags leads to an extra source term of friction force, F(z) [N m-3], in the momentum equations:

$$F(z) = \frac{1}{2}\rho_0 C_D \emptyset(z) n(z) |u(z)| u(z)$$

Where:

ρ_0 = the fluid density [kg m-3]

C_D = the drag coefficient [-]

$\phi(z)$ = the diameter of the plant structure [m] at height z [m] above the bottom

n(z) = the number of plant structures per unit area [m-2] at height z

u(z) = the horizontal flow velocity [m/s] at height z.

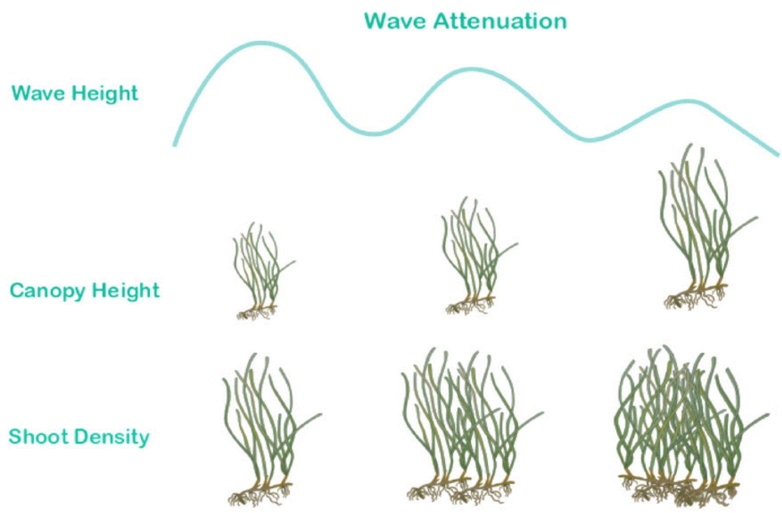

Figure 23. Source: Twomey (2021). Increases in canopy height, shoot density, meadow length and shoot width all contribute to an increase in wave attenuation.

A wide range of drag coefficients are found in the literature (Table 11 and Table 12), although it is true that most of the experimental analysis carried out is to determine the drag coefficient (C_D) of seagrass, recently attention is being paid to experimentation focused on marsh vegetation.

Reference	Type	Species	Mean C_D	Range C_D
Weitzman et al. (2015)	Seagrass	*Thalassia testitudinum*	0.02	0–0.09
John et al. (2015)	Seagrass	*Enhalus acoroides*	0.12	0.07–0.15
Sánchez-González et al. (2011)	Seagrass	*Posidonia oceanica*	0.18	0.01–0.41
Stratigaki et al. (2011)	Seagrass	*Posidonia oceanica*	0.55	0.33–0.71
Cao et al. (2013)	Seagrass	*Posidonia oceanica*	0.74	0.29–1.28
Manca et al. (2012)	Seagrass	*Posidonia oceanica*	1.74	0.7–2.77
Koftis et al. (2013)	Seagrass	*Posidonia oceanica*	0.68	0.29–1.23
Prinos et al. (2010)	Seagrass	*Posidonia oceanica*	1.05	0.56–1.47
Fonseca and Cahalan (1992)	Seagrass	*Halodule wrightii*	1.79	1.79
		Syringodium filiforme	5.12	5.12
		T. testudinum	0.99	0.99
		Zostera marina	0.48	0.48
Nowacki et al. (2017)	Seagrass	*S. filiforme*	0.19	0.13–0.33
Infantes et al. (2012)	Seagrass	*P. oceanica*	2.6	0.71–4.44
Méndez et al. (1999)	Seagrass	-	5.75	-
Paul and Amos (2011)	Seagrass	*Zostera noltii*	0.13	-
Hu et al. (2014)	Stiff wooden rods	-	1.69	-
Abdelrhman, 2007	Seagrass	*Zostera marina*	0.7	-
Pinsky et al. (2013)	Seagrass	-	2.5	-
Bouma et al. (2005)	Seagrass	*Zostera noltii and*	0.46	-
Bradley and Houser (2009)	Seagrass	*Thalassia testitudinum*	4.37	-
Cox et al. (2003)	Seagrass	*Posidonia autralis mimics*	3.06	-
Huber (2003)	Seagrass	*Zostera marina*	0.78	-
Ota et al. (2004	Seagrass	-	3.89	-
Wallace and Cox (2001)	Seagrass	*Posidonia autralis mimics*	0.85	-

Table 11. Drag coefficients for seagrass obtained from: Pinsky et al., 2013; Vuik et al., 2016 and Twomey et al., 2021.

Reference	Type	Species	Mean C_D	Range C_D
Bouma et al. (2005)	Marsh	*Spartina anglica*	0.68	-
Bouma et al. (2010)	Marsh	*Spartina anglica* *Puccinellia maritima*	2.33	-
Cooper (2005)	Marsh	*Puccinellia maritima, Salicornia europaea, Atriplex portulacoides, Spartina alterniflora*	0.85	-
Moller (2006)	Marsh	*Spartina anglica, Salicorniaspp., Suaeda maritima*	2.58	-
Möller et al. (1999)	Marsh	*Limonium vulgare Aster tripolium Atriplex portulacoides Salicorniaspp Spartinaspp Suaeda maritima Plantago maritima Puccinellia maritima*	0.01	-
Shi etal. (2000	Marsh	*Scirpus mariqueter*	0.01	-
Tschirky et al. (2001)	Marsh	*Scirpus validus*	3.24	-
Pinsky et al. (2013)	Marsh	-	2.6	-
Yiping et al., (2015)	Marsh	*Phragmites australis*	0.25	0.061-0.301
Zhao et al., (2017)	Marsh	*Juncus*	0.27	-
Möller et al. (2014)	Marsh	*Elymus athericus*	0.25	-
Jadhav and Chen (2012)	Marsh	*Spartina alterniflora,*	2.96	-
Pinsky et al. (2013)	Marsh	-	0.14	-
Anderson and Smith (2014)	Marsh	*Spartina*	1.45	-

Table 12. Drag coefficients for marsh vegetation obtained from: Pinsky et al., 2013; Vuik et al., 2016 and Twomey et al., 2021.

For vegetation models, the drag coefficient, C_D, is obtained by averaging the drag coefficients found from published studies. The values shown in this study ignore variations of C_D with the Reynolds' number. In the literature review we did not find the C_D value for all mapped species. In those where the information is not available, the C_D value of the species that presents the most similar morphological conditions to it will be used.

As discussed in (Vuik, 2016), empirical formulas and process-based descriptions of wave attenuation are mostly applied for bridging the gap between measured conditions and extreme conditions. These instruments are mainly based on measurements carried out during low condition, which leads to uncertainties when applying them to storm conditions.

2.3 Carbon sinks

A carbon sink is any process, activity or mechanism that removes CO_2 from the atmosphere and stored it in any other component of the climate system that act as a carbon reservoir.

Vegetated coastal ecosystems (i.e. saltmarshes, seagrass meadows and mangroves forests) remove CO_2 from the atmosphere through photosynthesis and store it in the form of organic carbon (C_{org}) as above (leaves and stems) and below ground (roots and rhizomes) biomass (Duarte et al., 2005; Nelleman et al., 2009) . Whereas above ground biomass can be exported, grazed or decomposed, belowground biomass accumulates in the sediment protected from currents, less accessible to herbivores and where the lack of oxygen reduced the activity of decomposer microorganisms (Nellemann et al., 2009). In addition, the canopy of these ecosystems acts as particle filter enhancing the sedimentation of organic particles from the water column derived from other sources (e.g. terrestrial detritus. macroalgae. phytoplankton), contributing to the enlargement of soil deposits (Kelleway et al., 2016; Kennedy et al., 2010). As a consequence, the largest and long-term C_{org} deposits in coastal vegetated ecosystems are allocated in the soil compartment (Serrano et al., 2019).

A carbon sink is characterized by the magnitude of the carbon deposit (stock) and by the rate at which carbon is being sequestered. In this study, the carbon sink capacity of estuarine ecosystems is proposed to be assessed through the quantification of the soil C_{org} stocks and burial rates of the most representative habitats in the estuaries of study.

In addition, data on soil C_{org} stocks and burial rates from other European marshes are compiled from the literature in order to provide a broader picture of the role saltmarshes play as carbon sinks at European scale.

The following sections describe how the quantification of C_{org} stocks was carried out.

2.3.1 Sampling of soil C_{org} deposits

Sampling was conducted between July and December 2020. In each estuary of study, between 3 to 4 sampling areas, distributed from the inner to the outer part of the estuary and containing different habitats were selected (see Figure 25 as an example). In each sampling area, a minimum of two different habitats at different marsh level were sampled (i.e. two sampling sites per area) (Figure 24). Soil C_{org} deposits were sampled by extracting 3 replicate soil cores in each sampling site (**¡Error! No se encuentra el origen de la referencia.**).

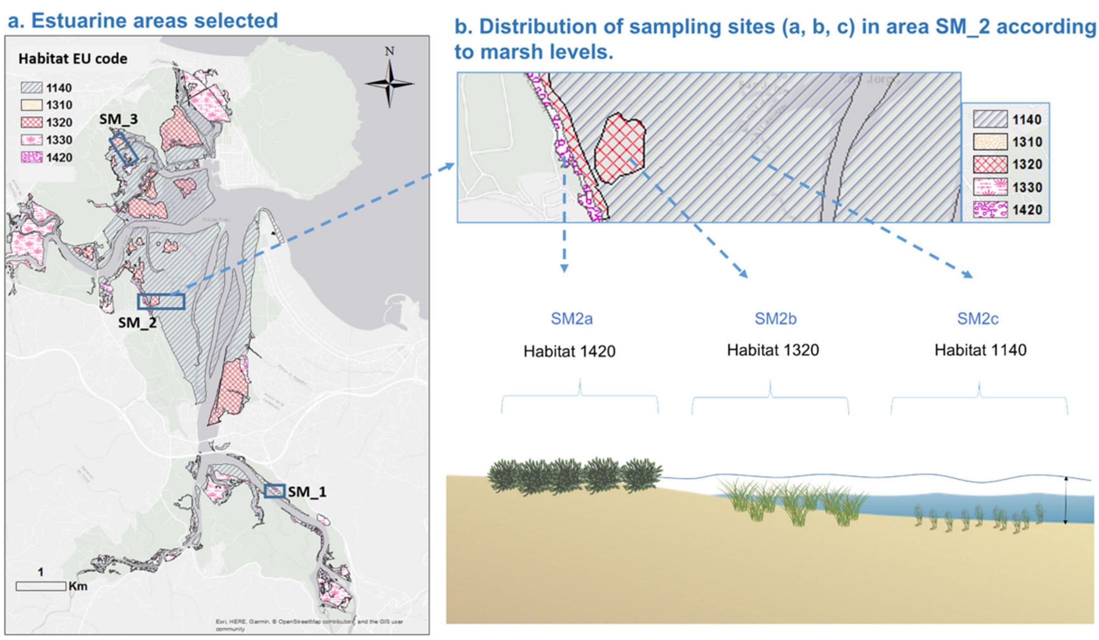

Figure 24. Sampling areas in the Santoña Marshes (SM) distributed from the inner (SM1) to the outer part (SM3) of the estuary and including different habitats. Right panel shows the distribution of three sampling sites within the sampling area (SM2) according to the marsh level.

Estuary	Sampling area	Lat / Long	EU Habitat	Marsh zone	Species composition	Core code	Compression (%)
Santander Bay	East_1	43.432096 / 3.758772	1330	High	*Juncus spp.*	BS1a_1	6.98
						BS1a_2	7.84
						BS1a_3	10.00
		43.43318 / - 3.758215	1320	Mid	*Spartina spp.*	BS1b_1	6.32
						BS1b_2	3.37
						BS1b_3	7.69
		43.433742 / - 3.758402	1140	Low	*Unvegetated tidal flat*	BS1c_1	3.05
						BS1c_2	0.00
						BS1c_3	3.45

Estuary	Sampling area	Lat / Long	EU Habitat	Marsh zone	Species composition	Core code	Compression (%)
	East_2	43.452136°/ - 3.748134°	1420	High	*Halimione spp.*	BS2a_1	0.00
						BS2a_2	0.00
						BS2a_3	0.83
		43.451940°/ - 3.748752°	1420	Mid	*Sarcocornea spp.*	BS2b_1	0.00
						BS2b_2	1.64
						BS2b_3	1.50
		43.451968° / - 3.753800°	1140	Low	*Zostera spp.*	BS2c_1	0.00
						BS2c_2	2.67
						BS2c_3	3.30
	West_1	43.409547/ - 3.808979	1420	High	*Halimione spp.*	BS3a_1	4.84
						BS3a_2	0.00
						BS3a_3	0.00
		43.409782 / - 3.809467	1140	Low	*Zostera spp.*	BS3c_1	10.89
						BS3c_2	8.81
						BS3c_3	7.45
	West_2	43.446924°/ - 3.772969°	1140	Low	*Zostera spp.*	EX_1	0.00
						EX_3	0.00
			1140	Low	*Unvegetated tidal flat*	SP_2	0.00
						SP_3	5.96
Santoña Marshes	1	43.368192°/ - 3.428633°	1330	High	*Juncus spp.*	MS1a_1	7.53
						MS1a_2	2.17
						MS1a_3	8.11
		43.368263° / - 3.428600°	1140	Low	*Unvegetated tidal flat*	MS1c_1	17.33
						MS1c_2	8.42
						MS1c_3	12.88
	2	43.419143° / - 3.480078°	1420	High	*Halimione spp.*	MS2a_1	2.41
						MS2a_2	0.00
						MS2a_3	0.00
		43.419399° / - 3.480063°	1320	Mid	*Spartina spp.*	MS2b_1	3.06
						MS2b_2	4.12
						MS2b_3	3.09
		43.419456° / - 3.479795°	1140	Low	*Zostera spp.*	MS2c_1	4.60
						MS2c_2	6.58
						MS2c_3	0.00
	3	43.448644°/ - 3.487925°	1320	Mid	*Spartina spp.*	MS3b_1	6.32
						MS3b_2	2.08

Estuary	Sampling area	Lat / Long	EU Habitat	Marsh zone	Species composition	Core code	Compression (%)
						MS3b_3	1.18
		43.448438°/ - 3.488090°	1140	Low	*Unvegetated tidal flat*	MS3c_1	24.00
						MS3c_2	18.00
						MS3c_3	12.00
Oyambre	East_1	43.373796°/ - 4.315541°	1330	HIgh	*Halimione spp.. Juncus spp.*	R_M1	12.87
						R_M2	12.22
						R_M3	10.35
		43.374078°/ - 4.315354°	1140	Low	*Unvegetated tidal flat*	R_P1	7.18
						R_P2	6.92
						R_P3	10.58
	East_2	43.382817°/ - 4.318047°	1420	High	*Halimione spp.. Juncus spp.*	N_M1	13.03
						N_M2	12.53
						N_M3	10.60
		43.383328°/ - 4.317465°	1140	Low	*Zostera spp.*	N_P1	15.77
						N_P2	10.58
						N_P3	7.35
	West_1	43.382675°/ - 4.335772°	Invasive species	High	*Juncus spp.. Baccharis spp.*	A2_M1	10.53
						A2_M2	7.88
						A2_M3	7.76
		43.383133°/ - 4.335868°	1140	Low	*Unvegetated tidal flat*	A2_P1	6.38
						A2_P2	4.35
						A2_P3	8.98
	West_2	43.385830°/ - 4.324631°	1420	High	*Halimione spp.. Juncus spp.*	A1_M1	0.00
						A1_M2	0.00
						A1_M3	7.00
		43.386026°/ - 4.324808°	1140	Low	*Unvegetated tidal flat*	A1_P1	6.29
						A1_P2	8.51
						A1_P3	9.79
Mondego	1	40.1191° / - 8.775068°	1320	Mid	*Spartina spp.*	MM3a1	3.21
						MM3a2	1.69
						MM3a3	8.66
		40.118167° / - 8.774267°	1140	Low	*Zostera spp.*	MM3b1	2.16
						MM3b2	22.86
						MM3b3	10.61
		40.118133° / - 8.774283°	1140	Low	*Unvegetated tidal flat*	MM3c1	100.00
						MM3c2	100.00

Estuary	Sampling area	Lat / Long	EU Habitat	Marsh zone	Species composition	Core code	Compression (%)
						MM3c3	80.00
	2	40.139017° / -8.808083°	1330	High	*Juncus spp.*	MM2a1	2.70
						MM2a2	0.00
						MM2a3	0.00
		40.140017° / -8.809621°	1140	Low	*Unvegetated tidal flat*	MM2b1	3.96
						MM2b2	6.77
						MM2b3	8.32
		40.140467° / -8.8112°	1140	Low	*Unvegetated tidal flat*	MM2c1	8.93
						MM2c2	10.55
						MM2c3	10.40
	3	40.13201° / -8.84815°	1330	High	*Juncus spp.*	MM1a1	6.55
						MM1a2	6.59
						MM1a3	16.67
		40.130783° / -8.846967°	1130	Mid	*Scirpus spp.*	MM1b1	12.53
						MM1b2	12.71
						MM1b3	12.24
		40.131283° / -8.845333°	1140	Low	*Unvegetated tidal flat*	MM1c1	6.37
						MM1c2	4.13
						MM1c3	6.12
Western Scheldt	1	51.364322° / 4.248053°	1130	High	*Phragmites australis*	WS1a_1	35.71
						WS1a_2	30.77
						WS1a_3	30.77
		51.364353° / 4.246972°	1130	Mid	*Scirpus spp.*	WS1b_1	16.67
						WS1b_2	13.04
						WS1b_3	13.04
		51.364042° / 4.245406°	1140	Low	*Unvegetated tidal flat*	WS1c_1	0.00
						WS1c_2	0.00
						WS1c_3	0.00
	2	51.397864° / 4.162592°	1320	High	*Spartina spp.*	WS2a_1	32.26
						WS2a_2	30.77
						WS2a_3	28.57
		51.397494° / 4.162875°	1130	Mid	*Scirpus spp.*	WS2b_1	19.05
						WS2b_2	14.29
						WS2b_3	14.29
		51.3957° / 4.1638°	1140	Low	*Unvegetated tidal flat*	WS2c_1	0.00
						WS2c_2	0.00

Estuary	Sampling area	Lat / Long	EU Habitat	Marsh zone	Species composition	Core code	Compression (%)
						WS2c_3	0.00
	3	51.387486° / 3.825075°	1320	High	*Spartina spp.*	WS3a_1	43.48
						WS3a_2	36.36
						WS3a_3	36.36
		51.387206° / 3.824794°	1320	Mid	*Spartina spp.*	WS3b_1	26.09
						WS3b_2	18.18
						WS3b_3	18.18
		51.385483° / 3.823778°	1140	Low	*Unvegetated tidal flat*	WS3c_1	7.69
						WS3c_2	0.00
						WS3c_3	0.00
	4	51.349617° / 3.719358°	1320	High	*Spartina spp.*	WS4a_1	36.36
						WS4a_2	30.00
						WS4a_3	30.00
		51.351169° / 3.720053°	1320	Mid	*Spartina spp.*	WS4b_1	25.93
						WS4b_2	20.00
						WS4b_3	20.00
		51.3523° / 3.721667°	1140	Low	*Unvegetated tidal flat*	WS4c_1	3.85
						WS4c_2	0.00
						WS4c_3	0.00

Table 13. Location of the soil cores sampled across the five estuaries of study. Sampling area numbers indicate the relative position within each estuary or estuary branch (for Bay of Santander and Oyambre), from inner sections (1) to outer sections (to a maximum of 4).

Soil cores were extracted by manually hammering PVC tubes (~60 cm long * ~7 cm D). During sampling, the length of the PVC tube and the inner and outer distance between the top of the tube and the sediment inside and outside the tube were measured in order to estimate the soil compression that occurs during hammering (Figure 25). A total of 136 soil cores (between 10-40 cm long) were sampled in a total of 46 different sites encompassing 5 different habitats and 1 invasive species (Table 13). In particular, 27 cores were sampled in 4 habitats in the Mondego estuary; 21 cores were sampled in 4 habitats in the Santoña Marshes estuary, 28 cores were sampled in 4 habitats in the Santander Bay estuary, 24 cores were sampled in 4 habitats in the Oyambre estuary and 36 cores were sampled in 3 habitats in the Western Scheldt estuary, distributed from the inner to the outer part of the estuary (Table 13). Soil cores were preserved frozen until processing in the laboratory.

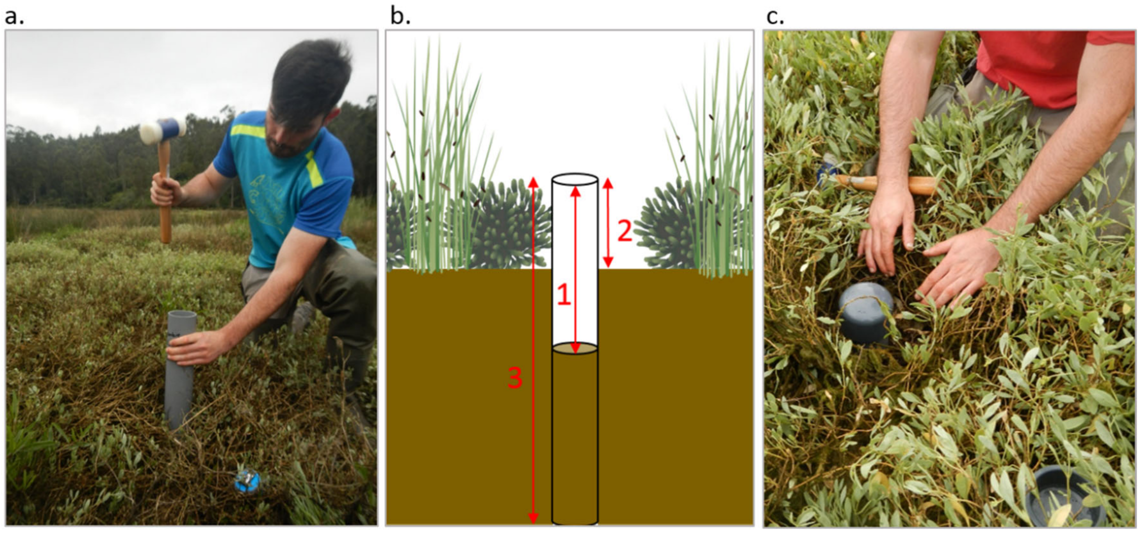

Figure 25. Steps during soil core sampling in saltmarsh communities: a. pipe hammering; b. measurements for compression estimate (1=inner distance. 2=outer distance and 3= pipe length) and c. pipe sealing before extracting.

2.3.2 Laboratory procedures

Soil cores processing

One of replicate soil core per sampling site was sliced every 1 cm along the whole sediment depth. The other two replicate cores were sliced every 2 cm for the top 20 cm and every 5 cm for deeper layers. Each sediment slice was measured for wet volume (cm^3) and wet weight (g) and dried at 60ºC for a minimum of 72 h (Figure 26). Dry weight of each sediment slice was measured and used along with wet volume to estimate sediment dry bulk density (DBD, g DW cm^{-3}) of each slice.

Figure 26. Example of different steps during core processing.

Biogeochemical analysis

Soil C_{org} content

From all the soil cores sampled, soil organic carbon content (C_{org} %DW) was measured every other two sediment depth sections distributed along the sediment depth profile. Organic carbon content was analyzed in the IHLab Bio laboratory of the Environmental Hydraulics Institute of the University of Cantabria using a TC analyzer (Shimadzu TOC-L + SSM-5000A). The C_{org} content (C_{org} %DW) of those sediment sections that were not analyzed was estimated as the average of the C_{org} content of the slices above and below in the depth profile.

Sediment dating

The age of the sediment is a critical variable to understand the role coastal ecosystems play as C_{org} sinks. It allows to identify if the ecosystem is actually acting as a sink (i.e. the reservoir of C_{org} is growing) and if so, to estimate a rate of C_{org} burial; if no net accumulation occurs or even if erosion occurs and the ecosystem is acting as a carbon source (i.e. carbon is been released) (Macreadie et al., 2014). In this study, the age of the sediment was determined in 22 of the sampling sites encompassing the wide variability of habitats and communities examined in the estuaries of studied (Table 14).

Region	Estuary	Location	Lat/Long	Marsh level	EU habitat	Dominant genera	Core code
Cantabria	Santander Bay	Inner	43.432096 / -3.758.772	High	1330	*Juncus. Halimione*	BS1A1
			43.43318 / -3.758215	Low	1320	*Spartina*	BS1B1
		Outer	43.452136°/ -3.748134°	High	1420	*Halimione*	BS2A1
			43.451940°/ -3.748752°	Low	1420	*Sarcocornea*	BS2B3
	Santoña Marshes	Inner	43.368192°/ -3.428633°	High	1330	*Junco.Festuca*	MSA2
		Outer	43.419143° / -3.480078°	High	1420	*Halimione*	MS2A3
			43.419399° / -3.480063°	Low	1320	*Spartina*	MS2B2
			43.419456° / -3.479795°	Mudflat / Sandflat	1140	*Zostera noltei*	MS2C3
	Oyambre	Outer	43.382817°/ -4.318047°	High	1420	*Halimione. Juncus*	NM3
			43.383328°/ -4.317465°	Mudflat / Sandflat	1140	*Zostera noltei*	NP2
		Inner	43.373796°/ -4.315541°	High	1330	*Halimione. Juncus. Suaeda. Limonium*	RM3
			43.374078°/ -4.315354°	Mudflat / Sandflat	1140	*unvegetated*	RP3
		Outer	43.385830°/ -4.324631°	High	1420	*Halimione. Inula. Elymus. Juncus*	A1M1
			43.386026°/ -4.324808°	Mudflat / Sandflat	1140	unvegetated	A1P1
		Inner	43.382675°/ -4.335772°	High	Invasive species	*Scirpus. Festuca. Atriplex. Juncus. Festuca. Halimione*	A2M3
			43.383133°/ -4.335868°	Mudflat / Sandflat	1140	unvegetated	A2P3
Coimbra	Mondego	Outer	40.13201° / -8.84815°	Low	1320	*Spartina*	MM1A1
			40.130783° / -8.846967°	Mudflat / Sandflat	1140	*Zostera noltei*	MM1B1
		Inner	40.140467° / -8.8112°	Mudflat / Sandflat	1140	unvegetated	MM2C1
Zeeland	Western Scheldt	Intermediate	51.397864° / 4.162592°	High	1320	*Spartina anglica*	WS2A1
			51.387206° / 3.824794°	Low	1320	*Spartina anglica*	WS3B1
		Outer	51.349617° / 3.719358°	High	1320	*Spartina anglica*	WS4A1

Table 14. Location, habitat and dominant species of the soil cores dated with ^{210}Pb per estuary of study. Sampling area indicates a gradient within the estuary, from inner estuary (1) to the estuary mouth (4).

Sediment age was determined applying ^{210}Pb dating techniques, especially suitable for the last 100-150 years (Appleby, 2001), the period where the largest impacts in coastal ecosystems have taken place. ^{210}Pb analysis were conducted in the Unit of Physics of Radiations from the

Autonomous University of Barcelona and in the Environmental Radioactivity Laboratory of Edith Cowan University (Perth). ^{210}Pb was analyzed in one of the replicate cores (sliced every 1 cm) of the sampling sites selected (Table 14). The age of the sediment was determined applying CF:CS models (Krishnaswamy et al., 1971).

2.3.3 Numerical procedures

Magnitude of Corg deposits

The magnitude of C_{org} deposits in this study were standardized to 30 cm soil depth by adding the C_{org} stock of the soil sections within the first 30 cm (decompressed) depth. The C_{org} stock for each soil section along the depth profile was estimated by multiplying the C_{org} content by the sediment dry bulk density and the section height. For those cores shorter than 30 cm long, top 30 cm stocks were estimated using the equation resultant from applying a linear regression of the C_{org} stock per soil section with depth.

C_{org} burial rates

C_{org} burial rate was estimated dividing the cumulative soil C_{org} stock to a certain depth section by the age of that sediment section. The C_{org} burial rates provided here correspond to average burial rates since 1950, as it is the oldest age reached by all the cores that could be dated.

Transformation of soil Corg stocks and burial rates into CO2

The C_{org} stocks and burial rates measured are also reported in terms of CO_2. Estimates of CO_2 were carried out by multiplying C_{org} stocks and burial rates by 44.01/12 (where 12 is the carbon molecular mass and 44.01 is the CO_2 molecular mass).

Trends examined

Top 30 cm soil C_{org} stocks were compared across dominant species and habitats considering the 46 communities examined in this study. For each of the estuaries of study differences in the magnitude of the top 30 cm soil C_{org} stocks were also compared across habitats and across different sections of the estuary (i.e. inner estuarine area vs. estuary mouth).

3 RESULTS AND DISCUSSION

3.1 Habitat cartography

The distribution of estuarine habitats mapped in the five estuaries of study is shown in Figures Figure 27-Figure 32).

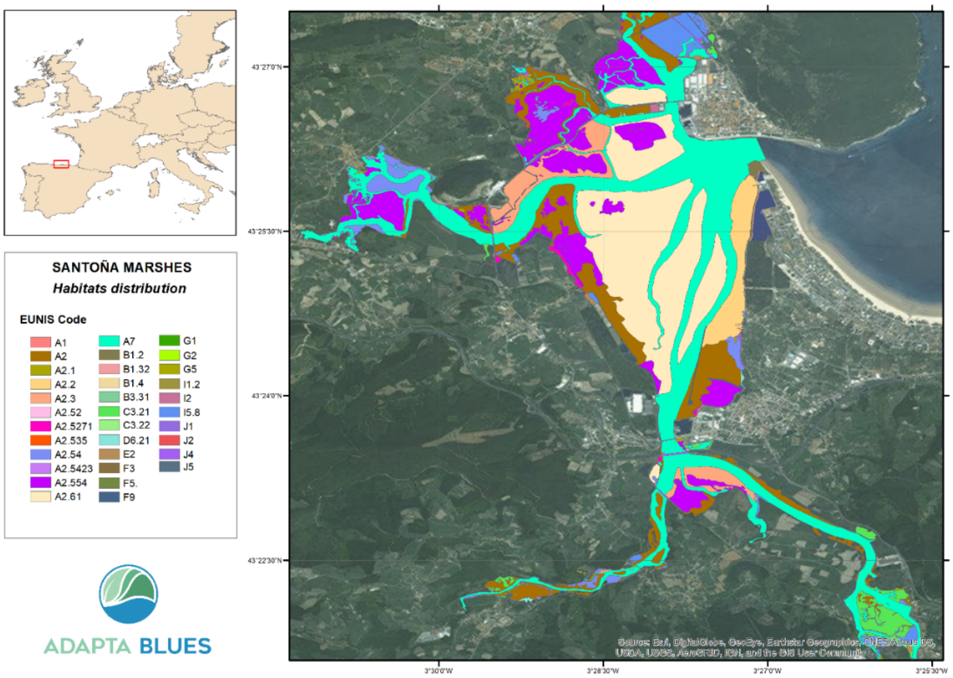

Figure 27.Cartography of estuarine habitats (EUNIS code), areas occupied by invasive species and tidal artificial barriers identified in Santoña Marshes (Cantabria).

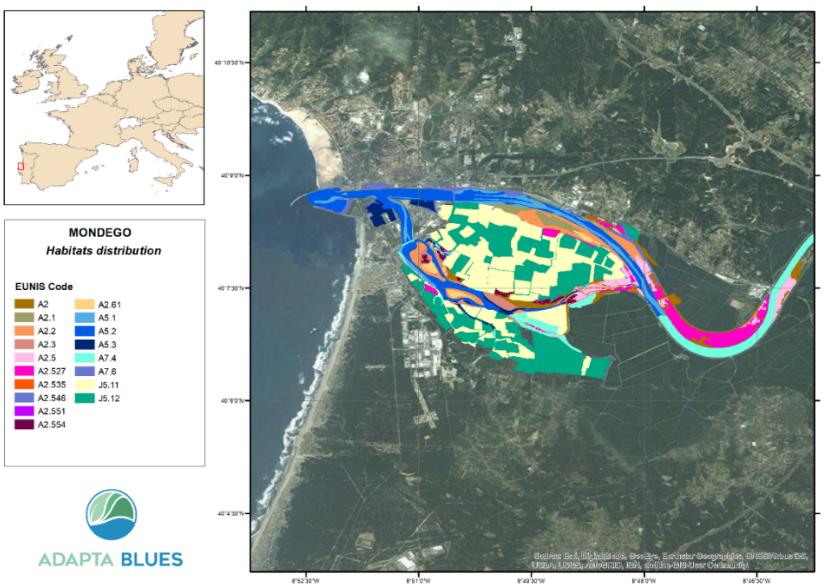

Figure 28. Cartography of estuarine habitats (EUNIS code), areas occupied by invasive species and tidal artificial barriers identified in the Mondego estuary (Cantabria).

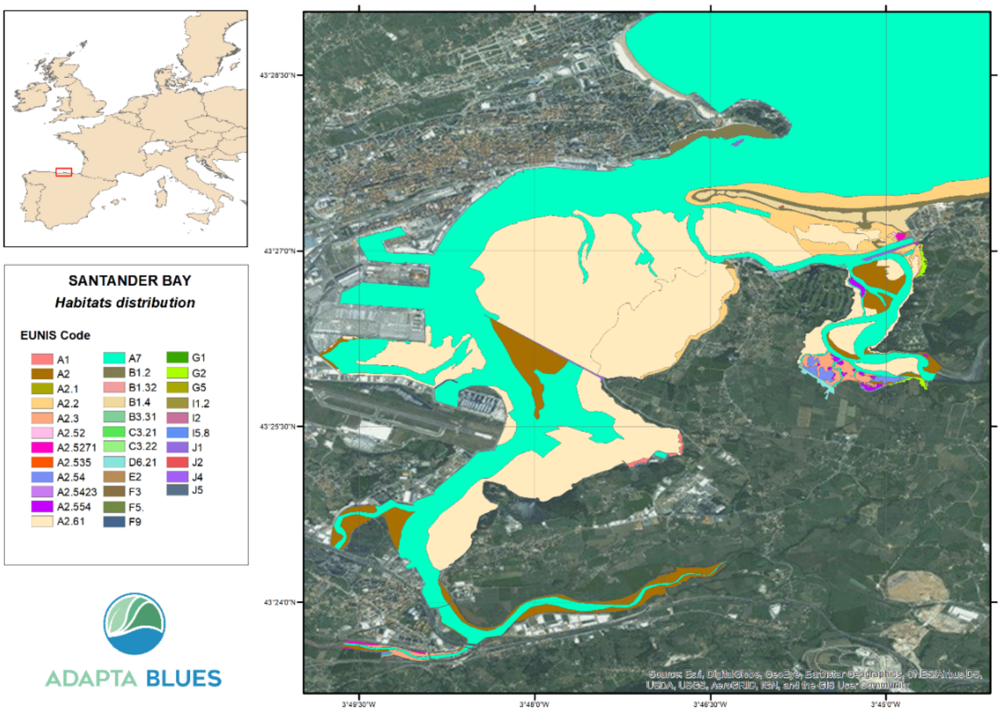

Figure 29. Cartography of estuarine habitats (EUNIS code), areas occupied by invasive species and tidal artificial barriers identified in Santander Bay (Cantabria).

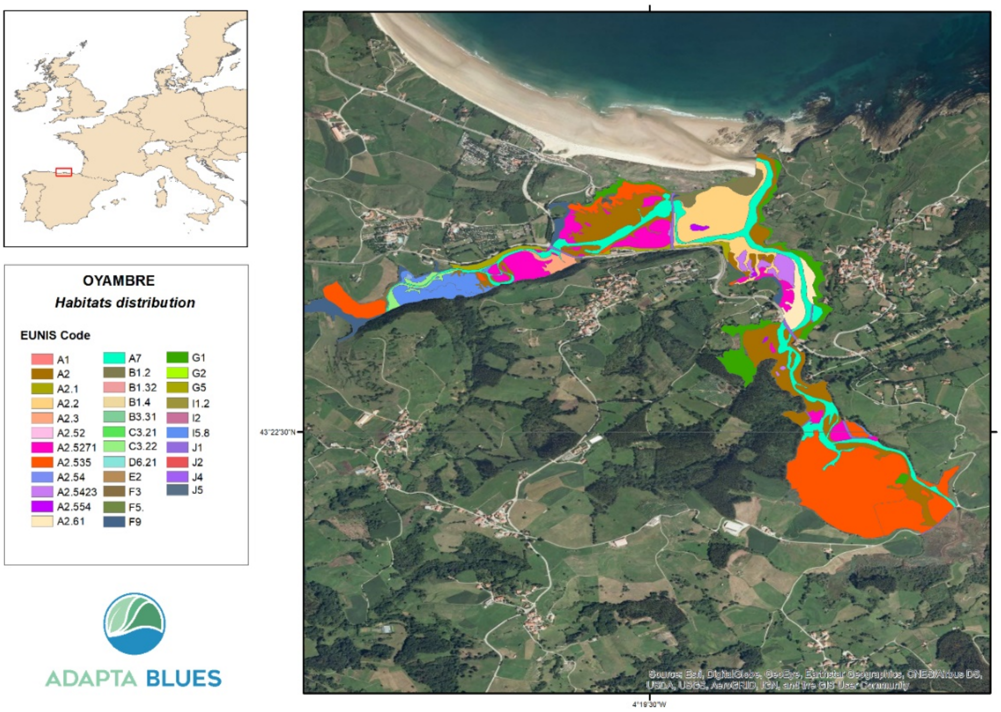

Figure 30. Cartography of estuarine habitats (EUNIS code), areas occupied by invasive species and tidal artificial barriers identified in Oyambre estuary (Cantabria).

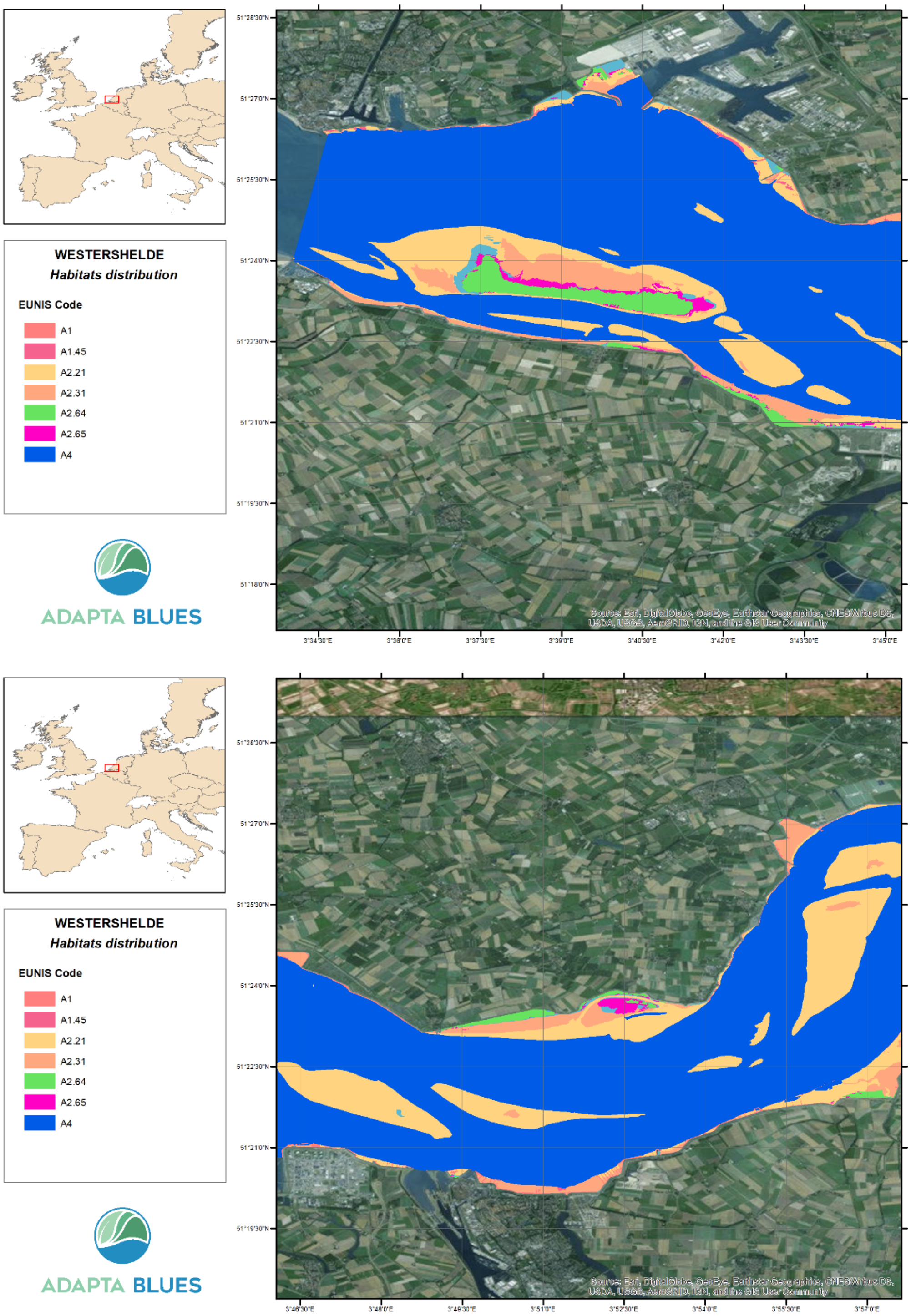

Figure 31. Cartography of estuarine habitats (EUNIS code), areas occupied by invasive species and tidal artificial barriers identified in the Western Scheldt estuary (Cantabria).

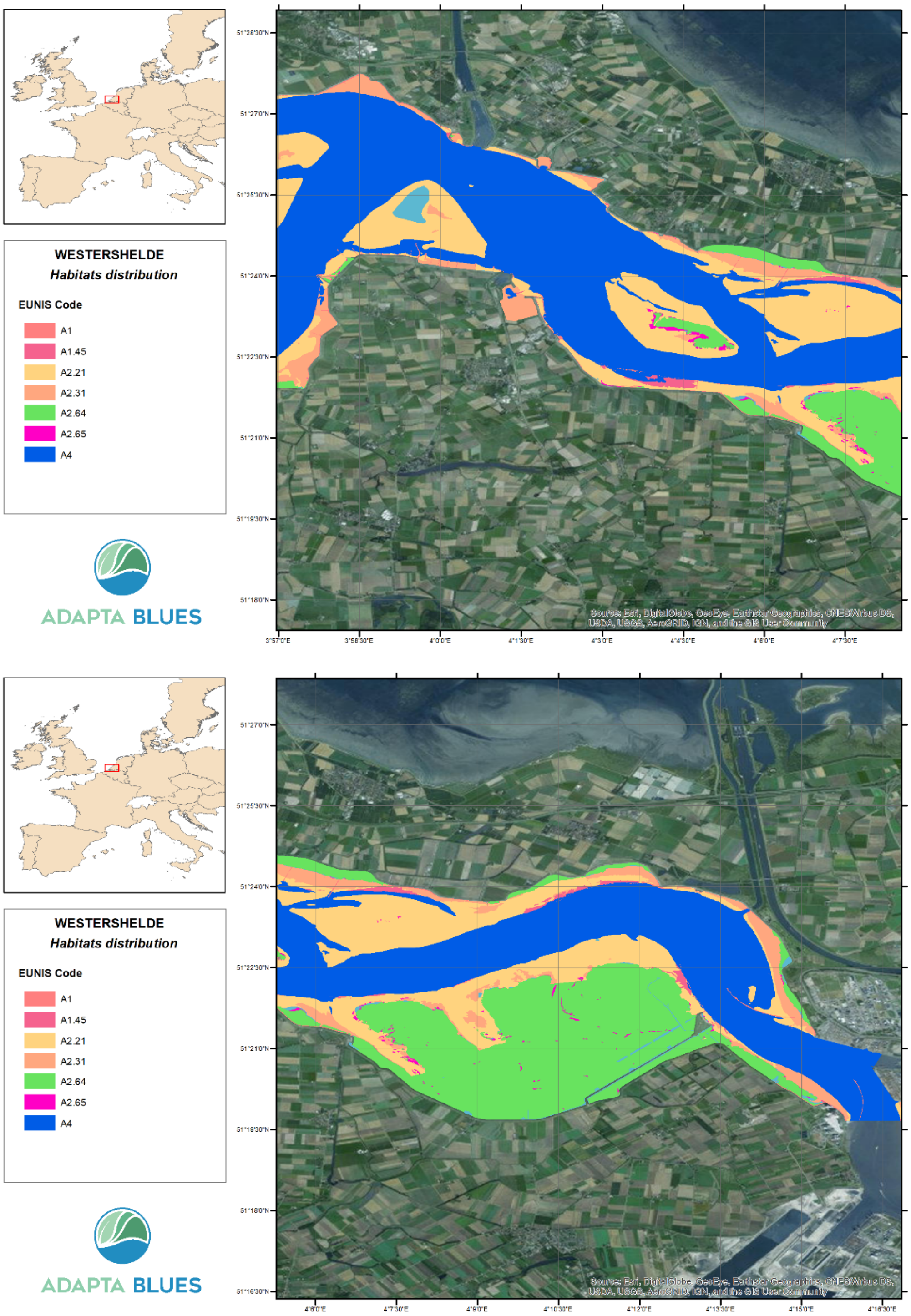

Figure 32.(continued) Cartography of estuarine habitats (EUNIS code), areas occupied by invasive species and tidal artificial barriers identified in the Western Scheldt estuary (Cantabria).

Subtidal habitats were dominant in Mondego estuary, Santander Bay and Western Scheldt whereas intertidal habitats dominated in Santoña marshes and Oyambre estuary (Table 15). Intertidal vegetated habitats (i.e. 1310, 1320, 1330 and 1420, Habitats Directive codes) contributed differently to each estuary, being Mediterranean and thermoatlantic halophilous scrubs (1420) the dominant vegetated habitat in the Mondego estuary. Spartina swards (1320) in Santoña Marshes and Atlantic salt meadows (1330) in Santander Bay, Oyambre and Western Scheldt.

EU habitat	Habitat description	Surface area (Ha) occupied per estuary of study				
		Mondego	Santoña Marshes	Santander Bay	Oyambre	Western Scheldt
1110	Sandbanks which are slightly covered by sea water all the time		440.16 (24.9%)	1954.3 (58.7 %)	11.16 (12.3 %)	10688 (25.8 %)
1130	Estuaries	1275.5 (49.8%)	143.05 (8.1%)	42.75 (1.3 %)	1.65 (1.8 %)	28338 (68.3 %)
1140	Mudflats or sandflats not covered by seawater in low tide	244.38 (9.54%)	805.57 (45.6 %)	1309.75 (39.4 %)	32.21 (35.6 %)	100 (0.24 %)
1310	Salicornea and other annual chenopodiaceous species	0.27 (0.01%)	0.22 (0.01 %)	0.05 (0.0 %)	1.99 (2.2 %)	103 (0.25 %)
1320	Spartina swards	15.22 (0.59%)	263.58 (14.9 %)	5.99 (0.2 %)	0.36 (0.4 %)	156 (0.38 %)
1330	Atlantic salt meadows	10.07 (0.39%)	51.84 (2.9 %)	10.22 (0.3 %)	29.53 (32.7 %)	2110 (5.08 %)
1420	Mediterranean and thermoatlantic halophilus scrubs	93.73 (3.66%)	6.99 (0.4 %)	3.69 (0.1 %)	8.99 (9.9 %)	
Invasive species			53.65 (3.0 %)	0.06 (0.0%)	4.48 (4.5 %)	
Total		2560.18	1765.07	3326.8	90.38	41495

Table 15. Total surface area (Ha) and percentage (in brackets) occupied by estuarine habitats identified in each estuary of study.

3.2 Coastal protection assessment

The assessment of the coastal protection provided by estuarine ecosystems will be analyzed from several perspectives:

- Vegetation role in coastal flooding analysis.
- Vegetation role in the velocity field analysis.
- Vegetation role in sediment trapping capacity.

Figures from Figure 33 to Figure 36 show water level time series at several points of the estuary considering the role of vegetation in the propagation of the tidal wave. The green line represents the result obtained from numerical modeling considering all vegetation communities in the estuary and the blue line represents the result obtained considering the estuary completely unvegetated.

Figure 33 shows the result in the Oyambre estuary. At Point 1 (located in the main channel), the tidal wave behavior overlaps in both scenarios, showing that there are no differences between the two scenarios analyzed. It is at the innermost points of the estuary where the greatest differences are observed. The propagation of the tidal wave suffers a time lag to reach high tide and its magnitude is attenuated by the role of vegetation. The behavior of the tidal wave during low tide is also modified, the drainage capacity of the estuary is reduced. At the points located in the innermost part of the estuary, reductions in the high tide level are observed, in the range of (16 - 57 cm). In the Santoña Marshes (Figure 34), a similar behavior is observed in the inner points, in high tide the amplitude of the tidal wave is reduced at a maximum of 15cm.

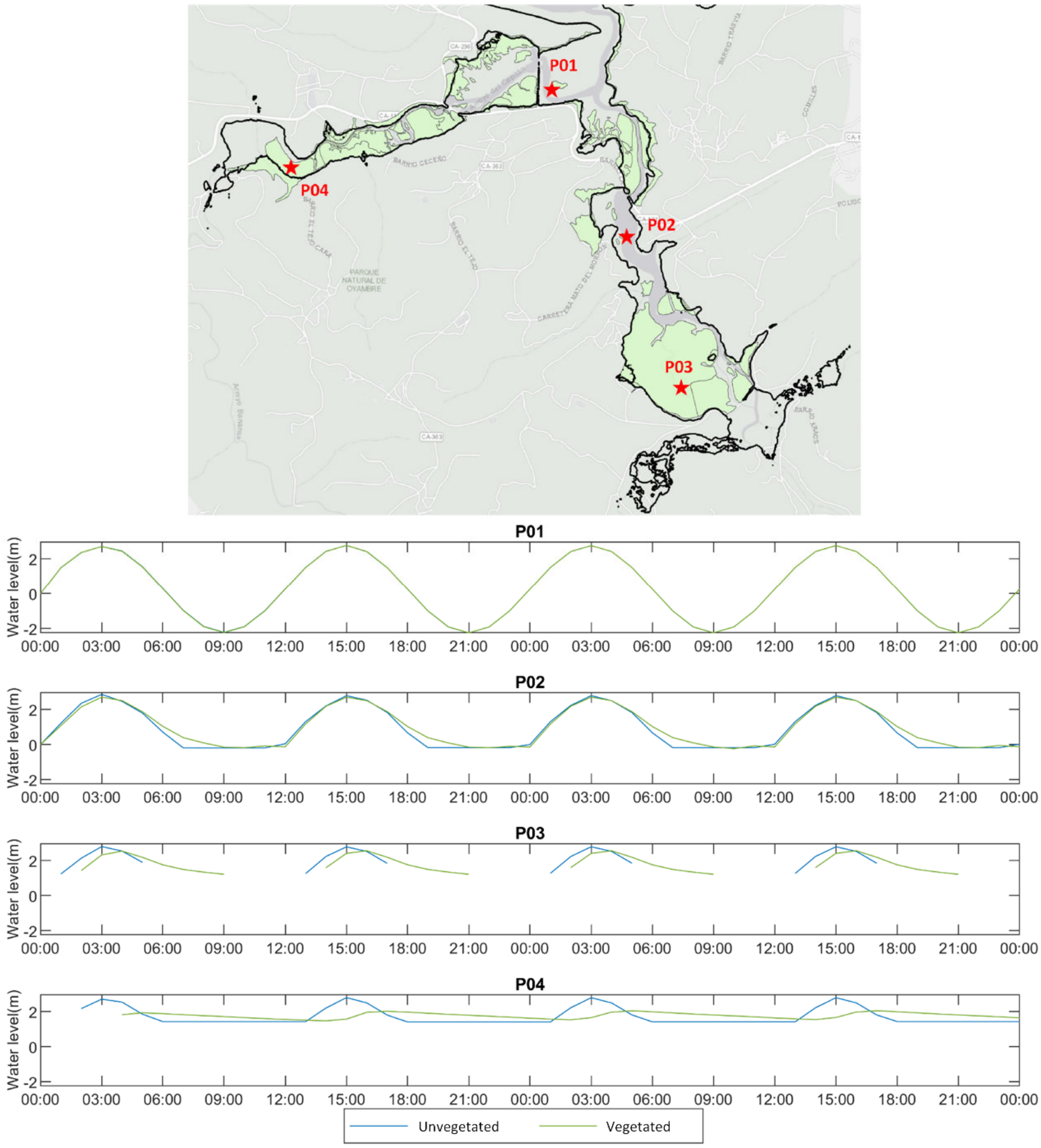

Figure 33. Water level time series in several points in Oyambre estuary. Comparison: vegetated and unvegetated.

In Santander Bay (Figure 35), in Point 1 (located in the main channel), no different exists between the scenarios (vegetated and unvegetated estuary) in the comparison of tidal wave. At the innermost points of the estuary, the greatest differences are observed. The propagation of the tidal wave suffers a time lag to reach high tide and its magnitude is attenuated by the role of vegetation. At the points located in the innermost part of the estuary, reductions in the high tide level are observed, in the range of (15 - 42 cm).

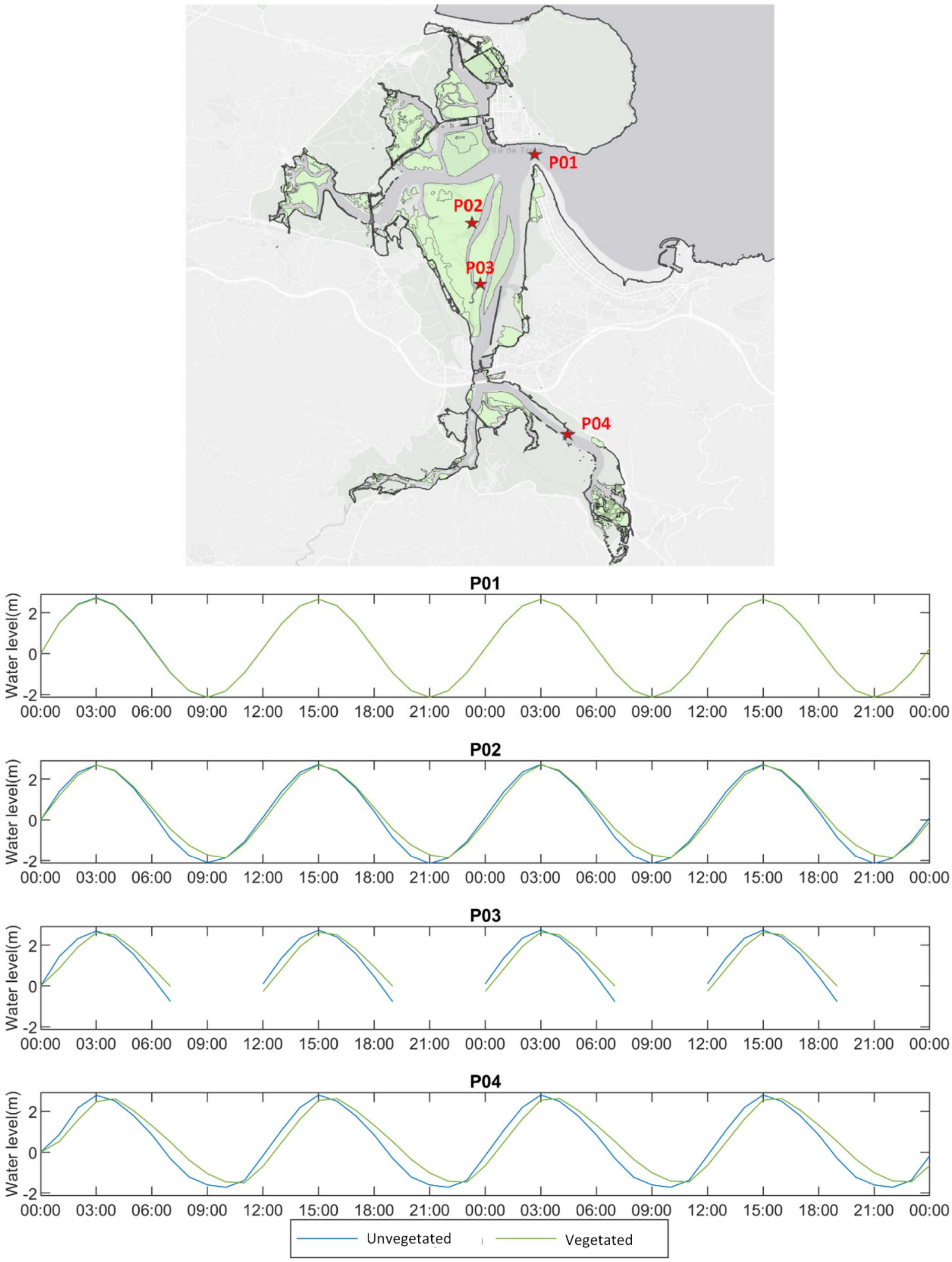

Figure 34. Water level time series in several points in Santoña marshes. Comparison: vegetated and unvegetated.

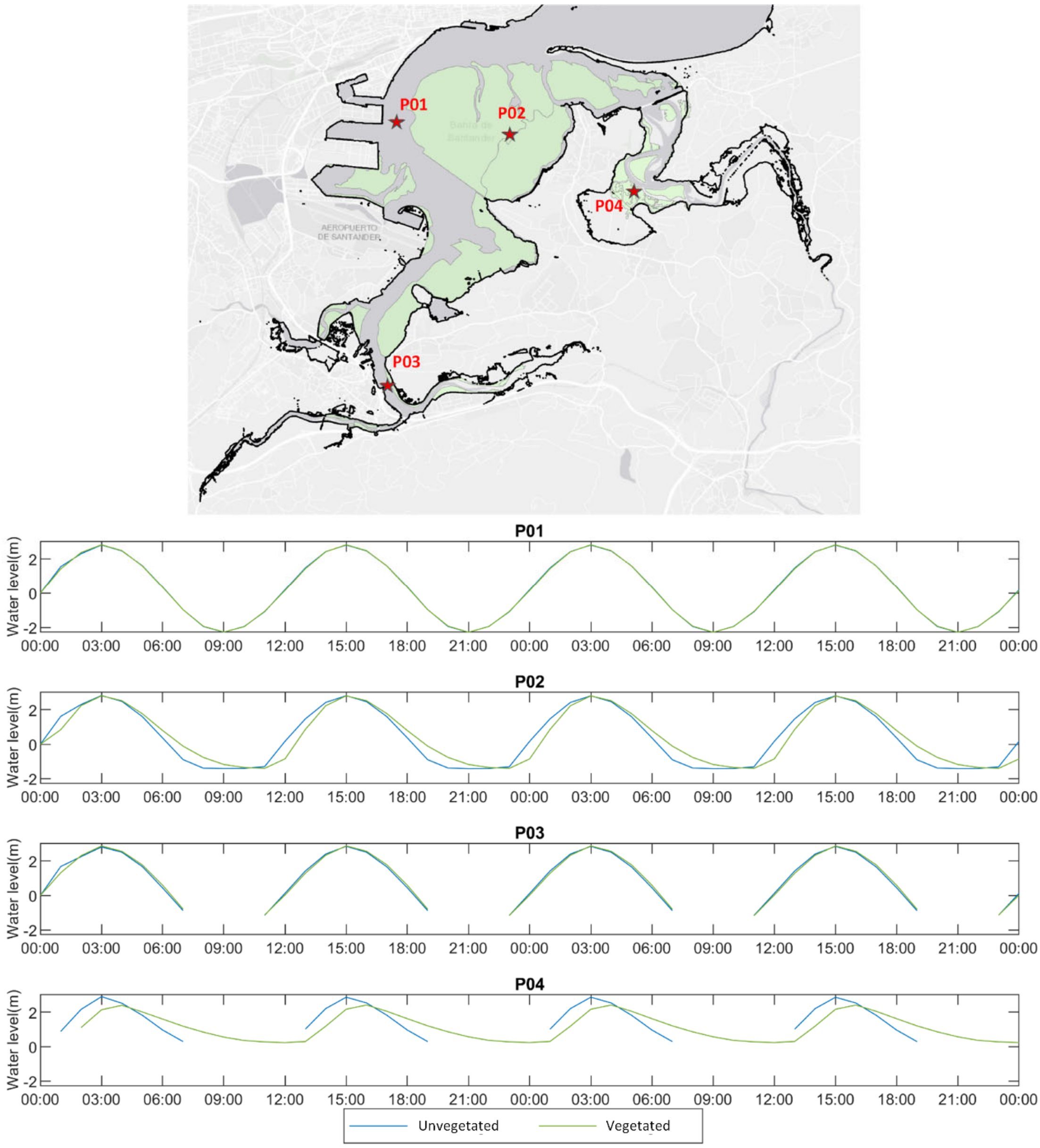

Figure 35. Water level time series in several points in Santander Bay. Comparison: vegetated and unvegetated.

Figure 36 shows the behavior of the tidal wave in the Mondego estuary. As it can be seen, the role of vegetation is not reflected in the tidal wave propagation. Differences of less than 5 cm are shown in the maximum high tide values. The Mondego estuary is the one where the smallest changes are observed under spring tide analysis.

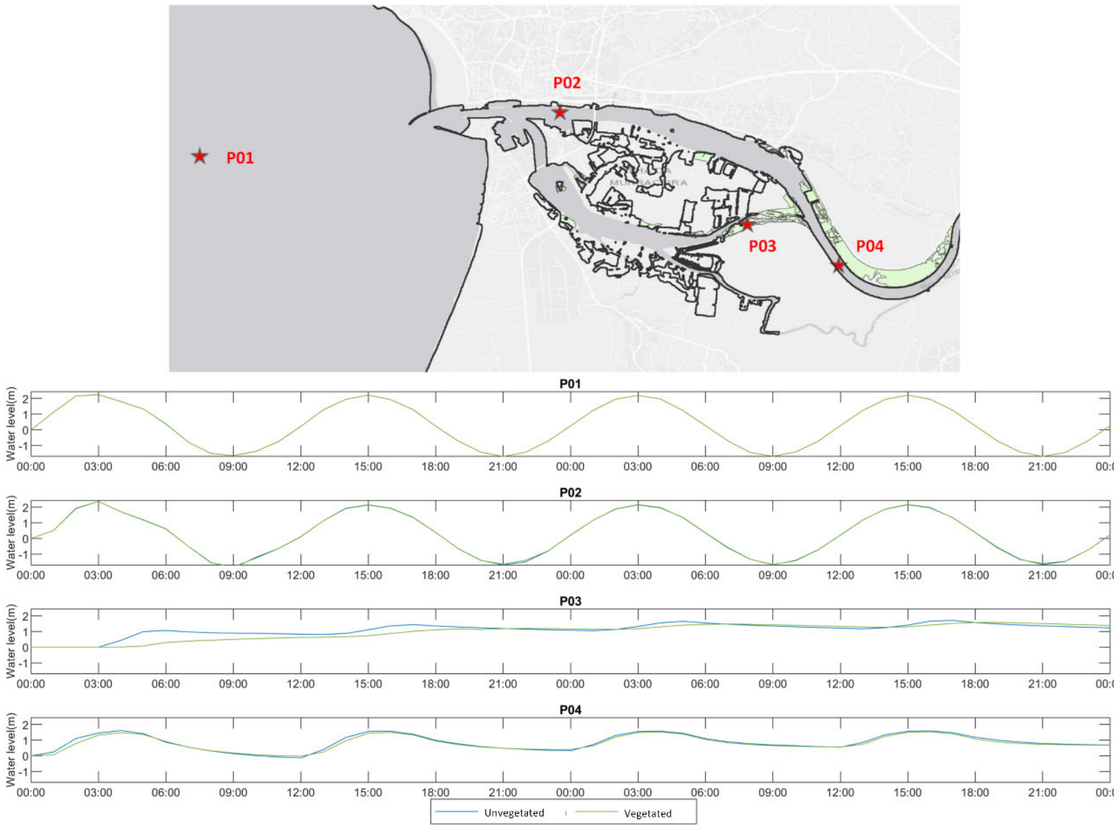

Figure 36. Water level time series in several points in Mondego estuary. Comparison: vegetated and unvegetated.

The coastal protection role that vegetation communities can provide may be due to the reduction in water level and to the attenuation capacity in the velocity fields. Figure 37 shows in its left panel the average of the maximum velocities in a tidal cycle in the bared scenario, in its middle panel the average of the maximum velocities in a vegetated scenario and finally in its right panel the differences between the two scenarios. As it can be observed, intertidal zones are where most of the vegetation species are located and it corresponds to the area where a decrease in the velocity is observed. The decrease in mean velocities in the Santander Bay estuary is around -0.17 m/s, in the Santoña estuary -0.24 m/s, in the Oyambre estuary -0.10 m/s and in the Mondego estuary -0.05 m/s.

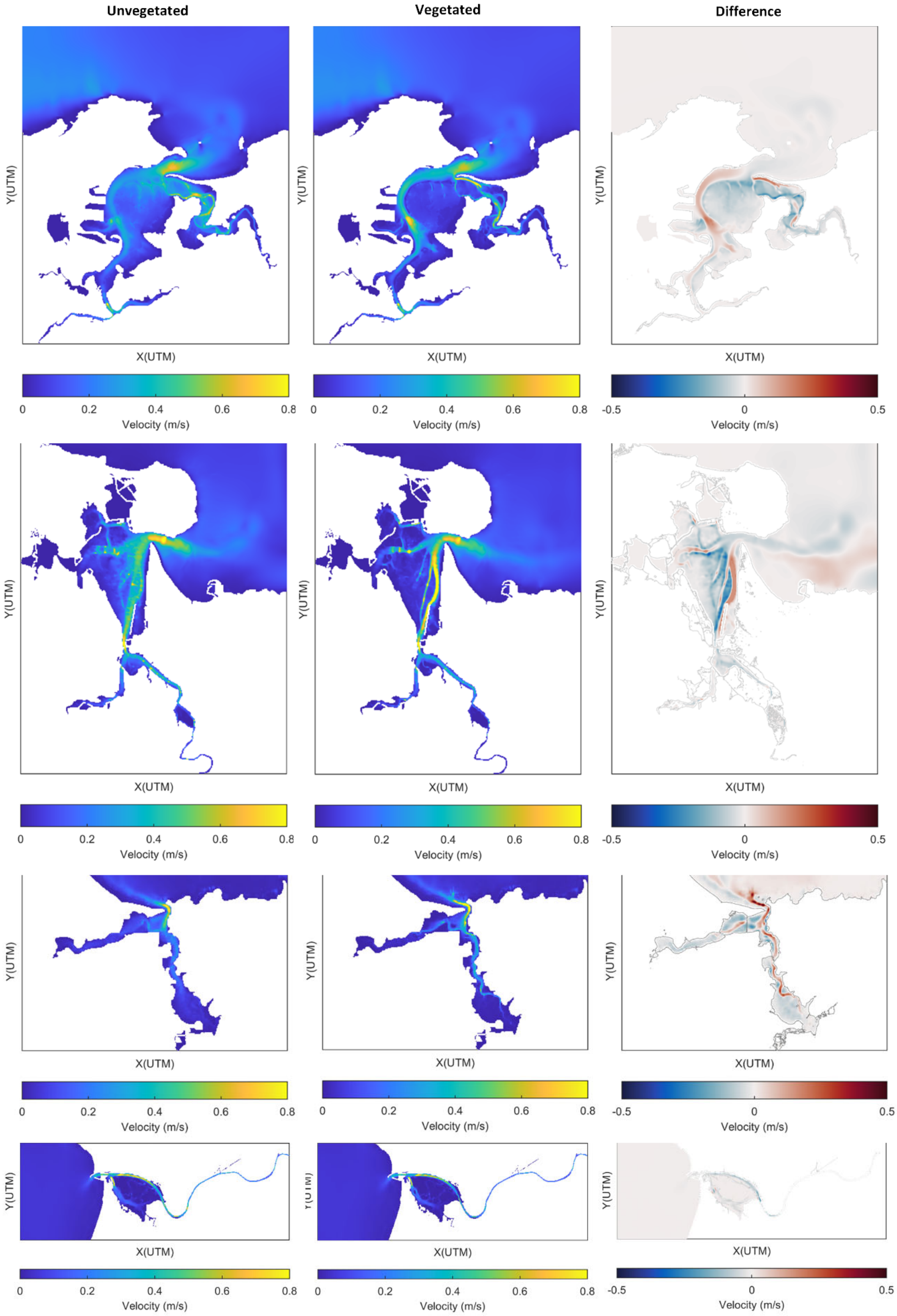

Figure 37. Mean depth averaged velocity (m/s) distribution. unvegetated (left panel) and vegetated (middle panel).

3.2.1 Flood maps

Figures from Figure 38 to Figure 53 show flood maps for return periods (10 and 100 years) of coastal and fluvial dynamics in bared and vegetated scenarios. All results are presented in Annex II

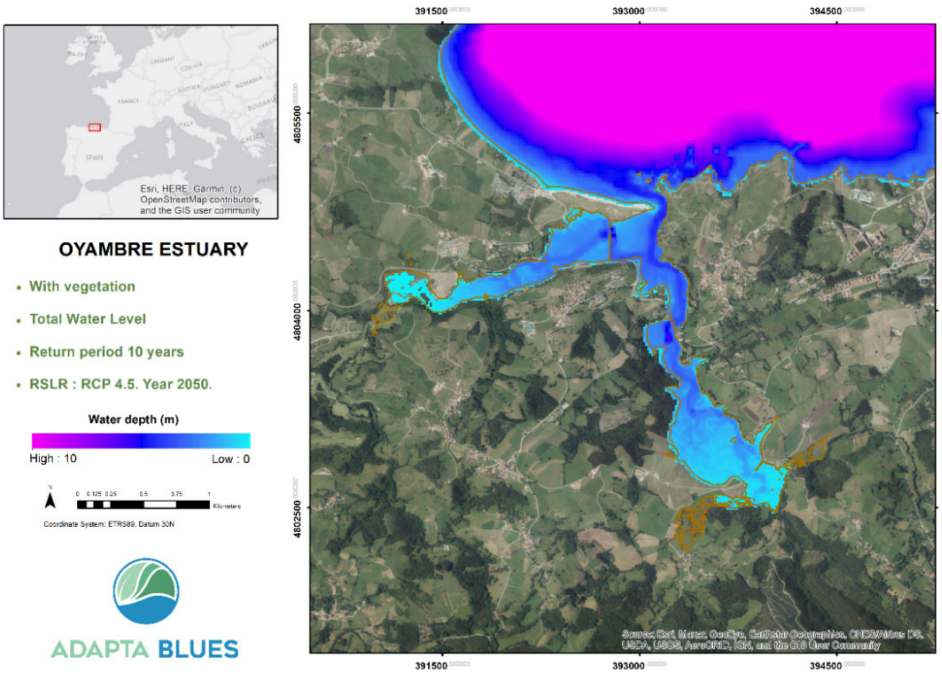

Figure 38. Flood area Oyambre estuary. Scenario: Vegetated. RCP 4.5. Year 2050. Return period= 10 years.

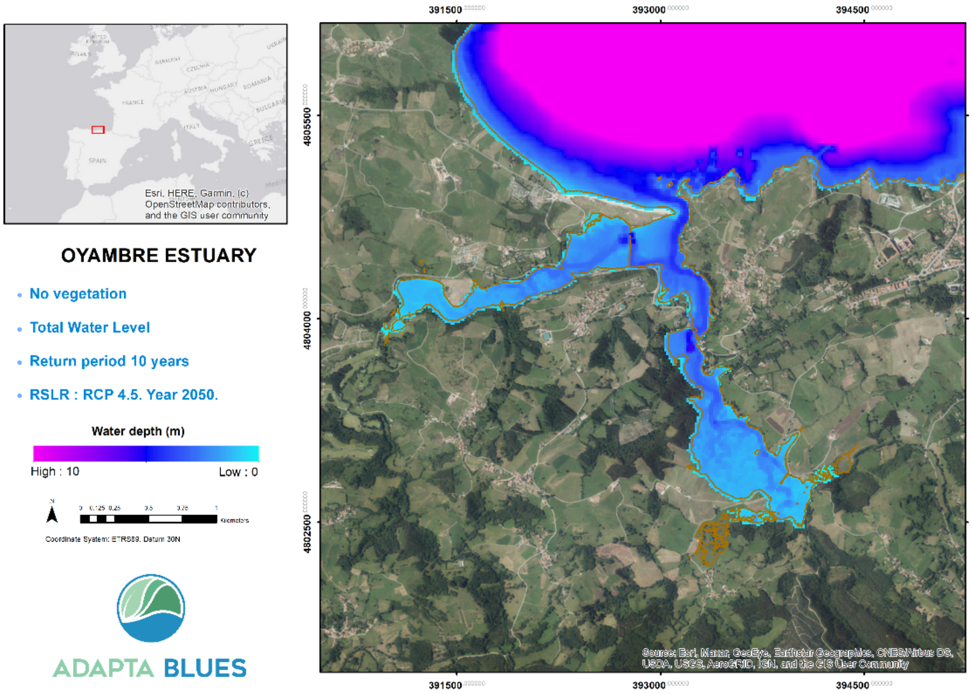

Figure 39. Flood area Oyambre estuary. Scenario unvegetated. RCP 4.5. Year 2050. Return period= 10 years

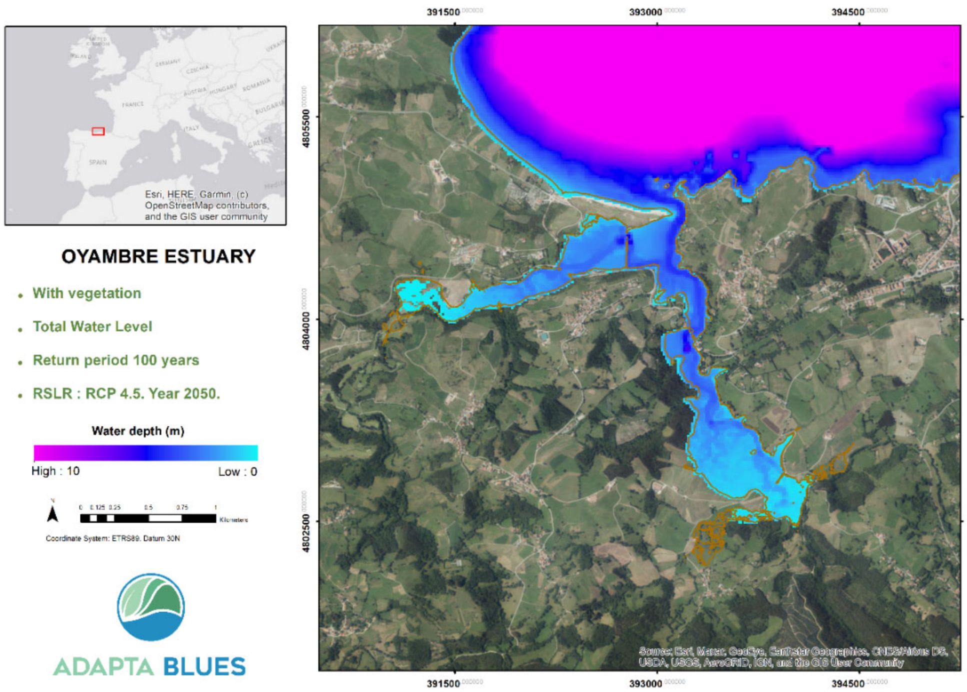

Figure 40. Flood area Oyambre estuary. Scenario vegetated. RCP 4.5. Year 2050. Return period=100 years.

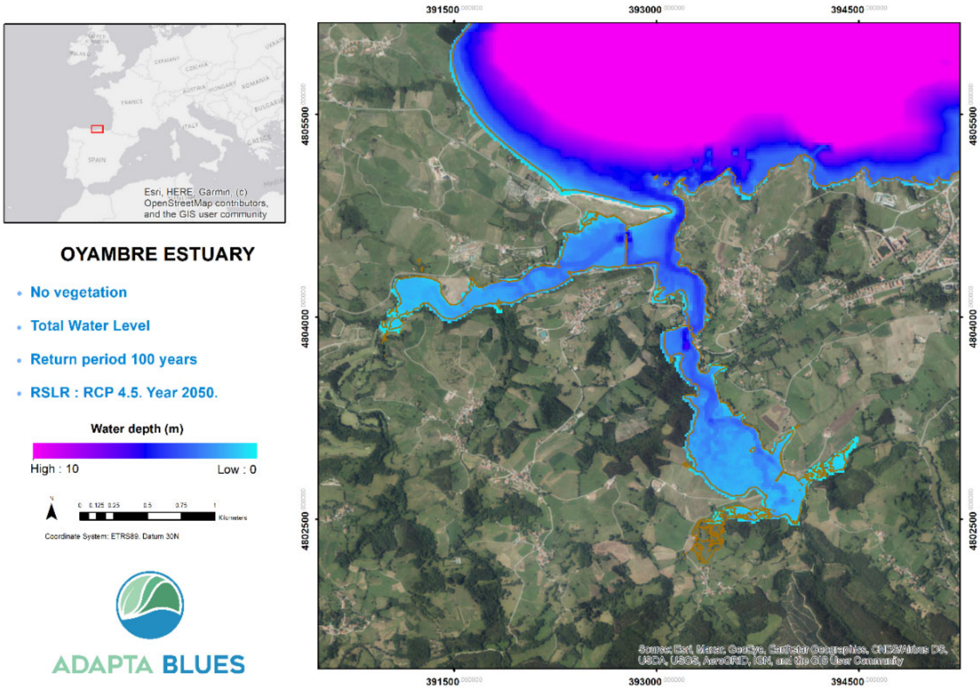

Figure 41. Flood area Oyambre estuary. Scenario unvegetated. RCP 4.5. Year 2050. Return period=100 years.

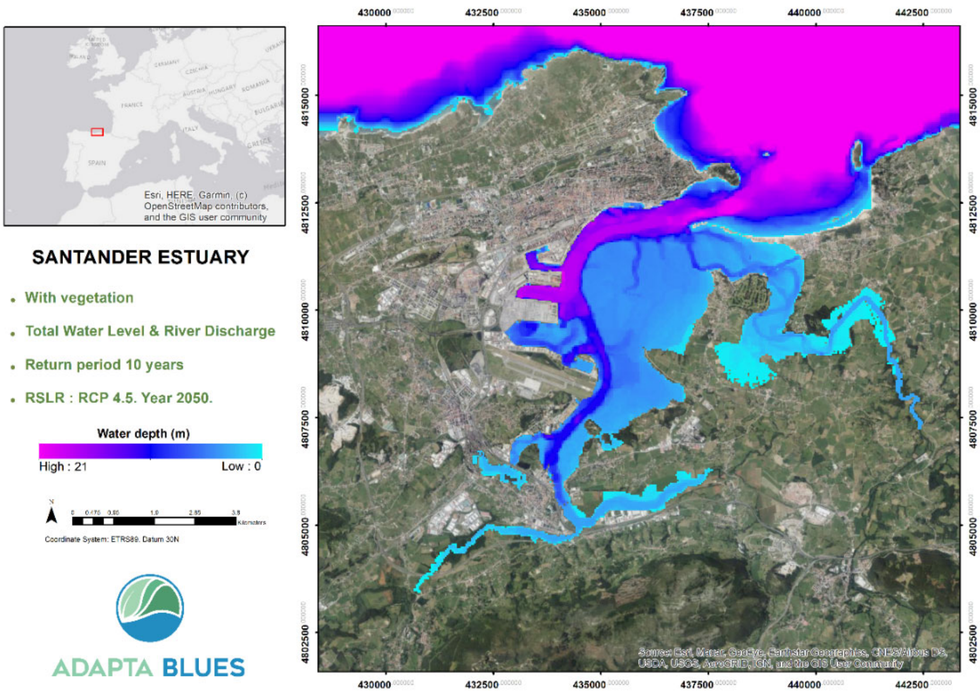

Figure 42. Flood area Santander Bay. Scenario: Vegetated. RCP 4.5. Year 2050. Return period= 10 years.

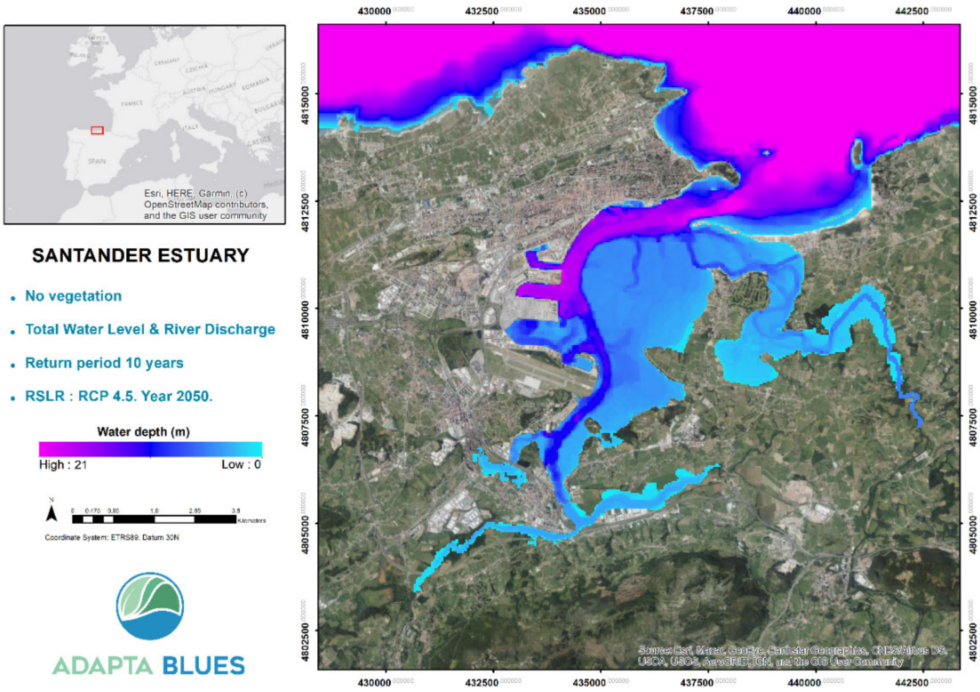

Figure 43. Flood area Santander Bay. Scenario: Unvegetated. RCP 4.5. Year 2050. Return period= 10 years.

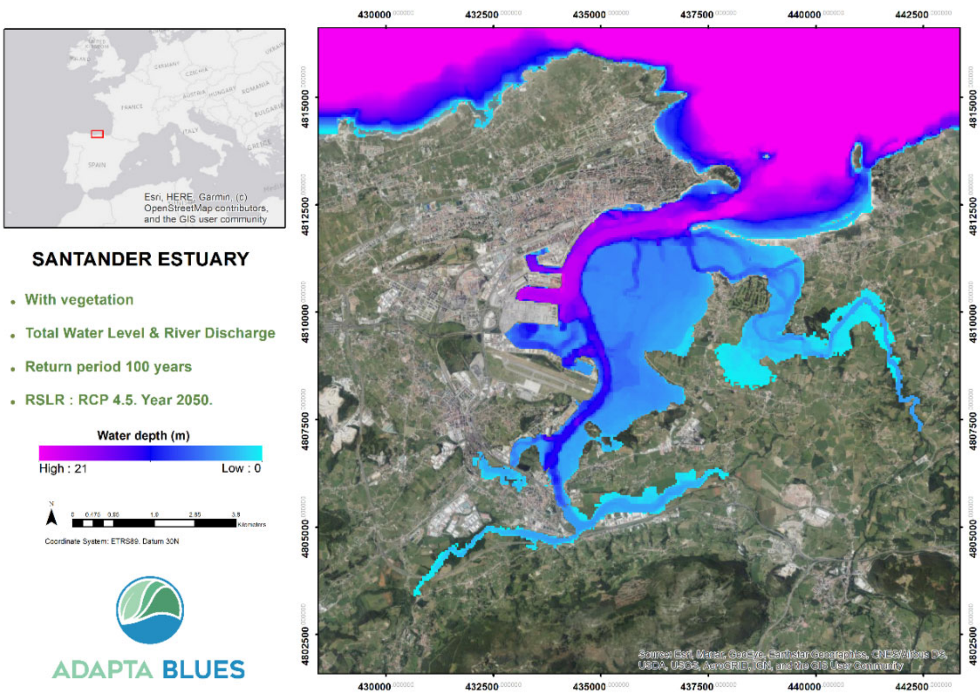

Figure 44. Flood area Santander Bay. Scenario: Vegetated. RCP 4.5. Year 2050. Return period= 100 years.

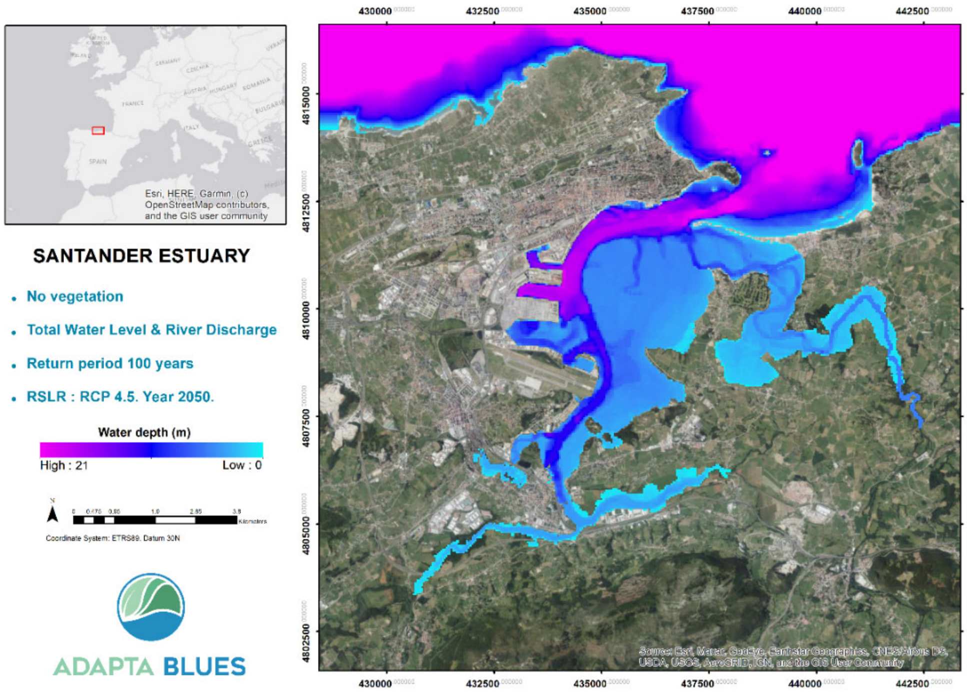

Figure 45. Flood area Santander Bay. Scenario: Unvegetated. RCP 4.5. Year 2050. Return period= 100 years.

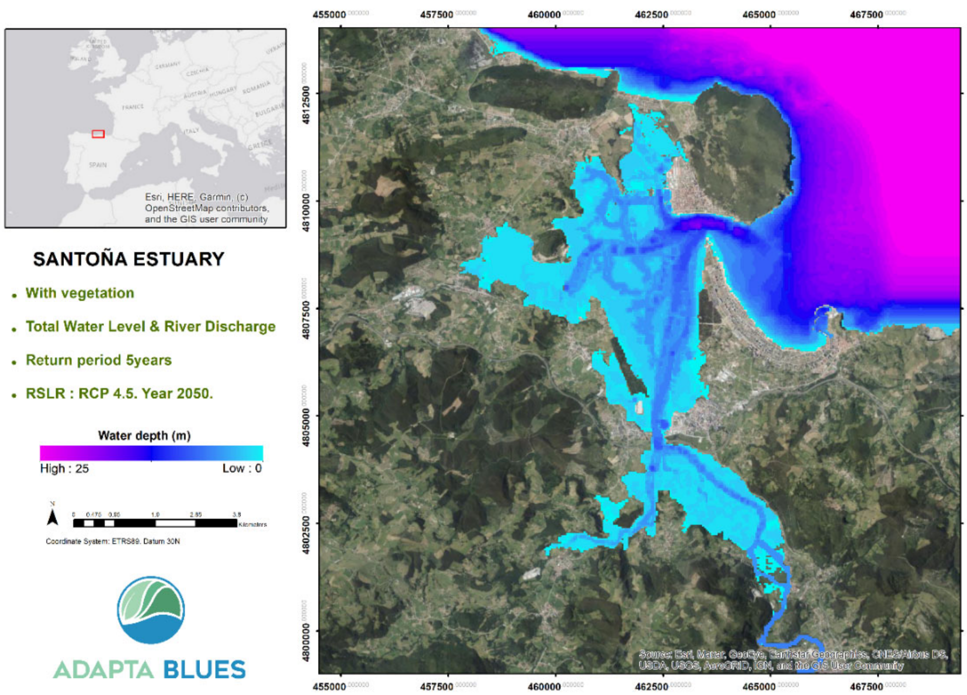

Figure 46. Flood area Santoña marshes. Scenario: Vegetated. RCP 4.5. Year 2050. Return period= 10 years.

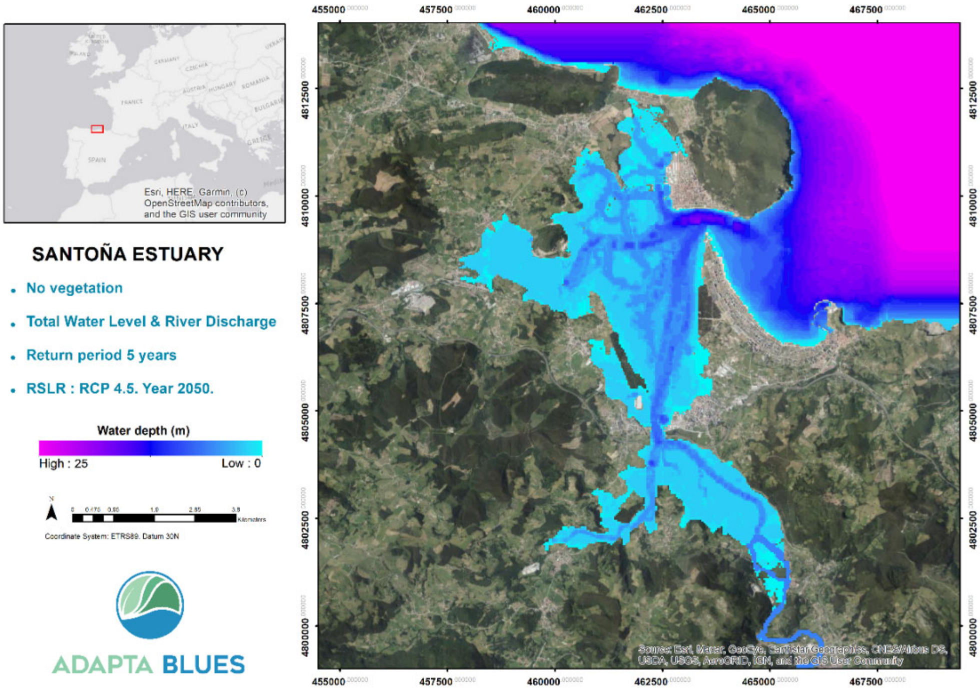

Figure 47. Flood area Santoña marshes. Scenario: Unvegetated. RCP 4.5. Year 2050. Return period= 10 years.

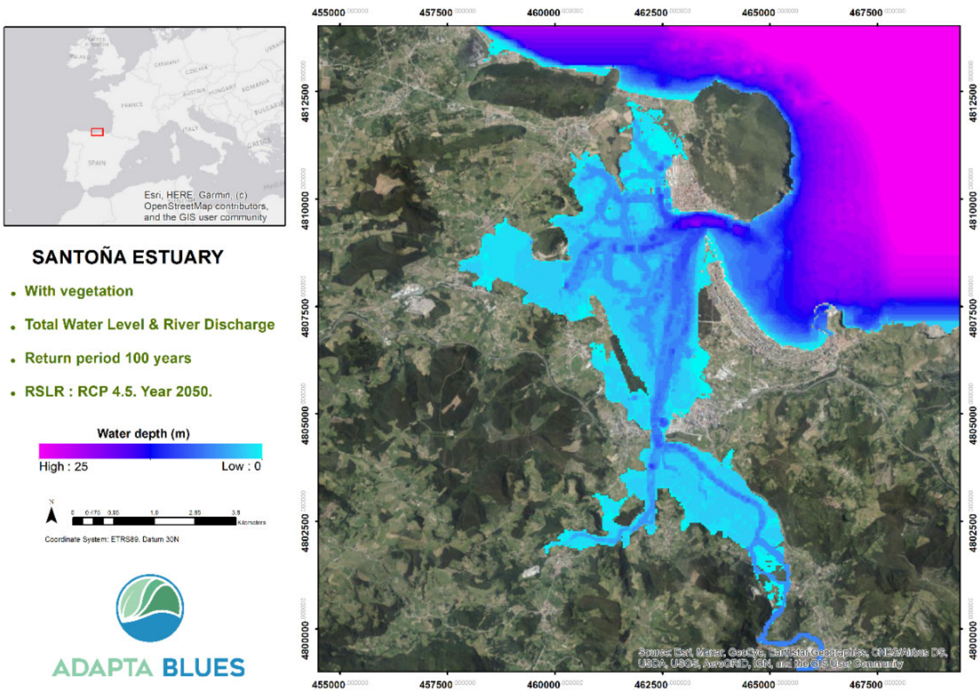

Figure 48. Flood area Santoña marshes. Scenario: Vegetated. RCP 4.5. Year 2050. Return period= 100 years.

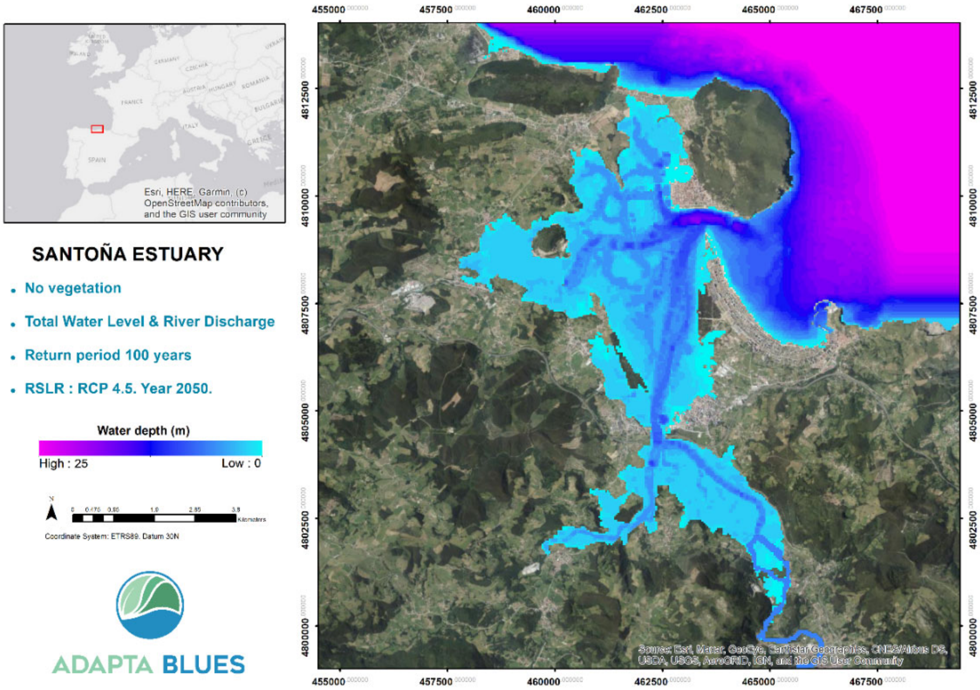

Figure 49. Flood area Santoña marshes. Scenario: Unvegetated. RCP 4.5. Year 2050. Return period= 100 years.

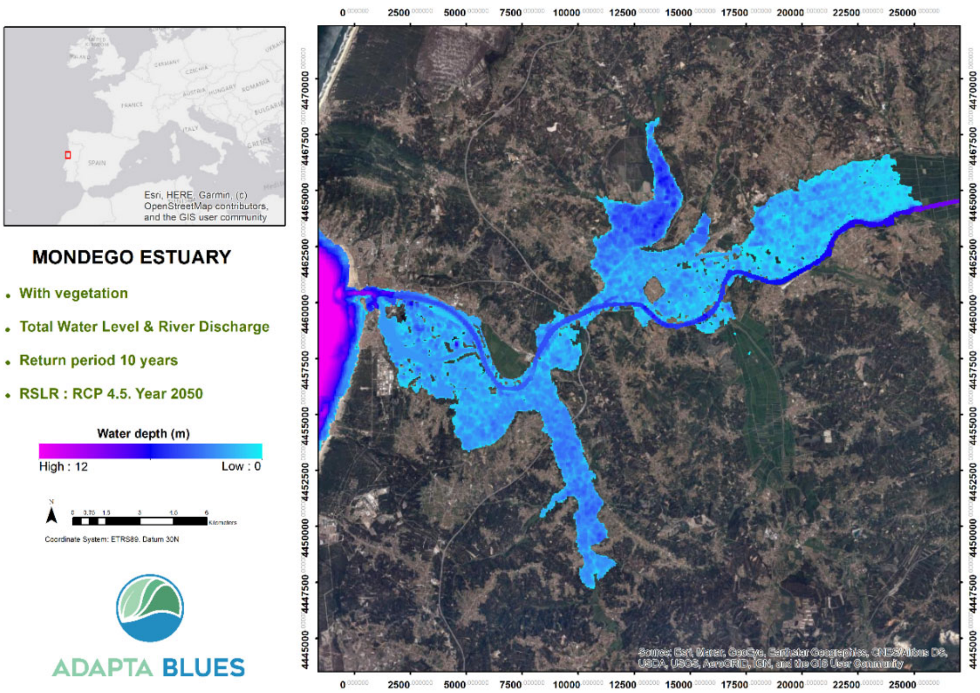

Figure 50. Flood area Mondego estuary. Scenario: Vegetated. RCP 4.5. Year 2050. Return period= 10 years.

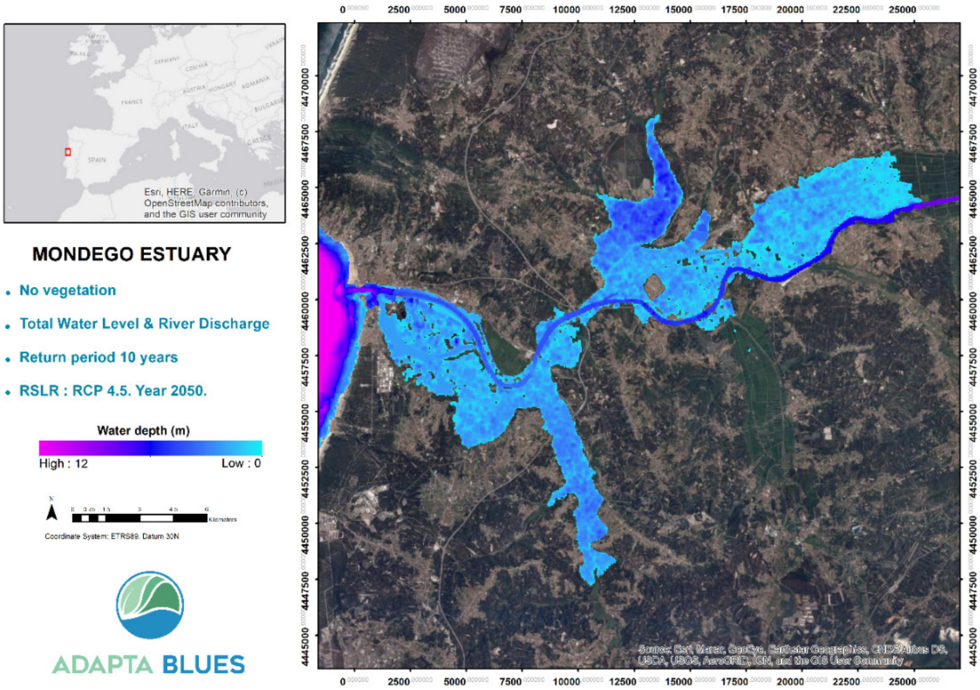

Figure 51. Flood area Mondego estuary. Scenario: Unvegetated. RCP 4.5. Year 2050. Return period= 10 years.

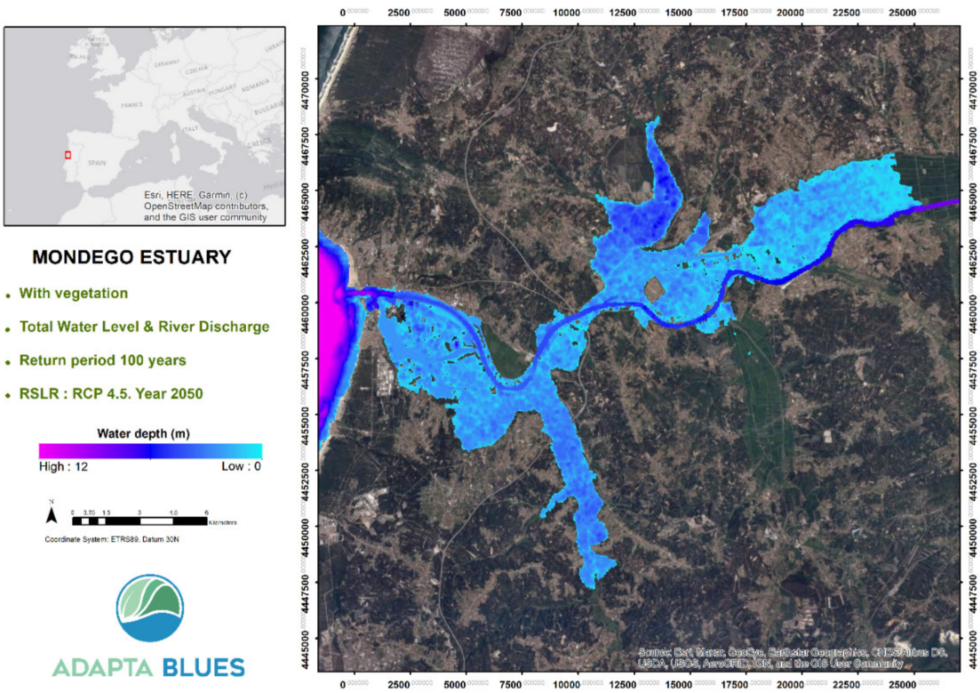

Figure 52. Flood area Mondego estuary. Scenario: Vegetated. RCP 4.5. Year 2050. Return period= 100 years.

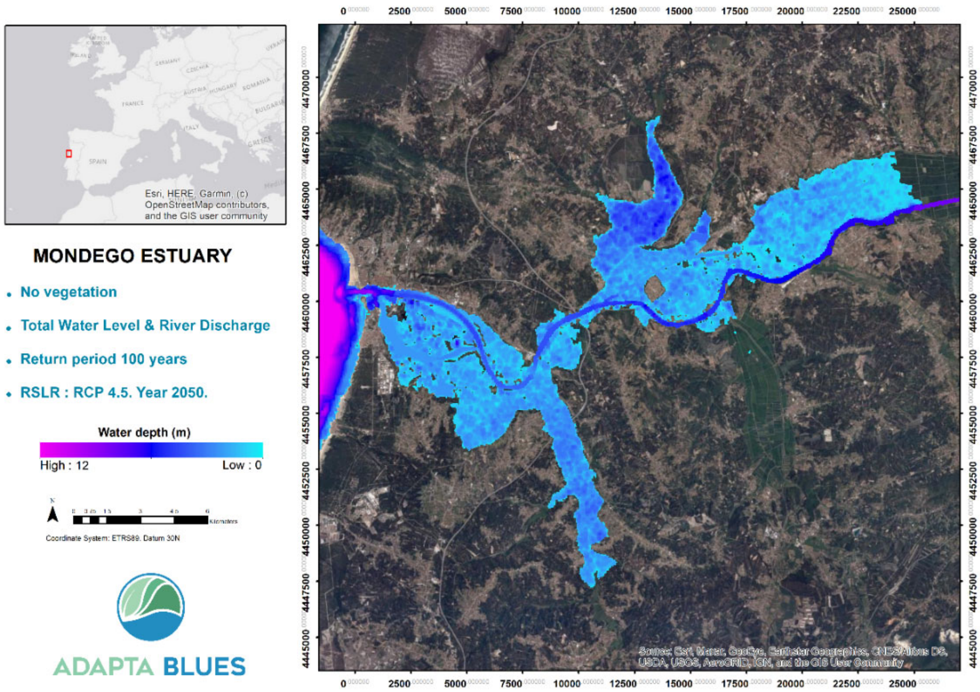

Figure 53. Flood area Mondego estuary. Scenario: Unvegetated. RCP 4.5. Year 2050. Return period= 100 years.

It should be noted that the possible regulation of flow by structures or gates has not been included in this analysis.

Figures from Figure 54 to Figure 57 show the maximum flood area in different climate change scenarios considering coastal and fluvial dynamics for several return periods. Santander Bay and Mondego are the estuaries where the vegetation role in terms of flooding area is less important. Furthermore, these two estuaries show small differences in the area to be flooded regardless of the climate change scenario analyzed. They are the estuaries which are best adapted to climate change.

The estuarine communities with the greatest capacity for protection against flooding are those existing in the estuaries of Oyambre and Santoña marshes. These estuaries are the two estuaries where intertidal habitats dominate. While in Santander Bay and Mondego estuary, subtidal habitats dominate.

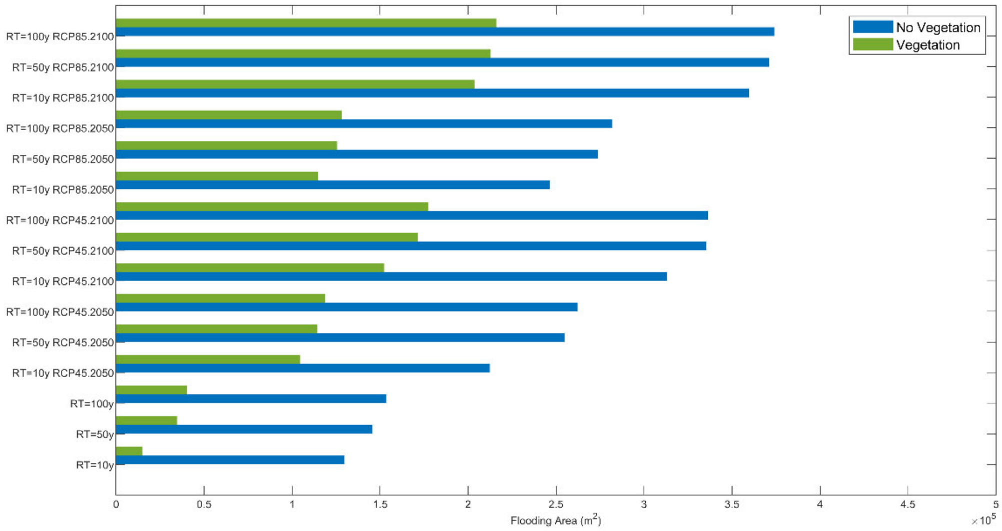

Figure 54. Flood area(m^2) in Oyambre estuary in different Climate Change scenarios

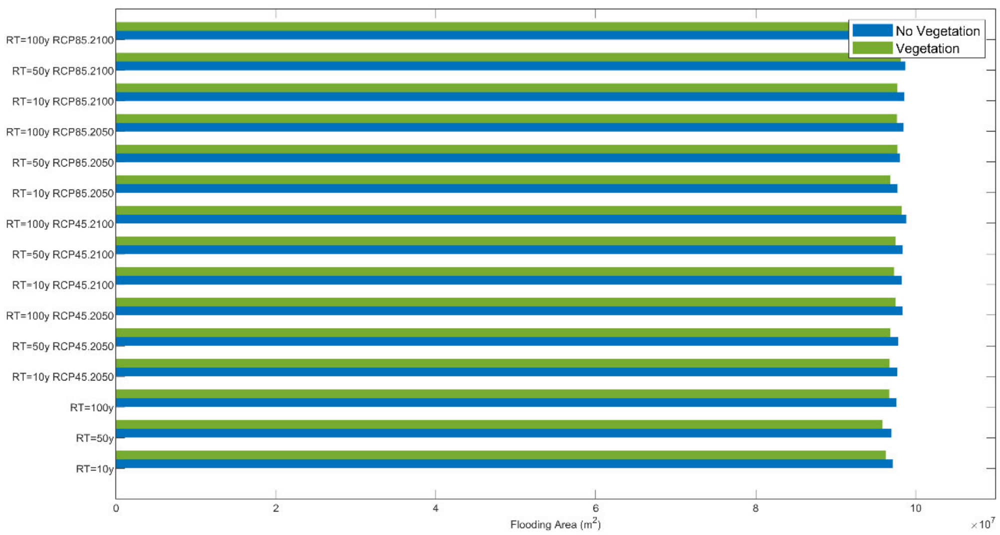

Figure 55. Flood area(m^2) in Santander Bay in different Climate Change scenarios.

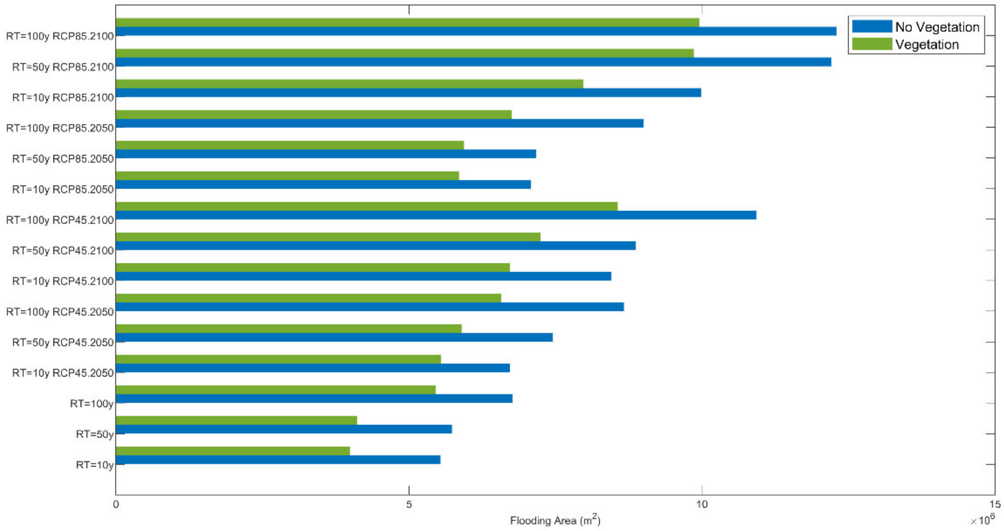

Figure 56. Flood area (m^2) in Santoña Bay in different Climate Change scenarios.

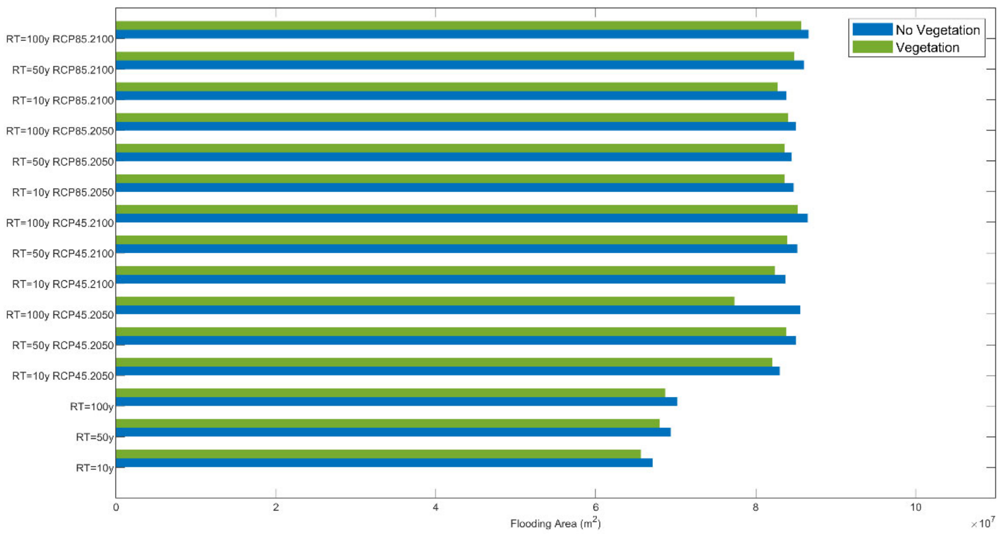

Figure 57. Flood area(m^2) in Mondego estuary in different Climate Change scenarios

Since 2017, the Dutch flood protection legislation establishes the safety standards for dike segments that are defined as the maximum allowed probability of flooding. Standards were set using a risk-based approach that considers the cost of the strengthening and the potential consequences of a flood. Although it is not the objective of this study to analyze the probability of failure of the dikes that protect the margins of the Western Scheldt estuary, this section aims to show the potential protective effect of vegetated foreshores in front of coastal dikes. This topic has only received limited attention in the literature, despite of the potential of this type of ecosystems to directly affect the flood risk in the area behind the flood defense (Vuik, 2016). Figure 58 shows the scheme for a dyke – foreshore system.

The presence of a vegetation foreshore influences the likelihood of dike breaching due to wave overtopping. Vuik, 2016 concludes that for small water depths, wave run-up is reduced by 60-100%, and the wave overtopping discharge diminishes until becoming negligible. For larger water depths, the influence of vegetation becomes more distinct, wave run-up under these conditions is only reduced by approximately 20% (0.6 m) for a 400 m wide, bare foreshore. The same foreshore covered by vegetation, resembling Spartina anglica, in winter state reduces the wave run-up by 55% (1.8 m).

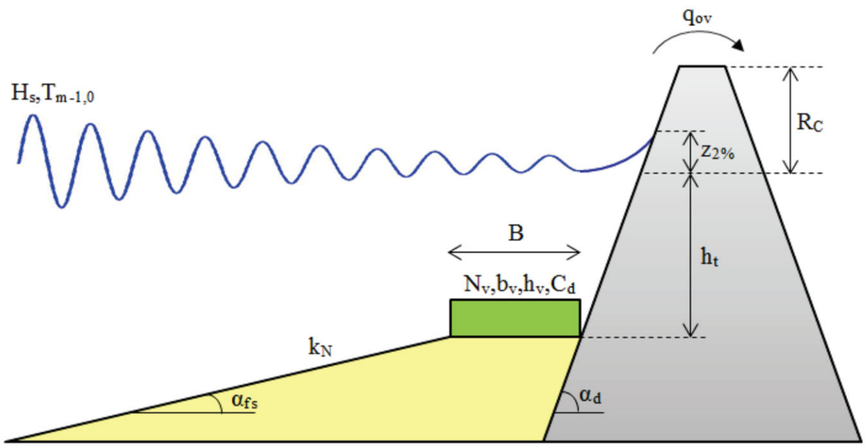

Figure 58.Source: Vuik, 2016. Definition sketch of a schematized dike-foreshore system: α_d *slope angle dike, RC Relative freeboard*, α_{fs} slope angle tidal flat, h_t *water depth at dike toe,* H_{m0} *offshore significant wave height,* $T_{m-1,0}$ *offshore spectral wave period,* k_N *Roughness length scale, B Width of flat part of foreshore,* N_v *stem density,* b_N*, stem diameter, hv vegetation height, Cd Bulk drag coefficient vegetation,* $Z_{2\%}$ *two percent wave run-up height,* q_{ov} *mean overtopping discharge.*

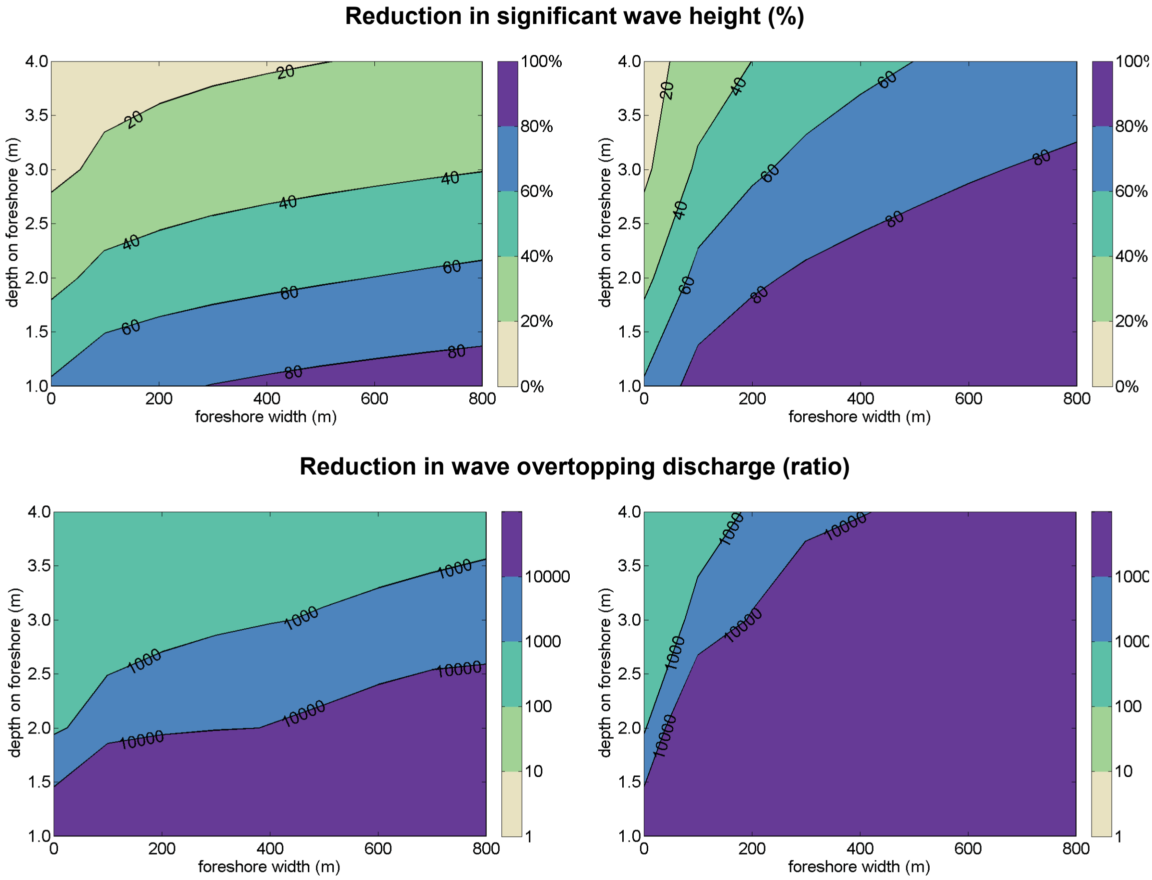

Figure 59. Source: Vuik, 2016. Relative reduction in significant wave height (top), and reduction factor in wave overtopping discharge (bottom), in case of bare foreshores (left panels) and vegetated foreshores (right panels).

Wave overtopping discharges still have significant values for bare foreshores in case of large water depths, whereas the presence of vegetation fully prevents the occurrence of overtopping. As concluded by Vuik, 2016 nature-based flood defenses can be considered as full alternatives for conventional flood defense, they need to be tested according to engineering standards for probability of failure (Van Wesenbeeck et al, 2014).

This analysis has been developed in the framework of the BE SAFE project which is financed by the Netherlands Organization for Scientific Research (NWO).

3.2.2 Erosion – Sedimentation patterns

The reduction in velocity field in the area where estuarine communities are develop causes an increase in sedimentation capacity and therefore may cause an increase the of bed level . Figure 60 shows the topographic distribution in the two scenarios analyzed in each estuary. The left-hand panel shows the unvegetated scenario. The middle panel shows the vegetated scenario, while in the right-hand panel shows the differences between the two scenarios. The main changes are observed in those areas where the changes in velocity field are more important.

Figure 61, shows the average change in the bed caused by each type of community. Nevertheless, it should be noted that the profile zonation of the different species can affect the trapping capacity of each one of them. In other words, all the analyses carried out in the different study zones show the three-dimensional interactions of all the communities simultaneously.

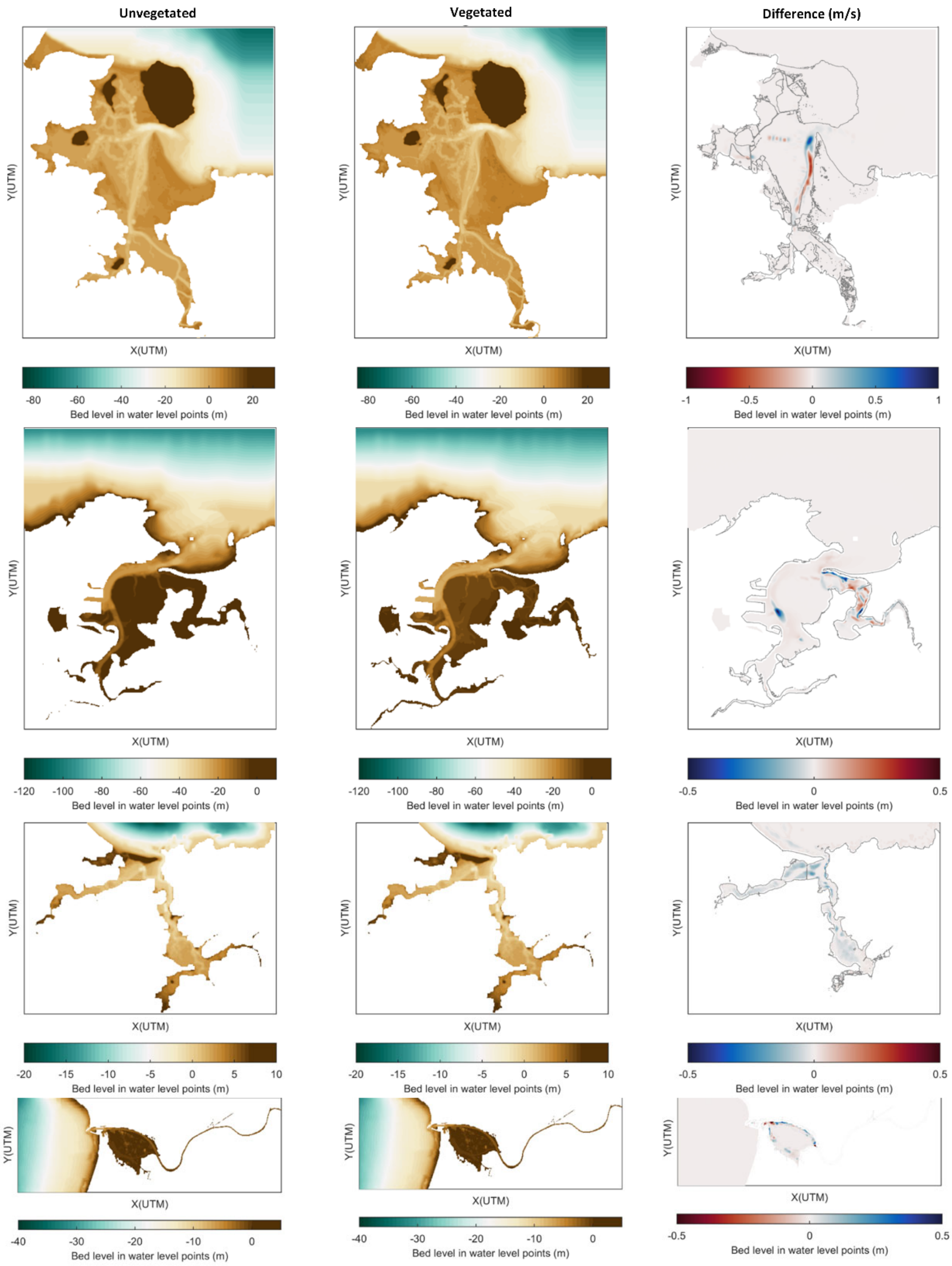

Figure 60. Bed level change (m) distribution. Comparison: unvegetated (left panel) and vegetated (middle panel).

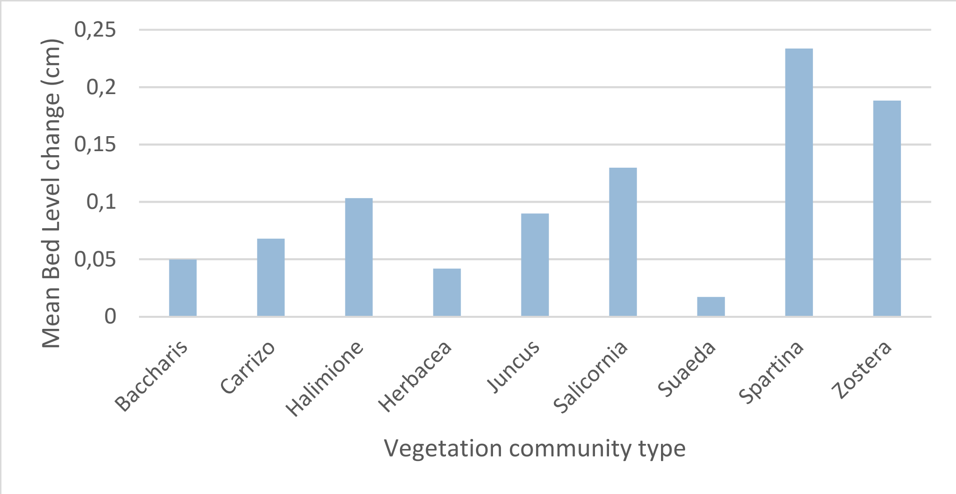

Figure 61. Averaged bed level change provided by vegetation communities.

3.2.3 Quantification of coastal protection provided by estuarine vegetation

The quantification of coastal protection of estuarine vegetation is obtained from the methodology described in section 2.2.4. The results obtained have been annualized for all the analyzed scenarios. Raw data are shown in Annex III.

Table 16 shows the quantification of the role of estuarine vegetation in Santander Bay. Table 16 shows exposed population and building area affected by flooding events, in the bared and vegetated scenarios. As can it can be seen, all scenarios show a decrease in the exposed population, regardless of the climate scenario analyzed. The population exposed decreases between a 2.9%-12.32% for scenarios RCP4.5 and it can be observed a decrease between 2.8%-6.5% in the RCP8.5 scenarios.

Santander estuary					
	Present	Year 2050		Year 2100	
		RCP45	RCP85	RCP45	RCP85
	Affected population (in person)				
Vegetated	434.935	512.705	534.34	519.13	581.295
Unvegetated	472.735	528.15	549.74	592.06	621.745
	2.80%	**2.92%**	**2.80%**	**12.32%**	**6.51%**
	Building affected (m^2)				
Vegetated	152077548	168426517	170971355	170978855	210172024
Unvegetated	173007867	176739893	178911203	194012321	215678536
	12.10%	**4.70%**	**4.44%**	**11.87%**	**2.55%**

Table 16. Exposed population and buildings in Santander Bay.

¡Error! No se encuentra el origen de la referencia. shows the exposed population in the Oyambre estuary. The population exposure decreases between 10%-12% it is observed for scenarios projected to 2100 year. Table 18 shows the exposed population in the Santoña estuary. The population exposure decreases by 31% - 44% for the RCP4.5 scenarios and a decrease between 29% - 39% is observed in the RCP8.5 scenarios. In the Mondego estuary (Table 19), the population exposure decreases by 1.60% - 2.18% for the RCP4.5 scenarios and a decrease between 1.78% - 2.48% in the RCP8.5 scenarios.

Oyambre estuary					
	Present	Year 2050		Year 2100	
		RCP45	RCP85	RCP45	RCP85
	Population exposed				
Vegetated	14.27	14.5	14.5	14.5	15.08
Unvegetated	14.27	14.5	14.56	16.53	16.82
	0.00%	**0.00%**	**0.41%**	**12.28%**	**10.34%**
	Infrastructure exposed (area m2)				
Vegetated	6319527.79	6351997.95	6351997.95	6351997.95	6426968.02
Unvegetated	6334532.66	6352680.47	6371745.46	7160423.56	7191318.05
	0.24%	**0.01%**	**0.31%**	**11.29%**	**10.63%**

Table 17. Exposed population and buildings in Oyambre estuary.

Santoña estuary					
	Present	Year 2050		Year 2100	
		RCP45	RCP85	RCP45	RCP85
	Affected population (in person)				
Vegetated	403.12	548.54	586.295	965.35	2439.455
Unvegetated	589.26	795.23	828.095	1724.665	4036.9
	31.59%	**31.02%**	**29.20%**	**44.03%**	**39.57%**
	Building affected (m^2)				
Vegetated	100159095	122009873	128785149	207605301	390088132
Unvegetated	131383628	158944289	169045407	319387555	613772824
	23.77%	**23.24%**	**23.82%**	**35.00%**	**36.44%**

Table 18. Exposed population and buildings in Santoña marshes.

Mondego estuary					
	Present	Year 2050		Year 2100	
		RCP45	RCP85	RCP45	RCP85
	Population exposed				
Vegetated	207.89	253.78	271.09	256.99	301.9
Unvegetated	214.88	259.445	275.505	261.65	309.575
	3.25%	**2.18%**	**1.60%**	**1.78%**	**2.48%**
	Infrastructure exposed (area m2)				
Vegetated	6439393	7860836	8397013	7960265	9351353
Unvegetated	6655908	8036309	8533767	8104609	9589086
	3.25%	**2.18%**	**1.60%**	**1.78%**	**2.48%**

Table 19. Exposed population and buildings in Mondego estuary.

Comparison between estuaries is shown in Figure 62. In this figure the changes of exposed population (%) in the comparison of vegetated and unvegetated estuaries is represented. The estuary for which the greatest protective role of all vegetation can be seen is the Santoña estuary. On the other hand, in the Mondego estuary and the Santander Bay the percentage of changes between vegetated and unvegetated decrease. The same pattern of behaviour is observed in the area affected by flooding on infrastructures and buildings (Figure 63).

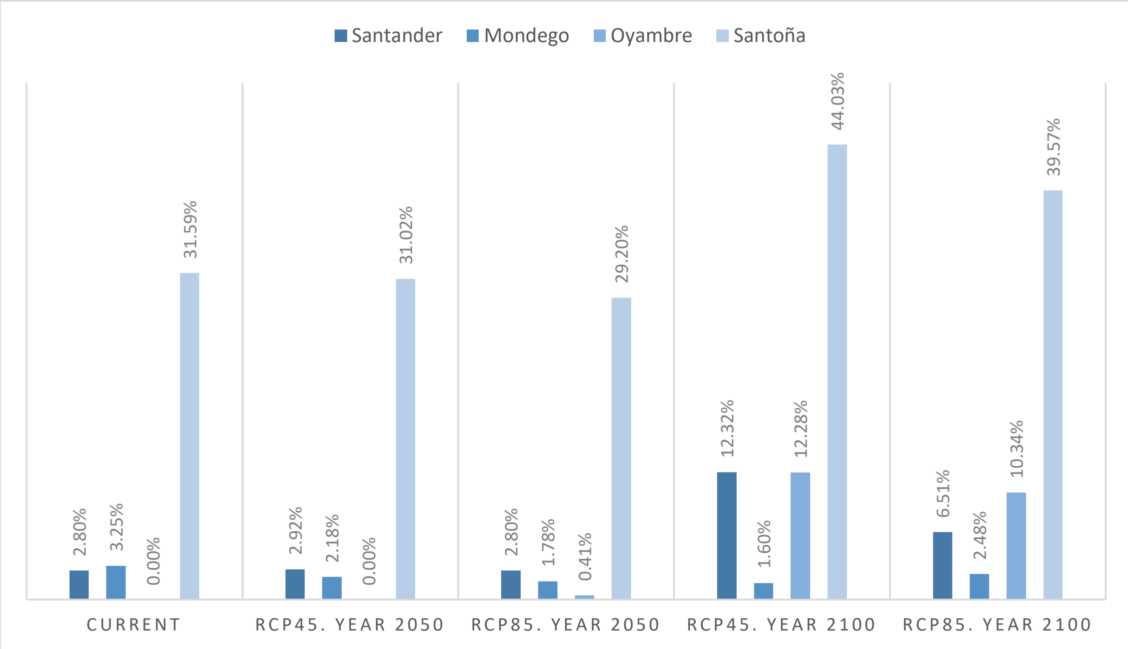

Figure 62. Exposed population changes (%) in the comparison of vegetated and unvegetated estuaries.

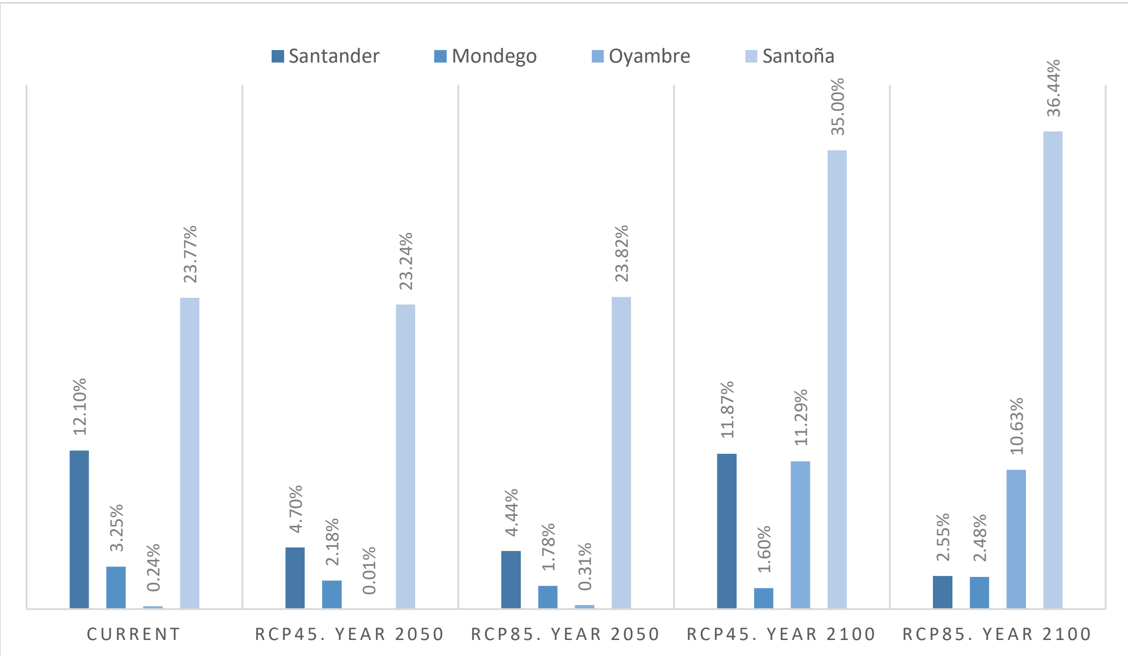

Figure 63. Exposed building area changes (%) in the comparison of vegetated and unvegetated estuaries.

Table 20 shows the consequences on the stock building and on the number of people protected by estuarine ecosystems. The Santoña estuary is the estuary that provides the greatest number of protections in terms of the number of people affected by flood events. The communities of the Mondego and Santander Bay estuaries show that the population protection capacity provided by the vegetation in these estuaries is reduced despite the fact that they are estuaries with a high population development on their margins. This fact shows that they are much more adapted to flooding events derived from climate change. The communities present in the Oyambre estuary protect a small number of people as it is an estuary that does not have a high level of urban development on its margins.

Regarding the economic stock that the existence of the estuarine communities represents, it can be seen that the communities of the Santoña marshes are the ones that generate the greatest protection in economic terms when compared to the communities of Mondego and Oyambre. Table 20 shows the value in €/ha of the protection value of these communities.

	Annual Protection Value. Nº People				
	Current	RCP45. Year 2050	RCP85. Year 2050	RCP45. Year 2100	RCP85. Year 2100
Santander	38	15	15	73	40
Oyambre	0	0	0	2	2
Santoña	186	247	242	759	1597
Mondego	7	6	5	4	8
	Annual Protection Value. Infrastructure exposed (€/ha)				
	Current	RCP45. Year 2050	RCP85. Year 2050	RCP45. Year 2100	RCP85. Year 2100
Santander	19248	7645	7302	21183	5064
Oyambre	235	11	309	12661	11971
Santoña	33881	40076	43685	121292	242713
Mondego	1423	1153	949	899	1563

Table 20. Annual Protection Value in People exposed and infrastructure value.

3.3 Carbon sequestration

3.3.1 Magnitude of soil C_{org} and CO_2 deposits

Across dominant species and habitats

The estuarine communities examined store an average of 50 ± 2 Mg C_{org} ha^{-1} in the top 30 of the soil, ranging from 3-100 Mg C_{org} ha^{-1} (Annex I), that equivalate to an average of 183 Mg CO_2 ha^{-1} sequestered in the soil compartment (12-368 Mg CO_2 ha^{-1}). The magnitude of soil C_{org} deposits and thus the amount of CO_2 sequestered per surface area vary across the communities examined according to the dominant species (Figure 64) and habitat type (Figure 65).

The largest stocks in the top 30 cm of sediment per surface area (65-100 Mg C_{org} ha^{-1}. 226-368 Mg CO_2 ha^{-1}) were found in communities dominated by large species, usually allocated in the high marsh zone, such as *Halimione spp.*, *Juncus spp.*, *Phragmatis spp.* and the invasive species *Baccharis halimifolia*. Communities formed by smaller size species, such as *Spartina spp*. and *Sarcocornea spp*., that develop in the low marsh level showed lower stocks per surface area (21-45 Mg C_{org} ha^{-1}, 76-164 Mg CO_2 ha^{-1}), comparable to those found in intertidal unvegetated mudflat and sandflat soils or occupied by intertidal seagrass meadows (*Zostera spp.*) (40-46 Mg C_{org} ha^{-1}, 136-147 Mg CO_2 ha^{-1}).

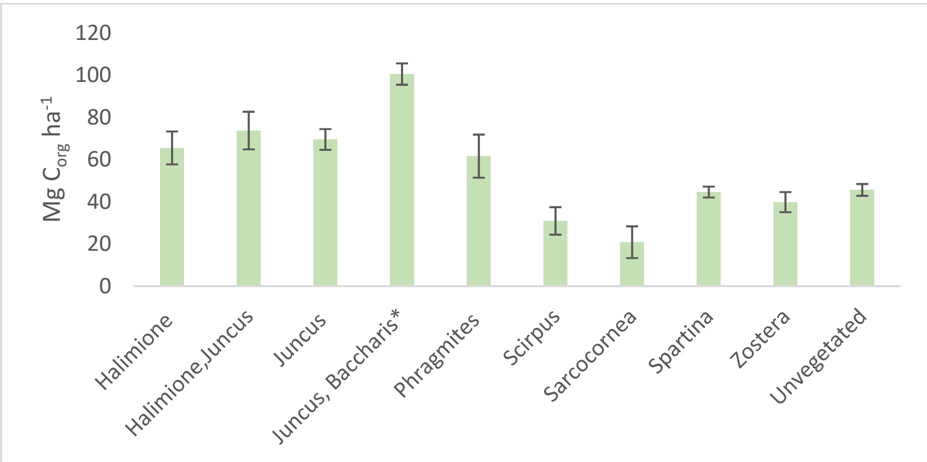

*Figure 64. Average (± SE) of top 30 cm soil C_{org} stocks across dominate species in the estuarine communities examined. *Invasive species*

In particular the largest stocks were found in an inner area within one of the branches of the Oyambre estuary (Ría de Capitan), occupied by high marsh species (e.g. *Juncus spp.*) but with a high incidence of the invasive species *Baccharis halimifolia*, a small tree species, native from north America, that has expanded in coastal and estuarine areas in the Bay of Biscay particularly where the natural tidal regime has been altered and salinity is reduced (Caño et al., 2013). It is known to cause negative impacts in formerly open habitats such as *Juncus maritimus* (i.e. habitat 1330) and *Halimione portulacoides* (i.e. habitat 1420) leading to a decrease in species richness and herbaceous cover and threating associated organisms (e.g. birds) by modifying habitat quality (Fried et al., 2016). Its particular structural characteristics, such as its larger size (compared to autochthonous estuarine species) and biomass, that enhance sediment trapping, and its lignified tissues that protect biomass from decomposition and remineralization could explain the largest soil C_{org} stock found in the area colonized by this invasive species. Yet, site characteristics such as the location within the estuary, the presence of large estuarine species (e.g. *Juncus maritimus* and *Halimione portulacoides*) or the hydrological regime might also favour the accumulation of large soil C_{org} stocks in this area of the Oyambre estuary. In order to understand if carbon sequestration ecosystem service could be enhanced under the colonization of *Baccharis halimifolia* a deep assessment should be carried out, encompassing a broader spectrum of estuaries and locations with each estuary.

Among estuarine habitats, habitat 1330 (Atlantic salt meadows) is the one showing the highest stocks per surface area (73 ± 5 Mg C_{org} ha^{-1}, 267 ± 17 Mg CO_2 ha^{-1}) followed by the habitat 1420 (Mediterranean and thermoatlantic halophilus scrubs) (57 ± 7 Mg C_{org} ha^{-1}, 210 ± 25 Mg CO_2 ha^{-1}) (Figure 65). The habitat 1320 (*Spartina* swards) showed a similar average C_{org} stock per surface area (45 ± 3 Mg C_{org} ha^{-1}, 164 ± 9 Mg CO_2 ha^{-1}) than habitats 1140 (Mudflats or sandflats not covered by seawater in low tide) and 1130 (Estuaries) (39-44 Mg C_{org} ha^{-1}, 142-161 Mg CO_2 ha^{-1}).

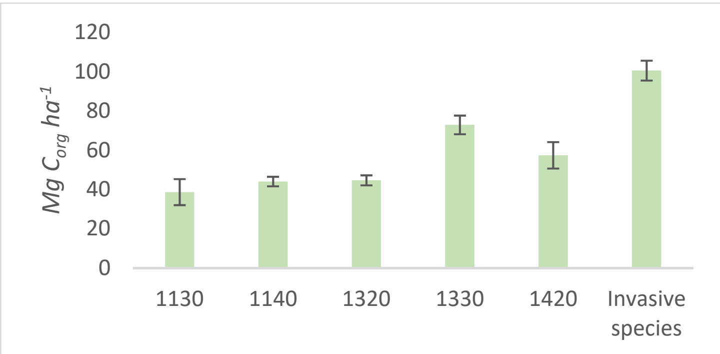

Figure 65. Average (± SE) of top 30 cm soil C_{org} stocks per surface area across habitats in the estuarine communities examined.

Within each estuary, the magnitude of the C_{org} stocks and CO_2 sequestered was also different across habitats (Figures 66-70). Habitats 1330 and 1420 tend to be the ones showing the largest stocks, followed by habitat 1320. Habitats 1140 and 1130 showed, in general, lower stocks per surface area in each of the estuaries of study. In the estuary of Oyambre the largest stocks were found in the area occupied by *Baccharis halimifolia* (Figure 66).

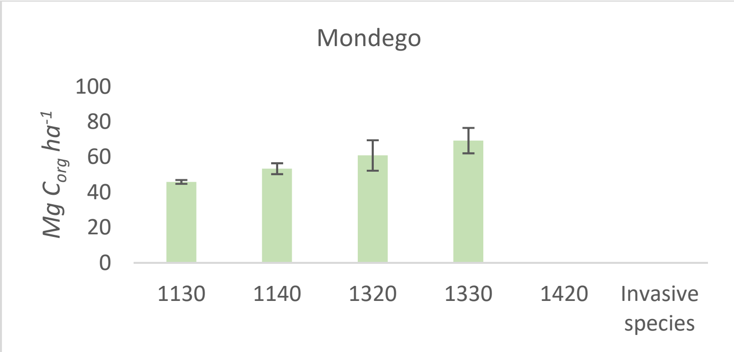

Figure 66. Average (± SE) of top 30 cm soil C_{org} stocks per surface area across habitats in the Mondego estuary. Habitats with no bars were not examined in this estuary.

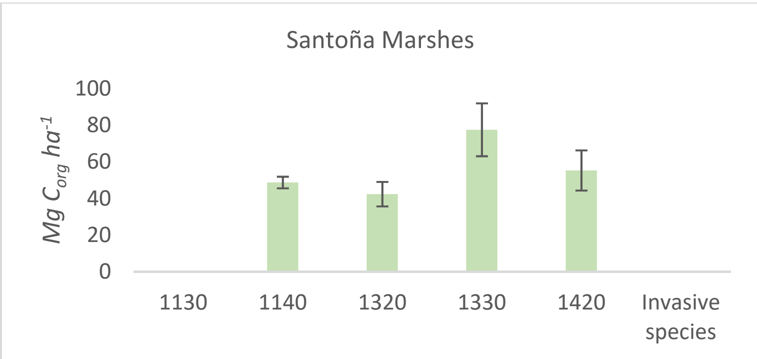

Figure 67. Average (± SE) of top 30 cm soil C_{org} stocks per surface area across habitats in Santoña marshes. Habitats with no bars were not examined in this estuary.

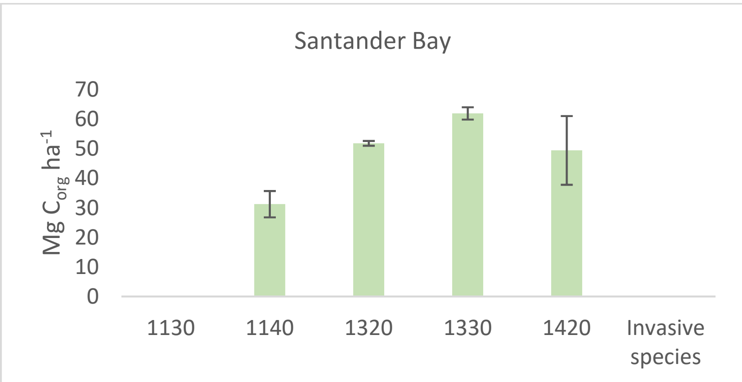

Figure 68. Average (± SE) of top 30 cm soil C_{org} stocks per surface area across habitats in Santander Bay. Habitats with no bars were not examined in this estuary.

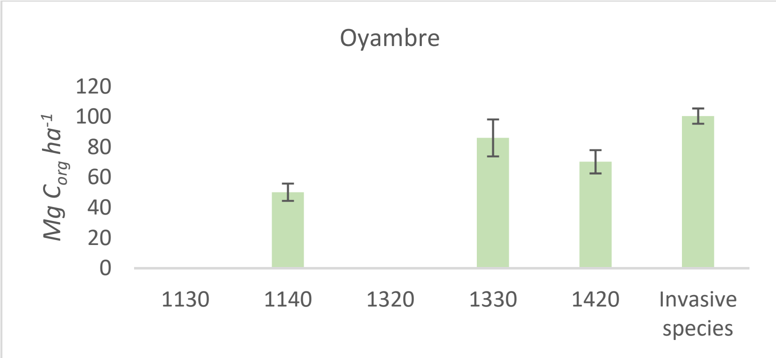

Figure 69. Average (± SE) of top 30 cm soil C_{org} stocks per surface area across habitats in the Mondego estuary. Habitats with no bars were not examined in this estuary.

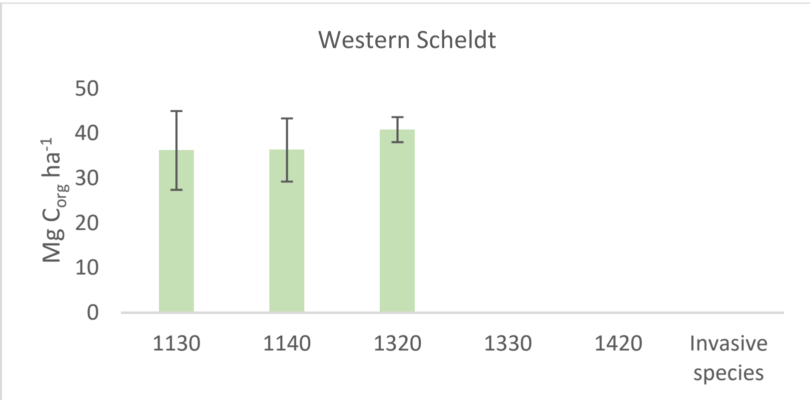

Figure 70. Average (± SE) of top 30 cm soil C_{org} stocks per surface area across habitats in the Western Scheldt estuary. Habitats with no bars were not examined in this estuary.

When considering the area occupied by each habitat sampled in the estuaries of study the habitats storing the largest C_{org} and CO_2 deposits in the top 30 cm were the mudflats or sandflats not covered by seawater in low tide (EU habitat 1140) in in Mondego estuary (58 ± 13 Gg C_{org}; 214 ± 5 Gg CO_2 ha^{-1}), Santoña marshes (39 ± 2 Gg C_{org}; 143 ± 9 Gg CO_2 ha^{-1}) and in Santander Bay (41 ± 6 Gg C_{org}, 150 ± 21 Gg CO_2 ha^{-1}), Atlantic salt meadows (EU habitat 1330) in Oyambre estuary (2.5 ± 3.6 Gg C_{org}, 9.3 ± 1.3 Gg CO_2 ha^{-1}) and the estuary habitat (EU habitat 1130) in the Western Scheldt (1025 ± 249 Gg C_{org}, 3759 ± 913 Gg CO_2 ha^{-1}) (Figures 71-75).

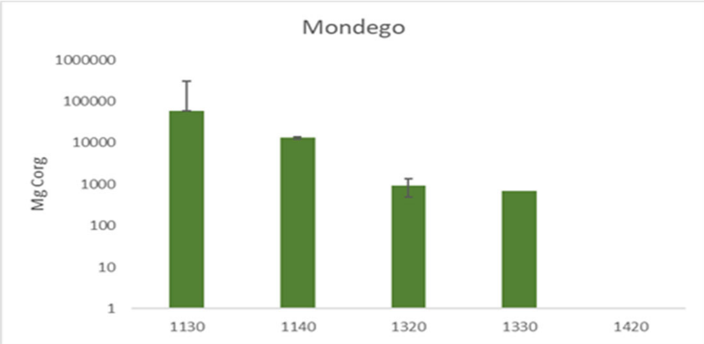

Figure 71. Top 30 cm soil C_{org} stocks (Mg) stored in each sampled habitat in the Mondego estuary. Habitats with no bars were not examined in this estuary.

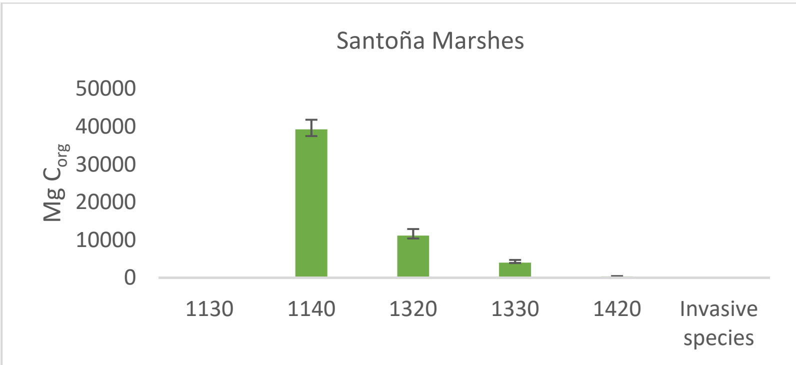

Figure 72. Top 30 cm soil C_{org} stocks (Mg) stored in each sampled habitat in the Santoña Marshes. Habitats with no bars were not examined in this estuary.

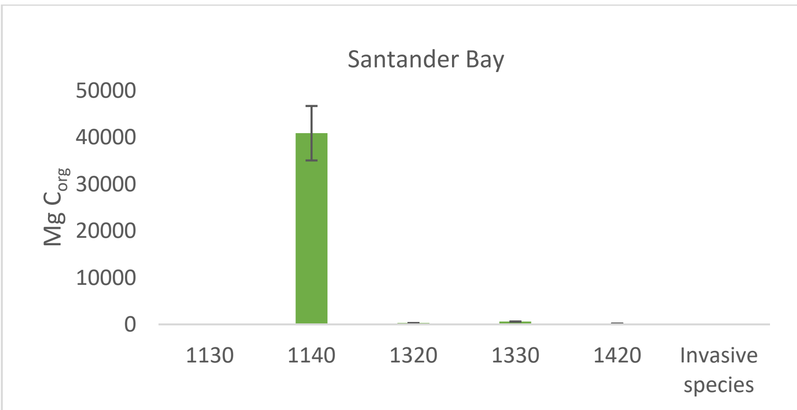

Figure 73. Top 30 cm soil C_{org} stocks (Mg) stored in each sampled habitat in Santander Bay. Habitats with no bars were not examined in this estuary.

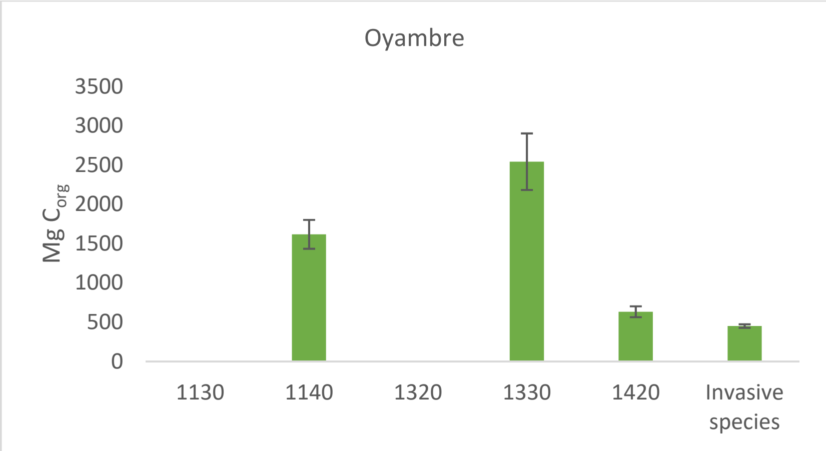

Figure 74. Top 30 cm soil C_{org} stocks (Mg) stored in each sampled habitat in Oyambre estuary. Habitats with no bars were not examined in this estuary.

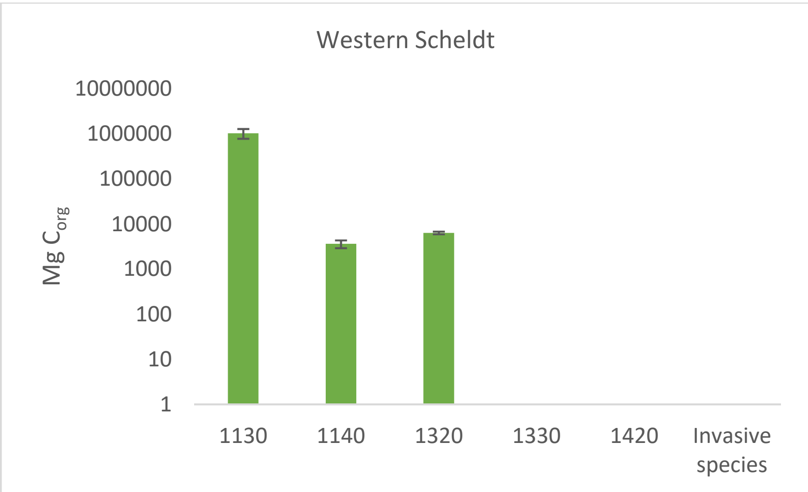

Figure 75. Top 30 cm soil Corg stocks (Mg) stored in each sampled habitat in Western Scheldt. Habitats with no bars were not examined in this estuary.

Across estuarine sections

For those habitats sampled in different sections of the estuaries, the soil C_{org} stocks and thus the amount of CO_2 sequestered per surface area were higher at the inner section of the estuaries compared to intermediate and outer sections, except in Oyambre estuary. This result is consistent to findings in previous studies developed in estuaries elsewhere and reflect the influence of the rivers as a source of organic matter (and thus C_{org} to estuarine habitats) (Kelleway et al., 2016; Ricart et al., 2020) .

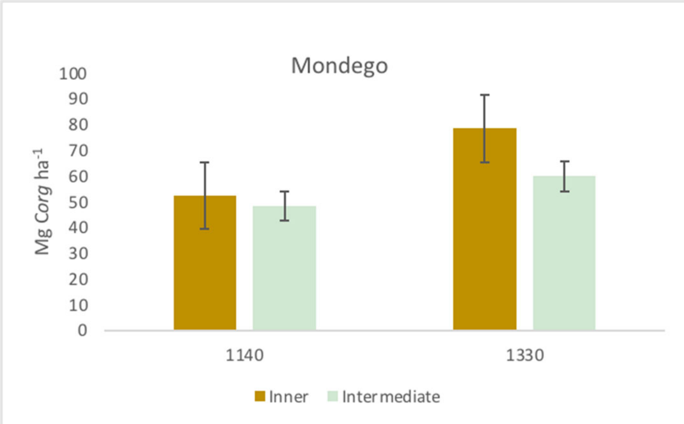

Figure 76. Average (± SE) top 30 cm soil C_{org} stocks per surface area found in the habitats 1140 and 1330 at the inner (brown bars) and intermediate (green bars) areas in the Mondego estuary.

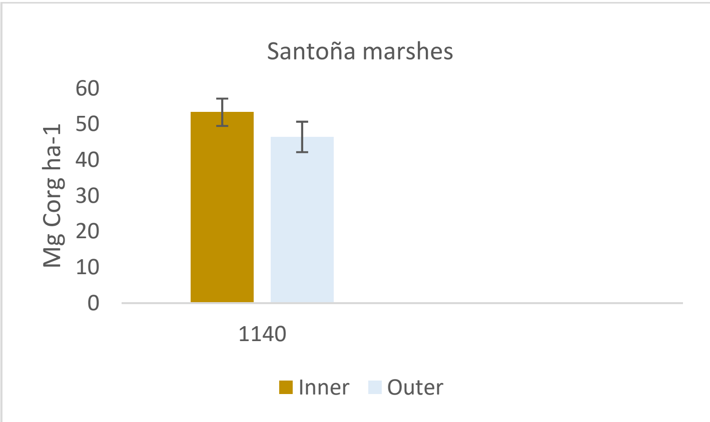

Figure 77. Average (± SE) top 30 cm soil C_{org} stocks per surface area found in the habitats 1140 at the inner (brown bars) and intermediate (blue bars) areas of the Santoña estuary.

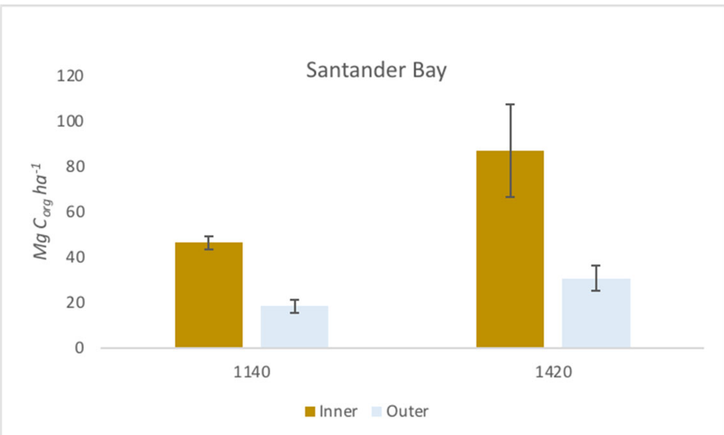

Figure 78. Average (± SE) top 30 cm soil C_{org} stocks per surface area found in the habitats 1140 and 1420 at the inner (brown bars) and intermediate (green bars) areas in Santander Bay estuary.

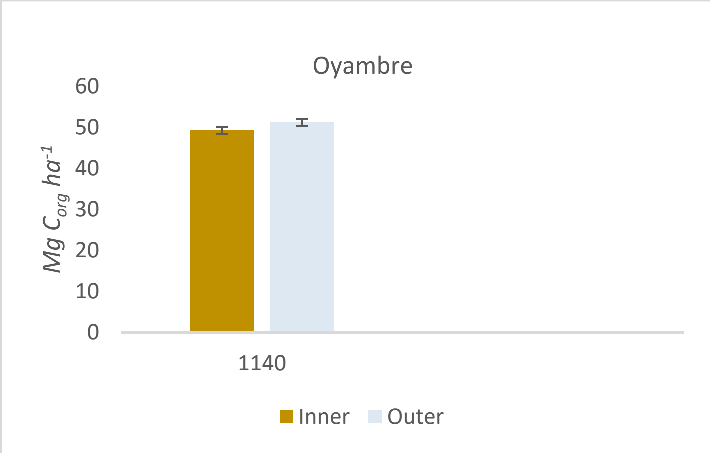

Figure 79 .Average (± SE) top 30 cm soil C_{org} stocks per surface area found in the habitat 1140 at the inner (brown bars) and outer (blue bars) areas in Oyambre estuary.

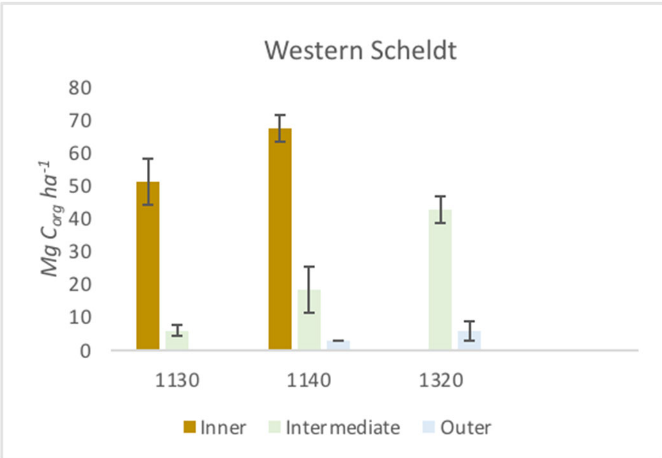

Figure 80. Average (± SE) top 30 cm soil Corg stocks per surface area found in the habitats 1130. 1140 and 1320 at the inner (brown bars). intermediate (green bars) and outer (blue bars) areas in the Western Scheldt.

3.3.2 C_{org} burial rates since 1950

The profiles of ^{210}Pb concentration with depth in the cores analyzed are provided in Annex II. In order to apply dating models to the ^{210}Pb concentration profile, ^{210}Pb concentration need to decline with depth (Arias-Ortiz et al., 2018). Only in 15 of them the ^{210}Pb was reliable to estimate the age of the sediment. Any of the cores from the Western Scheldt that were analyzed for ^{210}Pb could be dated. Thus, the results provided here are based on only 15 soil cores. Estimates of C_{org} burial and CO_2 sequestration rates from the dated cores are shown in Table 21.

Region	Estuary	Location	EU habitat	Marsh level	Dominant genera	Core code	C_{org} burial Mg ha^{-1}y^{-1} (avg ± se)	CO_2 sequestration Mg ha^{-1} y^{-1} (avg ± se)

Cantabria	Santander Bay		1330	High	*Juncus. Halimione*	BS1A1	0.59±0.05	2.15±0.19
		Inner	1320	Low	*Spartina*	BS1B1	0.46±0.04	1.68±0.13
		Outer	1420	High	*Halimione*	BS2A1	0.19±0.03	0.68±0.1
	Santoña Marshes		1420	High	*Halimione*	MS2A3	0.68±0.16	2.51±0.57
			1320	Low	*Spartina*	MS2B2	0.16±0.02	0.6±0.06
		Intermediate	1140	Mudflat / Sandflat	*Zostera*	MS2C3	0.3±0.02	1.09±0.09
	Oyambre		1420	High	*Halimione. Juncus*	NM3	0.99±0.1	3.62±0.37
		Outer	1140	Mudflat / Sandflat	*Zostera*	NP2	0.41±0.03	1.5±0.11
		Inner	1140	Mudflat / Sandflat	*bare*	RP3	0.07±0.01	0.25±0.04
			1420	High	*Halimione. Juncus*	A1M1	0.26±0.06	0.96±0.2
		Outer	1140	Mudflat / Sandflat	*bare*	A1P1	0.67±	2.45±
		Inner	Invasive species	High	*Juncus. Baccharis*	A2M3	1.16±0.06	4.27±0.22
Coimbra	Mondego		1320	Low	*Spartina*	MM1A1	0.57±0.05	2.09±0.17
		Outer	1140	Mudflat / Sandflat	*Zostera*	MM1b1	1.28±0.06	4.71±0.21
		Intermediate	1140	Mudflat / Sandflat	*bare*	MM2C1	0.65±0.02	2.37±0.08

Table 21. Average (± se) C_{org} and CO_2 burial rates (Mg C_{org} ha^{-1} y^{-1}) estimated for the 15 cores that could be dated.

The communities examined bury C_{org} at an average rate of 0.56 ± 0.1 Mg C_{org} ha^{-1} y^{-1}, which equivalates to a rate of CO_2 sequestration in the soil of 2.1 ± 0.3 Mg CO_2 ha^{-1} y^{-1}. The C_{org} burial rate did not vary across different dominant genera (Figure 81). The highest C_{org} burial and CO_2 sequestration rate was identified for the high marsh community dominated by *Juncus maritimus* and the invasive species *Baccharis halimifolia* in Oyambre estuary (1.16 Mg C_{org} ha^{-1} y^{-1}; 4.3 Mg CO_2 ha^{-1} y^{-1}). Yet, this result is based on a single dated core.

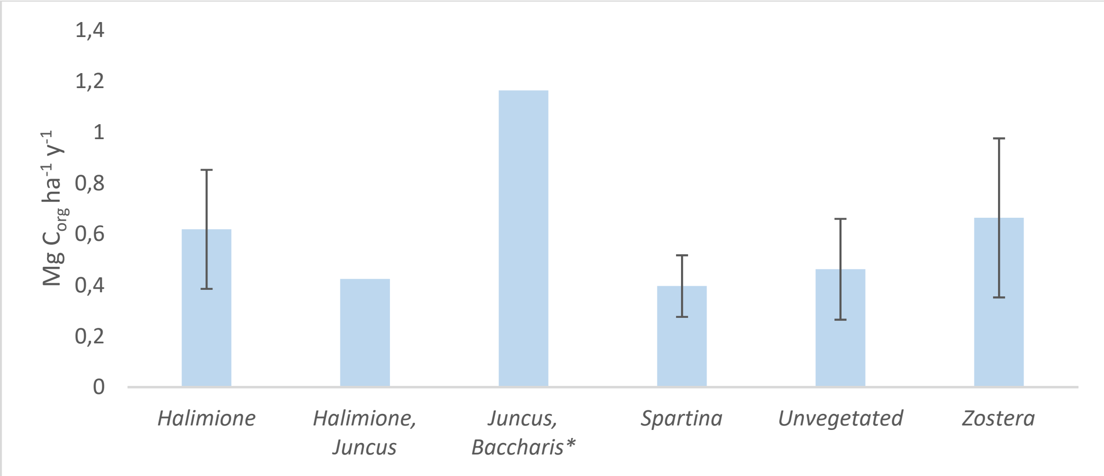

*Invasive species

Figure 81. C_{org} burial rates (avg. ± se) estimated since 1950 across dominant species and unvegetated soils.

When examined the differences in C_{org} burial and CO_2 sequestration rates across habitats examined, we found no differences except for the habitat occupied by the invasive species *Baccharis halimifolia* (Figure 82). We expected larger C_{org} burial rates in high marsh communities, that develop larger biomass and larger soil C_{org} stoks, compared to low marshes, bare tidal flats and seagrass meadows. Yet, these habitats, that are located at a lower intertidal range compared to high marsh, are subject to more frequent and longer hydroperiods that favor a higher accumulation of organic and inorganic particles from the water column compared to high marsh communities. Thus, C_{org} burial rates in these habitats are comparable to that found in high marsh communities, despite their lower biomass accumulation (Chmura and Hung, 2004; Santos et al., 2019).

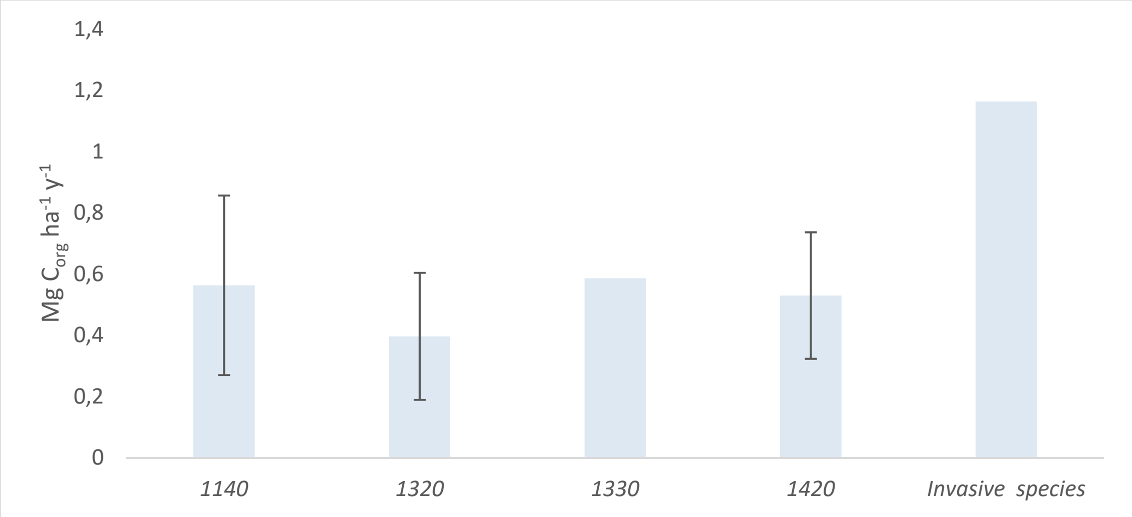

Figure 82. C_{org} burial rates (avg. ± se) estimated since 1950 across habitats.

No C_{org} burial rates could be estimated for estuarine communities in the Western Scheldt as the ^{210}Pb profiled obtained suggest no net accumulation

The number of data on C_{org} burial rates available is not enough to examine differences across habitats within each estuary.

3.3.3 C_{org} stocks and burial rates in other European saltmarshes

By looking at the scientific and grey literature a total of 46 data on soil C_{org} density (g C_{org} cm^{-3}) or organic matter density (g OM cm^{-3}), 10 data on top 100 cm soil C_{org} stocks and 51 data on C_{org} burial rate in the soils of European saltmarshes were found. Most of the data were already compiled in the previous global reviews by Chmura et al. (2003) and Ouyang and Lee (2014) and this review includes data from two additional scientific studies published after 2014 and the results of EU LIFE BLUE NATURA project. In order to be able to compare with the soil C_{org} stocks estimated in this project we used the data on on C_{org} density reported in the original source to estimate top 30 cm soil C_{org} stocks, assuming a constant bulk density along the depth profile. In cases where only organic matter density was available C_{org} density was estimated applying the formula by Craft et al. (1991).

$$C_{org} = (0.40* LOI)+(0.0025*LOI^2)$$

where LOI (Loss of Ignition) is used as a proxy of organic matter content. As C_{org} density tends to decrease with depth particularly in high marsh soils this approach might have led to some overestimation. In the cases were top 100 cm soil C_{org} stocks were reported (i.e. data for Andalucian saltmarshes from [EU LIFE BLUE NATURA project]) soil stocks were normalized to 30 cm depth). The estimated top 30 cm soil C_{org} stocks and burial rates are shown in Table 22.

Country	Location	Lat / Long	Marsh level	Dominant genera	Top 30 cm C_{org} stocks Mg ha^{-1}	C_{org} burial Mg ha^{-1} y^{-1}	Dating technique	Source
United Kingdom	Stiffkey Marsh	52.9 / 0.9	Low	*Spartina*	123	1.59	^{137}Cs	Callaway et al.. 1996; Ouyang and Lee 2014
United Kingdom	Stiffkey Marsh	52.9 / 0.9	High	*Armeria*	123	1.1	^{137}Cs	
United Kingdom	Dengie Marsh	51.7 / 0.9	Low	*Halimione*	123	1.87	^{137}Cs	Callaway et al.. 1996; Ouyang and Lee 2014
United Kingdom	Dengie Marsh	51.7 / 0.9	High	*Halimione*	123	1.39	^{137}Cs	
United Kingdom	The Humber estuary	53.7 / -0.1	Low	*Puccinellia*	171	7.93	^{137}Cs	Andrews et al.. 2008; Ouyang and Lee 2014
United Kingdom	The Humber estuary	53.7 / -0.1	Pioneer	*Spartina*	171	11.33	^{137}Cs	
United Kingdom	The Blackwater estuary 1	52 / -0.7			54	0.96 [b]	na	Adams et al.. 2012; Ouyang and Lee. 2014
United Kingdom	The Blackwater estuary 2	52 / -0.7	High	*Halimione*	69	1.27 [b]	na	
United Kingdom	The Blackwater estuary 3	52 / -0.7	Mid	*Salicornea*	36	0.66[b]	na	
United Kingdom	Hut marsh	53 / 0.7		*Aster*	81	1.65	MH	French and Spencer. 1993; Chmura et al.. 2003
United Kingdom	Hut marsh	53 / 0.7		*Halimione*	81	0.77	MH	
Denmark	Skallingen	55.5 / 8.3			63		^{137}Cs	Morris and Jensen. 1998; Chmura et al.. 2003

Country	Location	Lat / Long	Marsh level	Dominant genera	Top 30 cm C_{org} stocks Mg ha^{-1}	C_{org} burial Mg ha^{-1} y^{-1}	Dating technique	Source
	Skallingen	55.5 / 8.3			63		^{137}Cs	
	Dieksander koog. Wadden Sea	53.9 / 8.9			45			Mueller et al.. 2019
	Westerhever. Wadden Sea	54.3 / 8.6			54			
	Sonke-Nissen-Koog. Wadden Sea	54.6 / 8.8			66			
	Skallingen Peninsula	55.5 / 8.3		*Puccinellia*	84	0.528	^{137}Cs	Andersen et al.. 2011; Ouyang and Lee 2014
The Netherlands	St. Annaland Marsh	51.5 / 4.1	Low	*Spartina*	123	2.77	^{137}Cs	Callaway et al.. 1996; Ouyang and Lee 2014
	St. Annaland Marsh	51.5 / 4.1	High	*Halimione*	123	1.39	^{137}Cs	
	Scheldt	51.5 / 4.1		*Spartina*	87	5.87	^{137}Cs	de Oenema and DeLaune. ; Chmura et al.. 2003
	Scheldt	51.5 / 4.1		*Spartina*	60	6.5	^{137}Cs	
Poland	Oder River	54.3 / 14.6	Low	*Phragmites*	63	1.48	^{137}Cs	Callaway et al.. 1996; Ouyang and Lee 2014
	Oder River	54.3 / 14.6	High	*Phragmites*	69	1.07	^{137}Cs	
	Vistula River	54.3 / 18.9	Low	*Phragmites*	60	3.81	^{137}Cs	Callaway et al.. 1996; Ouyang and Lee 2014
	Vistula River	54.3 / 18.9	High	*Phragmites*	93	2.54	^{137}Cs	
France	Rhone. riverine	43.3 / 4.6		*Juncus*	81	3.57	MH	Hensel et al.. 1999; Ouyang and Lee 2014
	Rhone. marine	43.3 / 4.6		*Arthrocnemun*	219	0.88	MH	

Country	Location	Lat / Long	Marsh level	Dominant genera	Top 30 cm C_{org} stocks Mg ha^{-1}	C_{org} burial Mg ha^{-1} y^{-1}	Dating technique	Source
	Rhone. impouded sites	43.3 / 4.6		*Arthrocnemun*	198	0.72	MH	
Portugal	Tagus estuary	38.8 / -8.9		*Spartina*	99	3.3	^{137}Cs	Sousa et al.. 2010a. Sousa et al.. 2010b.
	Tagus estuary	38.8 / -8.9		*Spartina*	225	7.5	^{137}Cs	Caçador et añ.. 2007; Castro 2005. Ouyang and Lee 2014
	Mondego estuary	40.1 / -8.6		*Spartina*	93	2.18	^{137}Cs	Sousa et al.. 2010a. Sousa et al.. 2010b. Caçador et añ.. 2007; Castro 2005. Ouyang and Lee 2014
Spain	Odiel	37.2 / -6.9		*Spartina*	45	3.24	MH	Curado et al.. 2013; Ouyang and Lee 2014
	The Palmones estuary	36.2 / -5.4	Low	*Spartina*		5.6[b]	na	Palomo and Niell 2009; Ouyand et al.. 2014
	Ebro Delta	40.71 / 0.75		*Sarcocornia*	132	2.72[a]	^{210}Pb	Fennesy et al.. 2019
				Sarcocornia	73	3.95[a]	^{210}Pb	
				Sarcocornia	256	4.35[a]	^{210}Pb	
				Phragmites. Juncus	7	2.26[a]		
				Sarcocornia	78	0.39[a]	^{210}Pb	
				Phragmites	52	2.19[a]	MH	
				Phragmites. Sarcocornia	11	0.32[a]	MH	
				Phragmites. Juncus	87	0.99[a]	^{210}Pb	
				Sarcocornia	156	0.49[a]	^{210}Pb	
				Phragmites	87	2.97[a]	^{210}Pb	
				Sarcocornia	52	0.53[a]	^{210}Pb	
				Phragmites	199	2.93[a]	MH	
				Cladium	62	1.42[a]	^{210}Pb	
				Phragmites. Scirpus	376	3.24[a]	MH	

Country	Location	Lat / Long	Marsh level	Dominant genera	Top 30 cm C_{org} stocks Mg ha^{-1}	C_{org} burial Mg ha^{-1} y^{-1}	Dating technique	Source
	Andalucia (Odiel and Cádiz Bay)	37 / -6.6	High	*High marsh spp.*	25	0.21	^{210}Pb	EU LIFE BLUE NATURA. Deliverable C2
			Medium	*Medium marsh spp.*	41	0.90	^{210}Pb	
			Low	*Low marsh spp.*	17		^{210}Pb	
			Low	*Spartina*	18	0.12	^{210}Pb	
			Low	*Sarcornea*	15		^{210}Pb	
			Low	*Bare*	31	0.15	^{210}Pb	
			Intertidal mudflat	*Zostera*	23	0.30	^{210}Pb	
			Re-wetted	*Salicornea.*	50	0.28	^{210}Pb	
			Re-vegetated	*Spartina*	20	0.99	^{210}Pb	
			Medium	*Salicornera*	5	1.81	^{210}Pb	

Table 22. Top 30 cm soil organic carbon stocks (Mg C_{org} ha^{-1}) and burial rates (Mg C_{org} ha^{-1} y^{-1}) estimated for European saltmarshes, extracted from the literature. [a]Burial rates provided correspond to total carbon burial rates, not C_{org}, so not included in estimate averages. [b]Direct measures of sediment accretion rates not provided, so they were excluded from analysis.

The data on soil C_{org} stocks (n= 78) and burial rates (n= 11) produced in the project LIFE ADAPTABLUES from 26 different saltmarsh communities increases the data available up to date in European saltmarshes carbon sinks in nearly 60% and 18% for soil C_{org} stocks and burial rates, respectively.

The top 30 cm soil C_{org} stocks estimated from previous studies (Table 22) are on average 88 ± 9 Mg C_{org} ha^{-1}, higher than the average stock measured in the high and low marshes examined in this project (65.5 and 38.7 Mg C_{org} ha^{-1}, respectively). This difference could be partly attributed to the way most of the top 30 cm soil C_{org} stocks for previous studies have been estimated (i.e. assuming a constant C_{org} density along the depth profile).

The C_{org} burial rate provided in the previous studies is also higher (2.5 ± 0.4 Mg C_{org} ha^{-1} y^{-1}) than the average C_{org} burial rate estimated in the high and low marsh communities examined in this project (0.64 and 0.40 Mg C_{org} ha^{-1} y^{-1}, respectively). This difference could be explained by the different approaches applied for sediment dating that provide a completely different temporal resolution. In the saltmarshes examined in this project all C_{org} burial rates were estimated applying radio chronological techniques; in particular ^{210}Pb radioisotope (sometimes combined with ^{137}Cs). which is ideal for studying pass 100 years sedimentation processes (Marland et al.. 2001) and can be applied to estimate long-term C_{org} burial rates. On the contrary. in most of the previous studies the age of the sediment was estimated using only ^{137}Cs. which provides a more recent temporal scale (since 1960 decade or using marker horizon techniques. that are used to measure current sedimentation rates during relatively short-time periods (~2 years) (Lynch et al., 2015). The differences in the methods used to estimate soil C_{org} stocks and burial rates limit the combination of all these data to produce accurate estimates of saltmarsh soil C_{org} stocks and burial rates at the European scale. The C_{org} burial rates obtained in the saltmarsh communities examined in this project (0.52 ± 0.3 Mg C_{org} ha^{-1} y^{-1}) is still slightly lower but in the same order of magnitude to average C_{org} burial rates estimated in saltmarsh communities within the project LIFE BLUE NATURA (0.72 ± 0.3 Mg C_{org} ha^{-1} y^{-1}), where sediment age and accumulation rate was also estimated through radiochronology (^{210}Pb).

3.3.4 Implication for Climate Change mitigation strategies

The European estuarine intertidal communities examined in this project, including saltmarshes, seagrass meadows and tidal flats, sequester CO_2 in their soils at an average rate per surface area of between 0- 4.3 Mg CO_2 ha^{-1} y^{-1} (median=1.6 Mg CO_2 ha^{-1}) and store an average of 183 Mg CO_2 ha^{-1} within the top 30 cm of soil. Both the rate of CO_2 burial and the magnitude of the soil deposits per surface area are higher than those estimated for terrestrial forests in Europe (0.23-1.64 Mg CO_2 ha^{-1} y^{-1}; 81 t CO_2 ha^{-1}; De Vos et al., 2015; Mol Dijkstra et al., 2009).

The degradation or Blue Carbon habitats leads to the loss of their CO_2 sequestration capacity and could lead to the emission of CO_2 sequestered in the soil compartment as C_{org} deposits get exposed to aerobic conditions and are remineralized (Lovelock et al., 2017; Pendleton et al., 2012). For instance, the degradation of the high marsh communities examined in this project and the subsequent erosion of top 30 cm C_{org} stocks (65.5 ± 3.5 Mg C_{org} ha^{-1}) could cause the release of approximately 40 Mg CO_2 ha^{-1} during the first year after habitat disturbance, considering the model for CO_2 emissions following saltmarsh degradation proposed by Lovelock et al., (2017). Thus, protecting the estuarine habitats of the estuaries examined contributes to Climate Change mitigation by maintaining the removal of CO_2 and avoiding CO_2 emissions derived from their degradation.

On the other hand, vast areas of European estuaries have been degraded or transformed to other uses during the last century (land claimed, Airoldi and Beck, 2007; Jimenez et al., 2012). For instance, only in the Cantabrian region, there are 139 concession areas (i.e. areas claimed and transformed for other uses) on a total of 10 estuaries distributed along 200 km of coast (Jimenez et al., 2012). Some of these areas can't be recovered back into intertidal areas due to the intense transformation they have suffered (e.g. converted into urban or industrial land). However, a large fraction of estuarine concessions in European estuaries are used as agricultural or livestock land or salt ponds, with some of them being currently abandoned. When concessions are used as croplands, soil C_{org} stocks might be comparable to those in natural saltmarsh communities (Yang et al., 2019). On the contrary, when claimed areas are not vegetated (e.g. those used as salt ponds), soil C_{org} stocks are lower compared to unaltered saltmarsh communities (Gulliver et al., 2020). In addition, in estuarine areas claimed for other uses, the influence of the tide, an important source of organic and inorganic particles to estuarine habitats soils, is highly limited or totally restricted by dykes, and thus the rate of C_{org} burial is usually lower than in natural estuarine areas (Gulliver et al., 2020; Tognin et al., 2021). In addition , tidal restriction leads to soil desiccation, which enhances soil C_{org} oxidation and the release of CO_2 along with other GHG such as CH4 (Kroeger et al., 2017). Finally, tidal restriction and the decrease in salinity in European estuaries have favored the spread of the invasive shrub species *Baccharis halimifolia* (Caño et al. 2013), that causes negative impacts in formerly open habitats such as *Juncus maritimus* (i.e. habitat 1330) and *Halimione portulacoides* (i.e. habitat 1420) leading to a decrease in species richness and herbaceous cover and threating associated organisms by modifying habitat quality (Fried et al. 2016).

The restoration of the natural tidal regime in claimed areas is known to lead to a rapid recovery of natural habitats (Warren et al., 2002), prevent the spread of invasive species *Baccharis halimifolia* (results of the project LIFE CONVIVE) and potentially contribute to increase C_{org} sequestration capacity and avoid GHG emissions (Kroeger et al., 2017). Thus, the restoration of claimed areas in European estuaries is an opportunity to restore biodiversity while contributing to Climate Change mitigation.

4 CONCLUSIONS

In the framework of this action the combined effect of all coastal dynamics (astronomical tide, meteorological tide and surge) and fluvial dynamics (river discharges) will be considered, with the aim of being able to holistically address the agents responsible for flooding in estuarine environments. Moreover, a simultaneous analysis has been carried out considering vegetated and unvegetated estuaries to quantify the current protection provided by these plant communities. It should be noted that a total of 11 plant communities (communities that currently exist in the study areas) have been considered within the analysis of the different estuaries.

Regarding the Coastal Protection Services:

- The estuarine vegetation provides a reduction in flooded area produced by the combination of continental and fluvial dynamics. In the Oyambre estuary and Santoña marshes the reduction in flooded area is greater than the reduction observed in the Mondego estuary and Santander. These differences are caused by:
  - Oyambre and Santoña marshes are dominated by intertidal spp. while Santander and Mondego estuaries are dominated by subtidal spp.
  - Santander bay and Mondego estuary are more adapted to climate change. Since their accommodation space is reduced due to the rigidification of the estuary margins.

  The average percentage reduction in flooding area provided by estuarine communities during all the scenarios analyzed (return periods: 10, 50, 100 years and climate change scenarios: -RCP 4.5-year 2050 and 2100- and -RCP 4.5 year 2050 and 2100-) ranges at about 20% for the Oyambre estuary, 44.8 % in the Santoña marshes, 2.04% in the Mondego estuary and 0.96% Santander Bay.

- Flow velocity attenuation is also a factor that must be evaluated in the assessment of flooding consequences. In Santander Bay a reduction of 0.17m/s is observed in the depth averaged velocity of the entire estuary. In Santoña marshes this decrease is 0.24 m/s, while in the Oyambre estuary it is 0.10 m/s. The Mondego estuary is the estuary where the role of vegetation is less important in flow reduction: it produces an average reduction in depth averaged velocities of 0.05m/s.

- The attenuation in velocity caused by the presence of vegetation communities can translate into increased sedimentation rates, since the bed shear stress can be lower than the critical bed shear stress that causes the sediment movement. The results from long-term morphodynamic simulations show that each zonation area presents different accretion rates:
  - Communities which dominate the subtidal zone area produce an accretion of 0.19 cm.
  - Communities which dominate the low intertidal zone area, provide a lower accretion rate of 0.15 cm, and in the high intertidal zone area the accretion rate is 0.12 cm.
  - The communities that dominate the supratidal have the highest accretion rate, reaching 0.21 cm.

  These results are similar (same order of magnitude) as those reported by the sensors in the *"Action A3.2. Capacity of tidal habitats to path with to sea level rise in European estuaries".*

- In terms of protection of the population against flooding events provided by the estuarine vegetation, we can conclude that there is great variability between estuaries. The estuary whose communities protect a higher percentage of the population compared to the bared scenario is Santoña marshes, that protects about of 35% more population if we compare it with the rest of estuaries that protect 5.47% in Santander Bay, 4.6% in Oyambre estuary and 2.26% in Mondego Estuary.

- In terms of economic cost of building protection provided by each hectare of estuarine vegetation against flooding events, it can be concluded that Santoña marshes protect about 28.45% of buildings, while this amount is reduced to 7.13% in Santander Bay, 4.5% in Oyambre estuary and 2.26% in Mondego estuary.

Regarding to Carbon sequestration

- The European estuarine intertidal communities examined in this project, including saltmarshes, seagrass meadows and tidal flats, sequester CO_2 in their soils at an average rate per surface area of between 0- 4.3 Mg CO_2 ha^{-1} y^{-1} (median=1.6 Mg CO_2 ha^{-1}) and store an average of 183 Mg CO_2 ha^{-1} within the top 30 cm of soil. Both the rate of CO_2

burial and the magnitude of the soil deposits per surface area are higher than those estimated for terrestrial forests in Europe (0.23-1.64 Mg CO_2 ha^{-1} y^{-1}; 81 t CO_2 ha^{-1}).

- Soil C_{org} stocks varied across habitats and estuarine locations.
    - The largest stocks in the top 30 cm of sediment per surface area were found in communities dominated by large species, usually allocated in the high marsh zone (*Halimione spp.*, *Juncus spp.*, *Phragmatis spp.)* whereas communities formed by smaller size species, such as *Spartina spp*. and *Sarcocornea spp*., that develop in the low marsh level showed lower stocks per surface area (comparable to those found in intertidal bare tidal flats or intertidal seagrass meadows (*Zostera spp.*).
    - Consistently, the largest C_{org} stocks per surface area were found in the habitat 1330 (Atlantic salt meadows) followed by the habitat 1420 (Mediterranean and thermoatlantic halophilus scrubs). The habitat 1320 (*Spartina* swards) showed similar average C_{org} stock per surface area than habitats 1140 (Mudflats or sandflats not covered by seawater in low tide) and 1130 (Estuaries).
    - Soil C_{org} stocks and thus the amount of CO_2 sequestered per surface area tended to be higher at the inner section of the estuaries compared to intermediate and outer sections, reflecting the influence of the river as a source of organic particles to estuarine habitats soil.
- The C_{org} burial rate did not vary across different dominant genera or habitat, despite the difference in biomass across habitats examined, likely due to longer and more frequent hydroperiods in low intertidal habitats (low marsh, seagrass meadows and bare flats) compared to high marsh habitats.
- Bare tidal flats are usually neglected in Blue Carbon research but the results found in this project suggest that they might play a comparable role as C_{org} sink to that of low marshes and seagrass meadows.
- This project generated data on C_{org} stocks (n= 78) and burial rates (n= 11) from 26 different saltmarsh communities, increasing the data available up to date in European saltmarshes carbon sinks in nearly 60% and 18% for soil C_{org} stocks and burial rates, respectively. Yet, the combination of the data generated in this project with that reported in previous studies to estimate soil C_{org} stocks and burial rates at the European level is constraint due to the different methodological approaches used.

The results obtained in this action will represent the basis for the development of the risk analysis described in Action 4 .("A.4) Risk of flooding: Assessing the risk associated to flooding in three estuarine regions of the Atlantic coast under future scenarios of Climate Change"). Subsequently, the results obtained from Action A4 combined with the information obtained in A.1 and A.3 will represent the basis for the definition of the technical recommendations of the different adaptation measures (Action C1) where the technical recommendations to establish the adaptation measures in each of the analyzed study sites will be specified.

5 REFERENCES

Abdelrhman, Mohamed. (2007). Modeling coupling between eelgrass Zostera marina and water flow. Marine Ecology-progress Series - MAR ECOL-PROGR SER. 338. 81-96. 10.3354/meps338081

Airoldi, L., Beck, M.W., 2007. Loss, status and trends for coastal marine habitats of Europe. Oceanogr. Mar. Biol. 45, 345–405. https://doi.org/10.1201/9781420050943.ch7

Appleby, P.G., 2001. IN RECENT SEDIMENTS Rn Pb Po 1, 171–203.

Arias-Ortiz, A., Masqué, P., Garcia-Orellana, J., Serrano, O., Mazarrasa, I., Marbá, N., Lovelock, C.E., Lavery, P.S., Duarte, C.M., 2018. Reviews and syntheses: 210Pb-derived sediment and carbon accumulation rates in vegetated coastal ecosystems - Setting the record straight. Biogeosciences 15, 6791–6818. https://doi.org/10.5194/bg-15-6791-2018

Anderson, M.E., Smith, J.M., 2014.Wave attenuation by flexible, idealized salt marsh vegetation. Coast. Eng. 83, 82–92

Barbier, E.B., Hacker, S.D., Kennedy, C., ..., 2011. The value of estuarine and coastal ecosystem services. Ecol. Monogr. 81, 169–193.

Booij, N., Ris, R. C., & Holthuijsen, L. H. (1999). A third-generation wave model for coastal regions: 1. Model description and validation. Journal of Geophysical Research, 104(C4), 7649. doi:10.1029/98JC02622

Bouma, T. J., M. B. De Vries, and P. M. J. Herman. 2010.Comparing ecosystem engineering efficiency of two plant species with contrasting growth strategies.Ecology 91:2696–2704.

Bouma, T. J., M. B. De Vries, E. Low, G. Peralta, I. C. Ta´nczos, J. van de Koppel, and P. M. J. Herman. 2005. Trade-offs related to ecosystem engineering: acase study on stiffness of emerging macrophytes. Ecology 86:2187–2199.

Bradley, K. and C. Houser. 2009. Relative velocity of seagrass blades: Implications for wave attenuation in low-energy environments. Journal of Geophysical Research 114:1–13.

Bunce R.G.H., Bogers M.M.B., Evans D., Halada L., Jongman R.H.G., Mücher C.A., Bauch B., De Blust G., Parr T.W. & Olsvig-Whittaker L., 2013a. The signiicance of habitats as indicators of biodiversity and their links to species. Ecological Indicators 33: 19-25.

Camus, P., Méndez, F. J., Medina, R., Tomás, A., and Izaguirre, C. (2013). High resolution downscaled ocean waves (DOW) reanalysis in coastal areas. Coastal Engineering, 72:56{68.

Caño, L., Campos, J.A., García-Magro, D., Herrera, M., 2013. Replacement of estuarine communities by an exotic shrub: Distribution and invasion history of Baccharis halimifolia in Europe. Biol. Invasions 15, 1183–1188. https://doi.org/10.1007/s10530-012-0360-4

Cao, H., Feng, W., Feng, X., 2013. Research on the Modification of Wave Attenuation in Flexible Vegetation with SWAN-VEG. The Twenty-Third International Offshore and Polar Engineering Conference. International Society of Offshore and Polar Engineers.

Cheong, S.-M., Silliman, B., Wong, P.P., van Wesenbeeck, B., Kim, C.-K., Guannel, G., 2013. Coastal adaptation with ecological engineering. Nat. Clim. Chang. 3, 787–791. https://doi.org/10.1038/nclimate1854

Chmura, G.L., Hung, G.A., 2004. Controls on salt marsh accretion: A test in salt marshes of eastern Canada. Estuaries 27, 70–81. https://doi.org/10.1007/BF02803561

Cid, A., Castanedo, S., Abascal, A.J., Menendez, M., and R. Medina, 2014. A high resolution hindcast of the meteorological sea level component for Southern Europe: the GOS dataset. Climate Dynamics, doi: 10.1007/s00382-013-2041-0.

Coco, G., Zhou, Z., vanMaanen, B., Olabarrieta, M., Tinoco, Townend, I., 2013. Morphodynamics of tidal networks: advances and challenges. Mar. Geol. 346, 1–16. https://doi.org/10.1016/j.margeo.2013.08.005.

Cohen-Shacham, E., Walters, G., Janzen, G., Maginnis, S., 2016. Nature-based solutions to address global societal challenges. IUCN, Gland, Switzerland. https://doi.org/10.2305/IUCN.CH.2016.13.en

Cooper, N. J. 2005. Wave dissipation across intertidal surfaces in the Wash tidal inlet, Eastern England. Journal of Coastal Research 21:28–40.

Cox, R., S. Wallace, and R. Thomson. 2003. Wave damping by seagrass meadows. Coastal and Port Engineering in Developing Countries (COPEDEC), VI. Engineering the Coastal Environment, Colombo, Sri Lanka.

Dawson, R. J., Dickson, M. E., Nicholls, R. J., Hall, J. W., Walkden, M. J., Stansby, P. K., Mokrech, M., Richards, J., Zhou, J., Milligan, J., Jordan, A., Pearson, S., Rees, J., Bates, P. D., Koukoulas, S., and Watkinson, A. R. (2009). Integrated analysis of risks of coastal flooding and cliff erosion under scenarios of long term change. Climatic Change, 95:249{288.

Del Jesus, M., Casado, J., Salvador, N., 2020. Return period evaluation of compound events of flooding using gaussian copulas. 6th IAHR Europe Congress, Warsaw, Poland

De Vos, B., Cools, N., Ilvesniemi, H., Vesterdal, L., Vanguelova, E., Carnicelli, S., 2015. Benchmark values for forest soil carbon stocks in Europe: Results from a large-scale forest soil survey. Geoderma 251–252, 33–46. https://doi.org/10.1016/j.geoderma.2015.03.008

Duarte, C.M., Losada, I.J.I.J., Hendriks, I.E., Mazarrasa, I., Marbà, N., 2013. The role of coastal plant communities for climate change mitigation and adaptation. Nat. Clim. Chang. 3, 961–968. https://doi.org/10.1038/nclimate1970

Duarte, C.M., Middelburg, J.J., Caraco, N., 2005. Major role of marine vegetation on the oceanic carbon cycle. Biogeosciences 2, 1–8. https://doi.org/10.5194/bg-2-1-2005

De Vriend, H. J., Capobinaco, M., Chesher, T., De Swart, H. E., Latteux, B., & Stive, M. J. F. (1993). "Approach to long-term modelling of coastal morphology: a review.", Coastal engineering, 21, 225-269.

Engelund F, Hansen E. 1967. A monograph on sediment transport in alluvial streams. Technical Report, Copenhagen, Danish Technical Press.

Fisher, R., & Tippett, L., 1928. Limiting forms of the frequency distribution of the largest or smallest member of a sample. Mathematical Proceedings of the Cambridge Philosophical Society, 24(2), 180-190. doi:10.1017/S0305004100015681

Fonseca, M. S. and J. A. Cahalan. 1992. A preliminary evaluation of wave attenuation by four species of seagrass. Estuarine Coastal and Shelf Science 35:565–576.

Fried, G., Caño, L., Brunel, S., Beteta, E., Charpentier, A., Herrera, M., Starfinger, U., Dane Panetta, F., 2016. Monographs on invasive plants in Europe: Baccharis halimifolia L. Bot. Lett. 163, 127–153. https://doi.org/10.1080/23818107.2016.1168315

Gulliver, A., Carnell, P.E., Trevathan-Tackett, S.M., Duarte de Paula Costa, M., Masqué, P., Macreadie, P.I., 2020. Estimating the Potential Blue Carbon Gains From Tidal Marsh Rehabilitation: A Case Study From South Eastern Australia. Front. Mar. Sci. 7, 1–13. https://doi.org/10.3389/fmars.2020.00403

Hallegatte, S., Green, C., Nicholls, R.J., Corfee-Morlot, J., 2013. Future flood losses in major coastal cities. Nat. Clim. Chang. 3, 802–806. https://doi.org/10.1038/nclimate1979

Hasselmann, K., T. P. Barnett, E. Bouws, H. Carlson, D. E. Cartwright, K. Enke, J. Ewing, H. Gienapp, D. E. Hasselmann, P. Kruseman, A. Meerburg, P. Müller, D. J. Olbers, K. Richter, W. Sell and H. Walden, 1973. "Measurements of wind wave growth and swell decay during the Joint North Sea Wave Project (JONSWAP)." Deutsche Hydrographische Zeitschrift 8 (12).

Hastie, T., Tibshirani, R., Friedman, J., 2001. The Elements of Statistical Learning. Springer, New York.

Hidralab+ ., 2016. Critical review of challenges for representing climate change in physical models. Adaptation for climate change. Deliverable 8.I. EC contract no 654110, HYDRALAB+

Hinkel, J., Lincke, D., Vafeidis, A. T., Perrette, M., Nicholls, R. J., Tol, R. S. J.,Marzeion, B., Fettweis, X., Ionescu, C., and Levermann, A. (2014). Coastal flood damage and adaptation costs under 21st century sea-level rise. Proceedings of the National Academy of Sciences of the United States of America, 111(9):3292{3297

Hinkel, J., van Vuuren, D.P., Nicholls, R.J., Klein, R.J.T., Vuuren, D.P., Nicholls, R.J., Klein, R.J.T., 2013. The effects of adaptation and mitigation on coastal flood impacts during the 21st century. An application of the DIVA and IMAGE models. Clim. Change 117, 783–794. https://doi.org/10.1007/s10584-012-0564-8

Holthuijsen, L., N. Booij and R. Ris, 1993. "A spectral wave model for the coastal zone." In Proceedings of 2nd International Symposium on Ocean Wave Measurement and Analysis, New Orleans, pages 630–641.

Houwing, E. J., I. C. Tánczos, A. Kroon and M. B. de Vries, 2000. "Interaction of submerged vegetation, hydrodynamics and turbidity; analysis of field and laboratory studies." Conference INTERCOH2000 .

Huber, C. 2003. Wave damping effects caused by seagrasses. Technical University Hamburg-Harburg,Germany.

Hu, Z., Suzuki, T., Zitman, T., Uittewaal,W., Stive, M., 2014. Laboratory study on wave dissipation by vegetation in combined current-wave flow. Coast. Eng. 88, 131–142.

Jadhav, R., Chen, Q., 2012. Field investigation of wave dissipation over salt marsh vegetation during tropical cyclone. Coast. Eng. Proc. 1, 111.

Infantes, E., Orfila, A., Simarro, G., Terrados, J., Luhar, M., Nepf, H., 2012. Effect of a seagrass (Posidonia oceanica) meadow on wave propagation. Mar. Ecol. Prog. Ser.456, 63–72.

IPCC (Intergovernmental Panel on Climate Change), 2014. Climate Change 2014: Impacts, Adaptation and Vulnerability. Working Group II. Contribution to the IPCC 5th Assessment Report.

John, B.M., Shirlal, K.G., Rao, S., 2015. Effect of artificial sea grass on wave attenuation and experimental investigation. Aquatic Procedia 4, 221–226.

Jiménez, M., Castanedo, S., Medina, R., Camus, P., 2012. A methodology for the classification of estuary restoration areas: A management tool. Ocean Coast. Manag. 69, 231–242. https://doi.org/10.1016/j.ocecoaman.2012.08.017

Kelleway, J.J., Saintilan, N., Macreadie, P.I., Ralph, P.J., 2016. Sedimentary Factors are Key Predictors of Carbon Storage in SE Australian Saltmarshes. Ecosystems 19, 865–880.

https://doi.org/10.1007/s10021-016-9972-3

Kennedy, H., Beggins, J., Duarte, C.M., Fourqurean, J.W., Holmer, M., Marbá, N., Middelburg, J.J., 2010. Seagrass sediments as a global carbon sink: Isotopic constraints. Global Biogeochem. Cycles 24, 1–8. https://doi.org/10.1029/2010GB003848

Koftis, T., Prinos, P., Stratigaki, V., 2013. Wave damping over artificial Posidonia oceanica meadow: a large-scale experimental study. Coast. Eng. 73, 71–83.

Krishnaswamy, S., Lal, D., Martin, J.M., Meybeck, M., 1971. Geochronology of lake sediments. Earth Planet. Sci. Lett. 11, 407–414.

Kroeger, K.D., Crooks, S., Moseman-Valtierra, S., Tang, J., 2017. Restoring tides to reduce methane emissions in impounded wetlands: A new and potent Blue Carbon climate change intervention. Sci. Rep. 7, 1–12. https://doi.org/10.1038/s41598-017-12138-4

Kron, W., 2013. Coasts: The high-risk areas of the world. Nat. Hazards 66, 1363–1382. https://doi.org/10.1007/s11069-012-0215-4

Lattuex, B. (1995). Techniques for Long Term Morphological Simulation under Tidal action. Marine Geology, 126, 129-141.

Lesser, G. R., Roelvink, J. A., van Kester, J. A. T. M., & Stelling, G. S. (2004). Development and validation of a three-dimensional morphological model. Coastal Engineering, 51(8-9), 883–915. doi:10.1016/j.coastaleng.2004.07.014

Lesser, G. R. (2009). An approach to medium-term coastal morphological modelling (PhD Dissertation). The Netherlands: CRC Press/Balkema.

Luijendijk, A. (2019). Crossing borders in coastal morphodynamic modelling. https://doi.org/10.4233/uuif:75ac8d9e-293f-4bff-90b3-467010352032.

Lovelock, C.E., Fourqurean, J.W., Morris, J.T., 2017. Modeled CO 2 Emissions from Coastal Wetland Transitions to Other Land Uses : Tidal Marshes , Mangrove Forests , and Seagrass Beds 4, 1–11. https://doi.org/10.3389/fmars.2017.00143

Macreadie, P.I., Baird, M.E., Trevathan-Tackett, S.M., Larkum, a W.D., Ralph, P.J., 2014. Quantifying and modelling the carbon sequestration capacity of seagrass meadows - A critical assessment. Mar. Pollut. Bull. 83, 430–9. https://doi.org/10.1016/j.marpolbul.2013.07.038

Manca, E., Caceres, I., Alsina, J.M., Stratigaki, V., Townend, I., Amos, C.L., 2012. Wave energy and wave-induced flow reduction by full-scale model Posidonia oceanica seagrass. Cont. Shelf Res. 50–51, 100–116.

Mccreless, E., Beck, M.W., 2016. Rethinking Our Global Coastal Investment Portfolio. J. Ocean Coast. Econ. 3.

Mendez, F.J., Losada, I.J., Losada, M.A., 1999. Hydrodynamics induced by wind waves in a vegetation field. Journal of Geophysical Research: Oceans 104, 18383–18396.

Mol Dijkstra, J.P., Reinds, G.J., Kros, H., Berg, B., de Vries, W., 2009. Modelling soil carbon sequestration of intensively monitored forest plots in Europe by three different approaches. For. Ecol. Manage. 258, 1780–1793. https://doi.org/10.1016/j.foreco.2008.09.011

Möller, I. 2006. Quantifying saltmarsh vegetation and its effect on wave height dissipation: Results from a UK East coast saltmarsh. Estuarine, Coastal and Shelf Science 69:337–351.

Möller, I., T. Spencer, J. R. French, D. J. Leggett, and M. Dixon. 1999. Wave transformation over salt marshes: a field and numerical modelling study from North Norfolk, England. Estuarine, Coastal and Shelf Science 49:411–426.

Moller, I., Kudella, M., Rupprecht, F., Spencer, T., Paul, M., Van Wesenbeeck, B.K., Wolters, G., Jensen, K., Bouma, T.J., Miranda-Lange, M., 2014. Wave attenuation over coastal salt marshes under storm surge conditions. Nat. Geosci. 7, 727.

Muis, S., Güneralp, B., Jongman, B., Aerts, J. C. J. H., and Ward, P. J. (2015). Flood risk and adaptation strategies under climate change and urban expansion: A probabilistic analysis using global data. Science of the Total Environment, 538:445{457.

Muis, S., Verlaan, M., Winsemius, H. C., Aerts, J. C. J. H., and Ward, P. J. (2016). A global reanalysis of storm surges and extreme sea levels. Nature Communications, 7(11969).

Narayan, S., Beck, M.W., Wilson, P., Thomas, C.J., Guerrero, A., Shepard, C.C., Reguero, B.G., Franco, G., Ingram, J.C., Trespalacios, D., 2017. The Value of Coastal Wetlands for Flood Damage Reduction in the Northeastern USA. Sci. Rep. 7, 1–12. https://doi.org/10.1038/s41598-017-09269-z

Nelleman, C., Corcoran, E., Duarte, C.M., Valdes, L., DeYoung, C., Fonseca, L., Grimsditch, G., 2009. Blue Carbon. A Rapid Response Assessment. GRID_Arendal.

Nellemann, C., Corcoran, E., Duarte, C.M., Valdés, L., De Young, C., Fonseca, L., Grimsditch, G., 2009. Blue Carbon. The role of healthy oceans in binding carbon. Birkeland Trykkeri AS, Norway.

Nowacki, D.J., Beudin, A., Ganju, N.K., 2017. Spectral wave dissipation by submerged aquatic vegetation in a back-barrier estuary. Limnol. ceanogr. 62, 736–753.

Ondiviela, B., Losada, I.J., Lara, J.L., Maza, M., Galván, C., Bouma, T.J., Belzen, J. Van, 2014. The role of seagrass in coastal protection in a changing climate. Coast. Eng. 87, 158–168.

Ota, T., N. Kobayashi, and J. T. Kirby. 2004. Wave and current interactions with vegetation. Coastal Engineering 2004:509–520.

Partheniades, E., 1965. "Erosion and Deposition of Cohesive Soils." Journal of the HydraulicsDivision, ASCE 91 (HY 1): 105–139. January.

Paul,M., Amos, C.L., 2011. Spatial and seasonal variation in wave attenuation over Zostera noltii. J. Geophys. Res. Oceans 116, 1–16.

Pendleton, L., Donato, D.C., Murray, B.C., Crooks, S., Jenkins, W.A., Sifleet, S., Craft, C., Fourqurean, J.W., Kauffman, J.B., Marbà, N., Megonigal, P., Pidgeon, E., Herr, D., Gordon, D., Baldera, A., 2012. Estimating Global "Blue Carbon" Emissions from Conversion and Degradation of Vegetated Coastal Ecosystems. PLoS One 7. https://doi.org/10.1371/journal.pone.0043542

Pérez, J., Menéndez, M., and Losada, I. J. (2017). GOW2: A global wave hindcast for coastal applications. Coastal Engineering, 124:1{11.

Pinsky, M. L., G. Guannel, and K. K. Arkema. 2013. Quantifying wave attenuation to inform coastal habitat conservation. Ecosphere 4(8):95. http://dx.doi.org/10.1890/ES13-00080.1

Potouroglou, M., Bull, J.C., Krauss, K.W., Kennedy, H.A., Fusi, M., Daffonchio, D., Mangora, M.M., Githaiga, M.N., Diele, K., Huxham, M., 2017. Measuring the role of seagrasses in regulating sediment surface elevation. Sci. Rep. 7, 11917. https://doi.org/10.1038/s41598-017-12354-y

Prinos, P., Stratigaki, V., Manca, E., Losada, I., Lopez Lara, J., Sclavo, M., Caceres Rabionet, I., Sanchez-Arcilla Conejo, A., 2010. Wave propagation over Posidonia oceanica: large scale experiments. In: 7th HYDRALAB III Joint Transnational Access User Meeting, pp. 57–60.

Ranasinghe, R., Callaghan, D., and Stive, M. J. F. (2012). Estimating coastal recession due to sea level rise: Beyond the Bruun rule. Climatic Change, 110:561{574.

Ranasinghe, R., Duong, T. M., Uhlenbrook, S., Roelvink, D., and Stive, M. (2013). Climate-change impact assessment for inlet-interrupted coastlines. Nature Climate Change, 3:83{87.

Reguero, B.G., Losada, I.J., Díaz-Simal, P., Méndez, F.J., Beck, M.W., 2015. Effects of Climate Change on Exposure to Coastal Flooding in Latin America and the Caribbean. PLoS One 10, e0133409. https://doi.org/10.1371%252Fjournal.pone.0133409

Ricart, A.M., York, P.H., Bryant, C. V., Rasheed, M.A., Ierodiaconou, D., Macreadie, P.I., 2020.

High variability of Blue Carbon storage in seagrass meadows at the estuary scale. Sci. Rep. 10, 1–12. https://doi.org/10.1038/s41598-020-62639-y

Ris, R., N. Booij and L. Holthuijsen, 1999. "A third-generation wave model for coastal regions, Part II: Verification." Journal of Geophysical Research 104 (C4): 7649–7666.

Roelvink, J.A., van Banning, G.K.F.M. (1994). Design and development of Delft3D and application to coastal morphodynamics. In: Verwey A, Minns AW, Babovic V (eds) Proceedings hydroinformatics 1994. Balkema, Rotterdam, p 451–456.

Roelvink J.A. (2006). "Coastal morphodynamic evolution techniques", Coastal engineering, Vol: 53(2-3), 277-287.

Rosenzweig, C., Solecki, W. D., Blake, R., Bowman, M., Faris, C., Gornitz, V., Horton, R., Jacob, K., LeBlanc, A., Leichenko, R., Linkin, M., Major, D., O'Grady, M., Patrick, L., Sussman, E., Yohe, G., and Zimmerman, R. (2011). Developing coastal adaptation to climate change in the New York City infrastructure-shed: Process, approach, tools, and strategies. Climatic Change, 406(1):93{127.

Sanchez-Gonzalez, J.F., Sanchez-Rojas, V., Memos, C.D., 2011. Wave attenuation due to Posidonia oceanica meadows. J. Hydraul. Res. 49, 503–514.

Santos, R., Duque-Núñez, N., de los Santos, C.B., Martins, M., Carrasco, A.R., Veiga-Pires, C., 2019. Superficial sedimentary stocks and sources of carbon and nitrogen in coastal vegetated assemblages along a flow gradient. Sci. Rep. 9, 1–12. https://doi.org/10.1038/s41598-018-37031-6

Schneiderbauer, S., and D. Ehrlich, 2004. Risk, Hazard and People's Vulnerability to Natural Hazards: A Review of Definitions, Concepts and Data. Luxembourg: Office for Official Publication of the European Communities.

Shi, Z., L. J. Hamilton, and E. Wolanski. 2000. Nearbed currents and suspended sediment transport in saltmarsh canopies. Journal of Coastal Research 16:909–914.

Stratigaki, V., Manca, E., Prinos, P., Losada, I.J., Lara, J.L., Sclavo, M., Amos, C.L.,Caceres, I., Sanchez-Arcilla, A., 2011. Large-scale experiments on wave propagation over Posidonia oceanica. J. Hydraul. Res. 49, 31–43.

Stockdon, H.H., Holman, R.A., Howd, P.A., Sallenger,A.H., 2006. Empirical parameterization of setup, swash, and runu. Coastal Engineering, Volume 53, Issue 7, Pages 573-588, ISSN 0378-3839, https://doi.org/10.1016/j.coastaleng.2005.12.005.

Serrano, O., Lovelock, C.E., B. Atwood, T., Macreadie, P.I., Canto, R., Phinn, S., Arias-Ortiz, A., Bai, L., Baldock, J., Bedulli, C., Carnell, P., Connolly, R.M., Donaldson, P., Esteban, A., Ewers Lewis, C.J., Eyre, B.D., Hayes, M.A., Horwitz, P., Hutley, L.B., Kavazos, C.R.J., Kelleway, J.J., Kendrick, G.A., Kilminster, K., Lafratta, A., Lee, S., Lavery, P.S., Maher, D.T., Marbà, N., Masque, P., Mateo, M.A., Mount, R., Ralph, P.J., Roelfsema, C., Rozaimi, M., Ruhon, R., Salinas, C., Samper-Villarreal, J., Sanderman, J., J. Sanders, C., Santos, I., Sharples, C., Steven, A.D.L., Cannard, T., Trevathan-Tackett, S.M., Duarte, C.M., 2019. Australian vegetated coastal ecosystems as global hotspots for climate change mitigation. Nat. Commun. 10, 1–10. https://doi.org/10.1038/s41467-019-12176-8

Spalding, M.D., Mcivor, A.L., Beck, M.W., Koch, E.W., Möller, I., Reed, D.J., Rubinoff, P., Spencer, T., Tolhurst, T.J., Wamsley, T. V., van Wesenbeeck, B.K., Wolanski, E., Woodroffe, C.D., 2014. Coastal ecosystems: A critical element of risk reduction. Conserv. Lett. 7, 293–301. https://doi.org/10.1111/conl.12074

Sutton-Grier, A.E., Wowk, K., Bamford, H., 2015. Future of our coasts: The potential for natural and hybrid infrastructure to enhance the resilience of our coastal communities, economies and ecosystems. Environ. Sci. Policy 51, 137–148. https://doi.org/http://dx.doi.org/10.1016/j.envsci.2015.04.006

Temmerman, S., Kirwan, M.L., 2015. Building land with a rising sea. Science (80-.). 349, 588 LP – 589.

Temmerman, S., Meire, P., Bouma, T.J., Herman, P.M.J., Ysebaert, T., De Vriend, H.J., 2013. Ecosystem-based coastal defence in the face of global change. Nature 504, 79–83. https://doi.org/10.1038/nature12859

Tognin, D., D'Alpaos, A., Marani, M., Carniello, L., 2021. Marsh resilience to sea-level rise reduced by storm-surge barriers in the Venice Lagoon. Nat. Geosci. 14, 906–911.

Tolman, H.L., 2014. User manual and system documentation of WAVEWATCH III version 4.18

Tschirky, P., K. Hall, and D. Turcke. 2001. Wave attenuation by emergent wetland vegetation. Coastal Engineering 2000:865–877.

Twomey, A.J., O'Brien, K.R., Callaghan, D.P., Saunders, M.I., 2020. Synthesising wave attenuation for seagrass: drag coefficient as a unifying indicator. Mar. Pollut. Bull. 160, 111661.Rijn, L. C. van, 1993. Principles of Sediment Transport in Rivers, Estuaries and Coastal Seas. Aqua Publications, The Netherlands.

Van Rijn, L. C. (2007a). Unified View of Sediment Transport by Currents and Waves . I : Initiation of Motion, Bed Roughness, and Bed-Load Transport, Journal of Hydraulic Engineering, 133(6), 649–667.

Van Rijn, L. C. (2007b). Unified View of Sediment Transport by Currents and Waves. II: Suspended Transport. Journal of Hydraulic Engineering, 133(6), 668–689. doi:10.1061/(ASCE)0733-9429(2007)133:6(668)

Van Wesenbeeck, B.K., Mulder, J.P.M., Marchand, M., Reed, D.J., de Vries, M.B., de Vriend, H.J., Herman, P.M.J. (2014). Damming deltas: A practice of the past? Towards nature-based flood defenses. Estuarine, Coastal and Shelf Science, 140, 1–6.

Vuik, V., Jonkman, S.N., Borsje, B.W., Suzuki, T., 2016. Nature-based flood protection: the efficiency of vegetated foreshores for reducing wave loads on coastal dikes. Coast. Eng. 116, 42–56.

Wallace, S. and R. Cox. 1997. Seagrass and wave hydrodynamics. Pages 69–73 in 13th Australasian Coastal and Ocean Engineering Conference and the 6th Australasian Port and Harbour Conference. Centre for Advanced Engineering, University of Canterbury, Christchurch, New Zealand.

Walstra, D.J.R, Hoekstra, R., tonnon, P.K., Ruessink, B.G., 2013. Input reduction for long morphodynamic simulations in wave-dominated coastal settings. Coastal engineering 77 (2013) 57-70.

Warren, R.S., Fell, P.E., Rozsa, R., Brawley, A.H., Orsted, A.C., Olson, E.T., Swamy, V., Niering, W.A., 2002. Salt marsh restoration in Connecticut: 20 years of science and management. Restor. Ecol. 10, 497–513. https://doi.org/10.1046/j.1526-100X.2002.01031.x

Weitzman, J.S., Zeller, R.B., Thomas, F.I., Koseff, J.R., 2015. The attenuation of currentand wave-driven flow within submerged multispecific vegetative canopies. Limnol. Oceanogr. 60, 1855–1874.

Wilmink, Rinse J. A.2015. “Accelerated morphological modelling : a schematized case study into the medium- and long-term morphological acceleration techniques Morfac and Mormerge.”

WL/Delft Hydraulics (2011). Delft3D-FLOW, simulation of multidimensional hydrodynamic flows and transport phenomena, including sediments, User Manual. Delft, 2011.

WL | Delft Hydraulics, 1998. Interaction of submerged vegetation and physical processes;Delft, The Netherlands. Research report, WL | Delft Hydraulics, Delft, The Netherlands. (in Dutch).

Wong, P. P., Losada, I. J., Gattuso, J.-P., Hinkel, J., Khattabi, A., and McInnes, K. (2014). Coastal systems and low-lying areas. In: Climate Change 2014: Impacts, Adaptation, and Vulnerability. Part A: Global and Sectoral Aspects. Contribution of Working Group II to the Fifth Assessment Report of the Intergovernmental Panel on Climate Change. [Field, C.B., V.R. Barros, D.J. Dokken, K.J. Mach, M.D. Mastrandrea, T.E. Bilir, M. Chatterjee, K.L. Ebi, Y.O. Estrada, R.C. Genova, B. Girma, E.S. Kissel, A.N. Levy, S. MacCracken, P.R. Mastrandrea, and L.L. White (eds.)]. Cambridge University Press, Cambridge, United Kingdom and New York, NY, USA, 361-409 pp.

Yang, W., Xia, L., Zhu, Z., Jiang, L., Cheng, X., An, S., 2019. Shift in soil organic carbon and nitrogen pools in different reclaimed lands following intensive coastal reclamation on the coasts of eastern China. Sci. Rep. 9, 1–10. https://doi.org/10.1038/s41598-019-42048-6

Yiping, Li & Anim, Desmond & Wang, Ying & Tang, Chunyang & Du, Wei & Lixiao, Ni & Yu, Zhongbo & Acharya, Kumud & Chen, Li. (2015). Laboratory simulations of wave attenuation by an emergent vegetation of artificial Phragmites australis: An experimental study of an open-channel wave flume. Journal of Environmental Engineering and Landscape Management. 23. 1-10. 10.3846/16486897.2015.1055750.

Zhao, Shujun & Cui, Yuanlai & Luo, Yufeng & Li, Peifeng. (2017). Experimental Study on Wetland Hydraulic Characteristics of Vegetated Drainage Ditches. Water (Switzerland). 9. 10.3390/w9050311.